

Department of Mechanical Engineering  
Integrated Masters in Mechanical Engineering

# **CFRP joints with hybrid laminates metal-carbon fibre**

Submitted by:

João Luís Cardoso Henriques Martins

Supervised by:

Lucas Filipe Martins da Silva

Co-supervised by:

Ricardo João Camilo Carbas

February 2018

*A todos aqueles que me acompanharam nesta pequena grande jornada.*

## Abstract

The aerospace and automotive industries are at the forefront with regard to technological advances in several areas of engineering. The materials and their bonding processes are in constant evolution, with special attention to the use of composite materials and structural adhesives. The fibre-metal laminates (FML) are hybrid materials which, as the name implies, consist of a structure composed by metal laminates and fibre reinforced polymer layers. This composite material arose in the 70's with the aim of strengthening a metal structure. A compromise was achieved between the best features of metallic materials, such as impact strength and good machinability, and the most interesting properties of fibre reinforced polymers, such as high mechanical strength, good resistance to fatigue and corrosion, among others. FMLs have been the target of several investigations by major aerospace companies, such as *Airbus* and *Boeing*, in order to replace certain metallic materials as constituents of structural components of vital importance in their aircrafts.

The theme of this thesis is based on the use of a similar concept to the FML to improve the peel strength of composite materials, as well as the adhesive joint strength itself that uses this material as an adherend. Using an epoxy matrix reinforced with carbon fibres as the composite material, its structural modification was performed by inserting one or two titanium sheets, during the production of the FML, in order to improve the through thickness properties of the composite. The main objective is to identify which configuration allows to obtain the best mechanical properties, when compared to the reference one, composed entirely of carbon fibre reinforced plastic (CFRP).

In order to find out the best configuration, four different designs were tested through tensile tests of single lap joints with two distinct overlaps – 12.5 and 50 mm. To predict the failure load and the failure mode of each one of the joints, several numerical models, using finite element analysis, were created to simulate the tensile tests of the adhesive joints experimentally manufactured, through the commercial software Abaqus®. The numerical models were improved for the purpose of correctly predicting the failure load and the joint strength.

It was verified that the delamination in the CFRP was less severe with the use of hybrid adherends constituted by titanium and CFRP. In addition, higher failure loads were obtained, as well as a greater joint's strength. An interesting failure mode was obtained characterized by an adhesive failure at the Ti-CFRP interface, that led to a progressive failure

instead of an abrupt one, which may be considered very appropriate with regard to the concept of safety, important to the aerospace industry.

With the purpose of optimizing the joint which featured the best behavior when tensile tested, the influence of the joint's thickness, the proportion of materials and the test conditions imposed was analyzed. It was confirmed that the failure load and the peel stresses along the joint were not significantly influenced by the joint's thickness or the percentage of titanium. However, when these joints were tested under impact conditions, the obtained failure load was expressively higher than the values achieved under static conditions.

A comparison between FMLs with different metallic sheets, aluminium and titanium, was made. The titanium presented the highest failure load for both static and impact conditions.

## Resumo

As indústrias aerospacial e automóvel encontram-se na vanguarda no que diz respeito aos avanços tecnológicos em diversas áreas da engenharia. As áreas dos materiais e dos seus processos de ligação apresentam-se em constante evolução, com especial atenção para a utilização de materiais compósitos e de adesivos estruturais. Os *fibre-metal laminates*, também designados por FML, são materiais híbridos que, tal como o nome indica, consistem numa estrutura composta por laminados metálicos e camadas de um polímero reforçado com fibras intercalados entre si. Este material compósito surgiu na década de 70, numa primeira instância, com o intuito de reforçar uma estrutura metálica. Assim, era obtido um compromisso entre as melhores características dos metais, como por exemplo a resistência ao impacto e boa maquinabilidade, e as propriedades mais interessantes dos polímeros reforçados com fibras, como a elevada resistência mecânica, boa resistência à fadiga e à corrosão entre outras. Os FMLs têm sido alvo de investigações por parte de grandes empresas aerospaciais, como a *Airbus* e a *Boeing*, no sentido de substituírem certos materiais metálicos como constituintes de componentes estruturais de crucial importância nas suas aeronaves.

O tema desta tese assenta na utilização de um conceito similar ao do FML para melhorar a resistência ao arrancamento de materiais compósitos, bem como a resistência da própria junta adesiva que utiliza esse material como aderente. Assim sendo, utilizando como material compósito uma matriz epóxida reforçada com fibras de carbono foi realizada a sua modificação estrutural ao introduzir um ou dois laminados de titânio durante a produção dos FML, de forma a melhorar as propriedades transversais do compósito. O principal objectivo consiste em identificar qual a configuração que permite obter as melhores propriedades mecânicas, quando comparada com a configuração de referência, constituída unicamente por polímero reforçado com fibras de carbono.

De forma a descobrir qual a melhor configuração, foram testadas quatro tipos de juntas através de ensaios de tração de juntas de simples sobreposição com dois comprimentos de sobreposição diferentes – 12.5 e 50 mm. Para obter uma previsão da força de rotura e da superfície de falha de cada configuração, foram criados diversos modelos numéricos, recorrendo à análise de elementos finitos, com o intuito de simular os ensaios de tração das juntas adesivas para as diferentes configurações, através do software comercial Abaqus®. Os modelos numéricos foram aperfeiçoados a fim de preverem o melhor possível a força de rotura e, também, a resistência mecânica da junta.

Verificou-se que a delaminação foi menos acentuada com a utilização dos aderentes híbridos de titânio e de CFRP. Para além disso, maiores forças de rotura foram obtidas, bem como uma maior resistência da junta. Um modo de falha interessante foi obtido, caracterizado por uma falha adesiva na interface titânio-CFRP que levou a uma rotura progressiva da junta o que pode ser considerado bastante relevante no que concerne ao conceito de segurança defendido pela indústria aeroespacial.

Com o propósito de otimizar a junta que apresentava um melhor comportamento quando testada à tração, foi analisada a influência da espessura, da proporção dos materiais e ainda da solicitação imposta. Confirmou-se que a força de rotura e as tensões de arrancamento ao longo da junta não eram, significativamente, influenciadas pela espessura da junta nem pela percentagem de titânio. No entanto, quando estas juntas eram testadas sob condições de impacto, a força de rotura obtida apresentava um valor significativamente maior àqueles alcançados em condições estáticas.

A comparação entre os FMLs usando diferentes metais, alumínio e titânio, foi realizada. O titânio apresentou os melhores valores de força de rotura para ambas as condições de teste.

## **Acknowledgments**

I would like to thank, primarily, Ricardo Carbas for his inexhaustible patience and availability during this semester. Also recognize that without his guidance and commitment this project would not be as successful as it was.

I would also like to thank Professor Lucas da Silva, for sharing his enormous knowledge and for challenging me with numerous tasks that made this investigation thesis even more motivating.

I would particularly like to show my endless gratitude to all members of ADFEUP, including Eduardo, José, Daniel and both Ana, for all opinions shared and all tips given during this project.

To my Master's colleagues, Mário and Paulo, I recognize that their help was of extreme importance.

I would like to thank the LADs, Ambrósio, Álvaro, Bernardo, Rocha, Manuel, José, Jolie, Antelo, Maria, Nando, Mário and Roque, for being there whenever I needed and for supporting me through this important journey.

I would like to especially thank my girlfriend, Catarina, for her patience through this semester, as well as her crucial advices given in every single decision I had to make.

Finally, to my father, my mother and my siblings, for the unconditional support and for turning the dream of being an engineer an eternal reality.

# Contents

Abstract .....	ii
Resumo .....	iv
Acknowledgments.....	vi
Nomenclature.....	ix
List of figures .....	xi
List of tables.....	xiv
<b>1. Introduction.....</b>	<b>1</b>
<b>1.1. Background and motivation .....</b>	<b>1</b>
<b>1.2. Objectives .....</b>	<b>3</b>
<b>1.3. Research methodology .....</b>	<b>3</b>
<b>1.4. Outline of the thesis .....</b>	<b>4</b>
<b>2. Literature Review.....</b>	<b>5</b>
<b>2.1. History of composite materials.....</b>	<b>5</b>
<b>2.2. Fibre reinforced composites.....</b>	<b>7</b>
2.2.1. <i>Matrices and fibres.....</i>	7
2.2.2. <i>Carbon fibre reinforced polymers.....</i>	7
2.2.2.1. <i>Mechanical properties and applications of CFRP's.....</i>	7
2.2.2.2. <i>Failure modes and failure mechanics of CFRP's.....</i>	10
<b>2.3. Adhesive bonding.....</b>	<b>11</b>
2.3.1. <i>Joint configurations .....</i>	12
2.3.2. <i>Failure modes in adhesive joints .....</i>	13
2.3.3. <i>Techniques to reduce the peel stresses in composite materials.....</i>	15
2.3.4. <i>Fibre metal laminates.....</i>	17
<b>2.4. Strength prediction of adhesively bonded joints .....</b>	<b>19</b>
2.4.1. <i>Numerical solutions.....</i>	19
<b>3. Experimental details .....</b>	<b>23</b>
<b>3.1. Adhesive .....</b>	<b>23</b>
<b>3.2. Adherends .....</b>	<b>24</b>
3.2.1. <i>CFRP.....</i>	25
3.2.2. <i>Titanium alloy .....</i>	25
<b>3.3. Specimens configurations.....</b>	<b>26</b>
<b>3.4. Specimens manufacture .....</b>	<b>27</b>
3.4.1. <i>CFRP plates.....</i>	27
3.4.2. <i>Surface treatment of the titanium alloy.....</i>	30
3.4.3. <i>Surface treatment influence.....</i>	32
3.4.4. <i>Manufacture of CFRP-Titanium laminates.....</i>	34
3.4.5. <i>Manufacture of single lap joints .....</i>	35
3.4.6. <i>Testing conditions .....</i>	38
<b>4. Experimental Results .....</b>	<b>40</b>
<b>4.1. CFRP-only SLJs.....</b>	<b>40</b>
4.1.1. <i>12.5 mm overlap length .....</i>	40
4.1.2. <i>50 mm overlap length .....</i>	41
<b>4.2. CFRP-Ti-CFRP SLJs.....</b>	<b>42</b>
4.2.1. <i>12.5 mm overlap length .....</i>	42
4.2.2. <i>50 mm overlap length .....</i>	43
<b>4.3. Ti-CFRP SLJs.....</b>	<b>44</b>
4.3.1. <i>12.5 mm overlap length .....</i>	44
4.3.2. <i>50 mm overlap length .....</i>	45
<b>4.4. Ti-CFRP-Ti SLJs .....</b>	<b>47</b>
<b>4.5. Comparison of SLJs' results .....</b>	<b>49</b>
4.5.1. <i>12.5 mm overlap SLJs.....</i>	49
4.5.2. <i>50 mm overlap SLJs .....</i>	50



5. Numerical Analysis .....	52
5.1. Model description .....	52
5.2. Triangular cohesive law vs Trapezoidal cohesive law .....	55
5.3. Numerical results .....	59
5.3.1. CFRP-only SLJs .....	60
5.3.1.1. 12.5 mm overlap length .....	60
5.3.1.2. 50 mm overlap length .....	61
5.3.2. CFRP-Ti-CFRP SLJs .....	62
5.3.2.1. 12.5 mm overlap length .....	62
5.3.2.2. 50 mm overlap length .....	64
5.3.3. Ti-CFRP SLJs .....	65
5.3.3.1. 12.5 mm overlap length .....	65
5.3.4. Ti-CFRP-Ti SLJs .....	66
5.3.4.1. 50 mm overlap length .....	66
6. Discussion .....	68
7. Optimization of Ti-CFRP-Ti single lap joints .....	72
7.1. Different thicknesses .....	72
7.2. Distinct proportion of materials .....	74
7.3. Impact conditions .....	76
8. Conclusions .....	80
9. Future work .....	82
10. References .....	83

## Nomenclature

### Acronyms

- ARALL – Aramid reinforced aluminium laminates
- CBBM – Compliance-based beam method
- CFRP – Carbon fibre reinforced polymer
- CNFs – Carbon nanofibres
- CTE – Coefficient of thermal expansion
- CZE – Cohesive zone elements
- CZM – Cohesive zone model
- DCB – Double cantilever beam
- ENF – End notched flexure
- FEA – Finite elements analysis
- FEM – Finite elements method
- FML – Fibre metal laminates
- FRP – Fibre reinforced polymer
- GLARE – Glass reinforced aluminium
- IA – Inter adherend
- SLJ – Single lap joint
- TAST – Thick adherend shear test
- TDCB – Tapered double cantilever beam

## Symbols

- $Al$  – Aluminium
- $b$  – Width of the joint
- $CO_2$  – Carbon dioxide
- $E$  – Young's Modulus
- $G$  – Shear modulus
- $G_{IC}$  – Fracture energy in mode I
- $G_{IIC}$  – Fracture energy in mode II
- $l$  – Overlap length
- $P$  – Load
- $t$  – Thickness of the adherend
- $Ti$  – Titanium
- $\delta$  - Displacement
- $\tau$  – Shear stress
- $\nu$  – Poisson's ratio

## List of figures

Figure 1 - Composition of A350 XWB [4].....	1
Figure 2 - Composition of Boeing 787 "Dreamliner" [5].....	1
Figure 3 - FML configuration [6].....	2
Figure 4 - Mongolian bow [8] .....	5
Figure 5 – Fiberglass [9].....	5
Figure 6 - Fiberglass boat [11] .....	6
Figure 8 - Carbon fibre reinforced epoxy matrix – prepreg form [15].....	8
Figure 7 - Prepreg production process [14] .....	8
Figure 9 - Automotive CFRP's applications [17] .....	9
Figure 10 – Failure modes of fibre reinforced polymers [19] .....	10
Figure 11 - Adhesive bonded joints [22] .....	12
Figure 12 - Typical loads of an adhesive joint: a) Normal stress; b) shear stress; c) cleavage stress; d) peel stress [21].....	13
Figure 13 - Failure mode for adhesives joints [23] .....	13
Figure 14 - Delamination of a FRP's adherend [24].....	14
Figure 15 - Internal taper and adhesive fillet [26].....	15
Figure 16 - Reduction of transverse stresses by internal taper and adhesive fillet [26].....	15
Figure 17 - Z-pins technique [27].....	16
Figure 18 - Crack growth resistance (R-) curves for the unreinforced and through-thickness reinforced laminates containing 0.82 vol% CNFs and/or 0.5 vol% z-pins under quasi-static [28] .....	16
Figure 19 - Inter-adherend-fibre joint [29] .....	17
Figure 20 - Classification of FMLs based on metal plies [31] .....	18
Figure 21 - Cohesive elements to simulate zero thickness failure paths [32] .....	21
Figure 22 - CZM laws with triangular, exponential and trapezoidal shapes available in Abaqus® [53] .....	22
Figure 23 - Cure cycle for the adhesive AF 163-2K [54].....	23
Figure 24 - Selected configurations for FML manufacturing.....	26
Figure 25 - Other possible FML configurations.....	26
Figure 26 - Application of releasing agent to the mould components .....	27
Figure 27 - Pre-heating of the CFRP layers with a hot air gun .....	28
Figure 28 - Cure cycle for CFRP plates .....	29
Figure 29 - Hot plates press machine <i>INTOCO</i> .....	29
Figure 30 - Diamond disc cutting from model DV 25 Batisti Meccanica.....	29
Figure 31 - Bonding between the steel blocks and the specimen CFRP-Ti-CFRP.....	32

Figure 32 - Loading scheme of traction test in mode I.....	32
Figure 33 – Most representative curve for Mode I traction test .....	33
Figure 34 - Typical failure of the samples in mode I traction test: (a) adhesive failure in Ti-CFRP interface; (b) cohesive failure in CFRP (delamination).....	33
Figure 35 - Stacking of the titanium laminates over the CFRP plate .....	35
Figure 36 - SLJs geometry (mm) [55] .....	36
Figure 37 - Adhesive in film placed on one adherend.....	36
Figure 38 - SLJs bonding .....	37
Figure 39 - MTS® model 810 .....	38
Figure 40 - Video system setup to observe the delamination phenomenon .....	39
Figure 41 - Load vs displacement typical curve of a CFRP-only SLJ with a 12.5 mm overlap .....	40
Figure 42 - Typical failure surface of 12.5 mm overlap CFRP-only SLJs.....	40
Figure 43 - Load vs displacement typical curve of a CFRP-only SLJ with a 50 mm overlap .	41
Figure 44 - Typical failure surface of 50 mm overlap CFRP-only SLJs.....	41
Figure 45 - Load vs Displacement typical curve of a CFRP-Ti-CFRP SLJ with a 12.5 mm overlap .....	42
Figure 46 - Typical failure surface of 12.5 mm overlap CFRP-Ti-CFRP SLJs .....	43
Figure 47 - Load vs displacement typical curve of a CFRP-Ti-CFRP SLJ with a 50 mm overlap .....	43
Figure 48 - Typical failure surface of 50 mm overlap CFRP-Ti-CFRP SLJs.....	44
Figure 49 - Load vs Displacement typical curve of a Ti-CFRP SLJ with a 12.5 mm overlap.	45
Figure 50 - Typical failure surface of 12.5 mm overlap Ti-CFRP SLJs .....	45
Figure 51 - Load vs displacement typical curve of a Ti-CFRP SLJ with a 50 mm overlap.....	46
Figure 52 - Failure surface of a 50 mm overlap Ti-CFRP SLJ .....	46
Figure 53 - Load vs displacement typical curve of a Ti-CFRP-Ti SLJ with a 50 mm overlap.	47
Figure 54 - Failure surface of a 50 mm overlap Ti-CFRP-Ti SLJ .....	48
Figure 55 - Distribution of CZE layers throughout the SLJ .....	52
Figure 56 - Schematic view of the physical boundary conditions in Abaqus® .....	53
Figure 57 - Schematic view of the thermal predefined field .....	53
Figure 58 - Ti-CFRP adherend's bending due to thermal stresses: a) Experimentally; b) Numerically .....	54
Figure 59 - Vertical displacement suffered by both adherends .....	54
Figure 60 - SLJ square mesh with 0.2 mm refinement.....	55
Figure 61 – AF 163-2K P- $\delta$ curves [55].....	56
Figure 62 - DCB test specimen's model.....	56
Figure 63 - Comparison between DCB experimental and numerical results .....	57
Figure 64 – ENF test specimen's model.....	57

Figure 65 - Comparison between ENF experimental and numerical results.....	58
Figure 66 - Comparison between the SLJs tests experimental and numerical results.....	59
Figure 67 – Numerical P- $\delta$ curve vs experimental P- $\delta$ curve for a 12.5 mm overlap CFRP-only SLJ.....	60
Figure 68 - Numerical failure surface of 12.5 mm overlap CFRP-only SLJ.....	61
Figure 69 - Numerical P- $\delta$ curve vs experimental P- $\delta$ curve for a 50 mm overlap CFRP-only SLJ.....	61
Figure 70 - Numerical failure surface of 50 mm overlap CFRP-only SLJ.....	62
Figure 71 - Numerical P- $\delta$ curve vs experimental P- $\delta$ curve for a 12.5 mm overlap CFRP-Ti-CFRP SLJ.....	63
Figure 72 - Numerical failure surface of 12.5 mm overlap CFRP-Ti-CFRP SLJ.....	63
Figure 73 - Numerical P- $\delta$ curve vs experimental P- $\delta$ curve for a 50 mm overlap CFRP-Ti-CFRP SLJ.....	64
Figure 74 - Numerical failure surface of 50 mm overlap CFRP-Ti-CFRP SLJ.....	64
Figura 75 - Numerical P- $\delta$ curve vs experimental P- $\delta$ curve for a 12.5 mm overlap Ti-CFRP SLJ.....	65
Figure 76 - Numerical failure surface of 12.5 mm overlap Ti-CFRP SLJ.....	66
Figure 77 - Numerical P- $\delta$ curve vs Experimental P- $\delta$ curve for a 50 mm overlap Ti-CFRP-Ti SLJ.....	67
Figure 78 - Numerical failure surface of 50 mm overlap Ti-CFRP-Ti SLJ.....	67
Figure 79 - Comparison between FEA predictions and experimental results for the failure load of 12.5 mm overlap SLJs.....	68
Figure 80 - Comparison between FEA predictions and experimental results for the failure load of 50 mm overlap SLJs.....	70
Figure 81 – Comparison between different Ti-CFRP-Ti adherend thicknesses in terms of failure load.....	72
Figure 82 - Comparison between different Ti-CFRP-Ti adherends' thicknesses in terms of peel stresses.....	73
Figure 83 - Comparison of the failure load between different titanium laminates thickness in Ti-CFRP-Ti joints.....	74
Figure 84 –Comparison of the peel stresses between different titanium laminates thickness in Ti-CFRP-Ti joints.....	75
Figure 85 - Schematic view of the physical boundary conditions for SLJs under impact conditions in Abaqus®.....	76
Figure 86 – Load vs Time curves for all SLJs under impact conditions.....	77
Figure 87 – Comparison of the failure load between quasi-static and impact conditions.....	78
Figure 88 – Failure mode of CFRP-only and CFRP-Ti-CFRP SLJs under impact conditions.....	78
Figure 89 - Failure mode of Ti-CFRP-Ti SLJs under impact conditions.....	78
Figure 90 - Comparison between Ti-CFRP-Ti and Al-CFRP-Al failure loads under quasi-static and impact conditions.....	79

## List of tables

Table 1 – Most important families of adhesives and their properties [21].....	11
Table 2 – AF 163-2K mechanical properties [55].....	24
Table 3 – Orthotropic components for a unidirectional CFRP ply [56].....	25
Table 4 – Mechanical properties of Ti-6Al-4V alpha-beta, annealed [58] .....	25
Table 5 – Failure load and type of failure for joints with a 12.5 mm overlap.....	49
Table 6 - Failure load and type of failure for joints with a 50 mm overlap .....	50
Table 7 – Cohesive parameters for CFRP interlaminar failure [55].....	53
Table 8 – Failure type obtained experimentally and numerically for the 12.5 mm overlap joints .....	69
Table 9 - Failure type obtained experimentally and numerically for the 50 mm overlap joints .....	71

# 1. Introduction

## 1.1. Background and motivation

The use of metallic materials has been replaced, throughout the years, by other materials that can offer interesting mechanical properties allied with a lower weight, which is one of the most wanted characteristics in aeronautical and aerospace industries. These materials are called composite materials.

The first composite materials were too expensive and those industries continued to prefer metallic alloys as aluminium or steel alloys. However, today we are able to find very good prices that allow the continuous bet in composite materials. For instance, the airbus A380 offers the lowest cost per seat in aerospace industry using advanced aluminium alloys (fuselage and wings) and composite materials in other structures as the centre wing box's primary structure, wing ribs or rear fuselage section [1]. The use of composite materials results in a reduction of fuel consumption per passenger and CO<sub>2</sub> emission which means a significant financial saving. Actually, the percentage of composite materials in the newest aircrafts can reach over 50%, like in A350 XWB and Boeing 787 "Dreamliner" aircrafts [2, 3], as seen in Figures 1 and 2.



Figure 1 - Composition of A350 XWB [4]

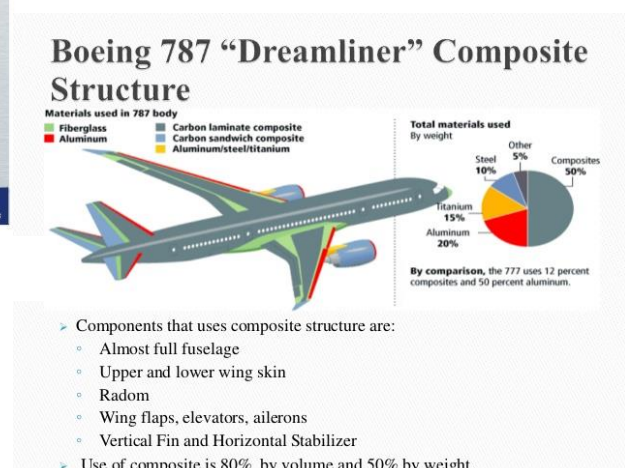


Figure 2 - Composition of Boeing 787 "Dreamliner" [5]



This group of materials shows some mechanical disadvantages in some directions due to their anisotropy. Nevertheless, they constitute the highest percentage of aircraft's materials which is explained not only with the advance of adhesive bonding technology but also with the invention of some techniques to increase the mechanical behavior through the weakest directions.

The adhesive bonding evolution have occurred parallelly with the growth of composite materials. Due to the decrease in their mechanical through thickness properties, the use of holes in order to bond two substrates with bolts or rivets must be avoided, which consents the election of adhesive bonding as ideal. This bonding process allows the achievement of a higher stiffness and a more uniform stress distribution, besides presenting a extremely low weight, in comparison with the use of bolts or rivets. However, adhesive bonding presents some disadvantages, such as the possibility of occurring delamination of the CFRP due to the peel loadings that adhesively bonded joints experience. Therefore, there are also some techniques that allow the improvement of these properties.

One of the techniques used to improve the mechanical properties through the thickness direction is the use of a similar concept of FML (Figure 3).



Figure 3 - FML configuration [6]

The study of these FML materials showed that the influence of the metal sheets was very positive by reducing significantly the fatigue crack growth rates in adhesive bonded sheet materials [7].

## **1.2. Objectives**

As said before, the main subject of this thesis is to study the influence of titanium laminates when used as a reinforcement of CFRP substrates. The concept is similar to that used in fibre metal laminates.

Therefore, the main objective is to find the best FML configuration that offers the optimal improvement related to peel strength of the composite and also joint strength of composite adhesive joints.

To test and find that optimal configuration, several numerical and experimental studies were made. The CFRP composite suffered a hybridization through its thickness, by including sheets of titanium. The combinations were tested since the only CFRP laminate until the optimal configuration.

## **1.3. Research methodology**

The following planning was done:

- a) Literature review on composite materials, mostly carbon fibre and FML, adhesive bonding, titanium laminates and SLJ's failure mechanisms;
- b) State of the art, focusing in FML material and its applications;
- c) Surface treatment of titanium laminates, manufacture of FML substrates and specimen's tests (Mode I);
- d) Numerical simulation of the tensile tests made with SLJs using Abaqus CAE software to validate the experimental data;
- e) Performance of experimental tests of SLJs for different combinations Ti-CFRP and analysis of the results;
- f) Numerical optimization of FML's configuration in order to find the best one that gives the most interesting mechanical properties to the substrates.

#### **1.4. Outline of the thesis**

The outline of the thesis will be described by chapter.

1. Introduction;
2. Literature review on composite materials, adhesive bonding, failure modes of composite and adhesives;
3. Experimental details;
4. Experimental results;
5. Numerical analysis;
6. Discussion;
7. Optimization of SLJs with different adherends thicknesses, distinct proportion of materials and under impact conditions;
8. Conclusions;
9. Future work;

## 2. Literature Review

### 2.1. History of composite materials

The first uses of composite materials date back to thousands of years BC, when northern African civilizations started joining more than one material to develop properties of their own buildings, ceramics and means of transport. In 1200 AD, the Mongols improved their bows using composite materials, as shown in Figure 4. Those combined wood, bone and “animal glue”.



Figure 4 - Mongolian bow [8]

During some centuries, these materials were forgotten. Their reappearance is directly connected with plastic's development. Until then, all resins used were animal or vegetable. In the beginning of 90's, some polymers such as vinyl, polystyrene, phenolic and polyester appeared in industry and even nowadays are used as matrixes for composite materials.

Nevertheless, it was not enough to provide the strength necessary for some structural applications. That is why studies were done to find a way to increase those mechanical properties and, in 1935, Owens Corning presented the first glass fibre, also called, fiberglass (Figure 5).



Figure 5 – Fiberglass [9]

The inclusion of glass fibres in a polymer matrix created a structure stronger than the polymer itself. Besides, the global structure was also lightweight which is one of the most interesting characteristics of a composite material. All these improvements had contributed for the origin of FRPs – fibre reinforced polymers [10].

Although this creation was made in a laboratory, during World War II, glass fibre started to be produced for applications in military industry such as aircrafts and radar equipment. After WWII, due to decrease in demand for military products, composite materials started to be applied in other fronts like sports and medicine (Figure 6).



Figure 6 - Fiberglass boat [11]

In 1970s the composite industry started an evolution that continues until today. Other resins and reinforcing fibres were created such as aramid fibre (Kevlar) and carbon fibre. These fibres replaced metal in some applications due to their high tensile strength and lower weight.

However, their manufacturing processes cost and the environmental issues have given some priority to the reintroduction of natural fibres as reinforcements of composite materials used in applications for men's protection such as fire helmets for example [10, 12].

The research for newer and better composite materials continues, particularly in nanomaterials and bio-based polymers areas. The use of FML's substrates is an area also studied in aerospace industry and is the main theme of this master's thesis.

## **2.2. Fibre reinforced composites**

### ***2.2.1. Matrices and fibres***

Composite materials have suffered several improvements since their creation. There are three types of composite materials: structural composites, fibre reinforced composites and particle reinforced composites. However, the main group of composite materials used in industry is the fibre reinforced one.

Fibre reinforced composites are composed by a matrix and reinforced fibres. The mechanical properties obtained at the end will be a mixture between all mechanical properties of the matrix and the fibres.

There are several types of matrices, such as thermosetting, thermoplastics, metals or even ceramics. Regarding the reinforcements used in composite materials, the carbon fibres and the glass fibres are the most used [13]. Regarding the fibres, they may be continuous (long) or short.

### ***2.2.2. Carbon fibre reinforced polymers***

#### ***2.2.2.1. Mechanical properties and applications of CFRP's***

As have been said before, the properties in FRP's composite materials are different depending on the direction assumed. Regarding CFRP composite, the weakest properties are the ones through thickness, since it is the polymer that controls them in that direction.

Due to the anisotropic behavior, typical when continuous fibres are used, it is important to realize how CFRP's mechanical properties differ with the direction. It will be strongly dependent on how the composite material is supplied.

Many suppliers provide CFRP as a prepreg, as seen in Figure 8, also called a semi-product, which consists in a combination of fibres and resin between silicone sheets that are pressed or rolled in order to ensure that all fibres are well wetted. The resin is partially cured to allow the prepreg handling. This process is represented in Figure 7.

Despite the component's proportion (50% of fibres) and the prepreg thickness (less than 0.5 mm), the supplier may change some characteristics during prepreg production to achieve some properties needed to a specific application [13].

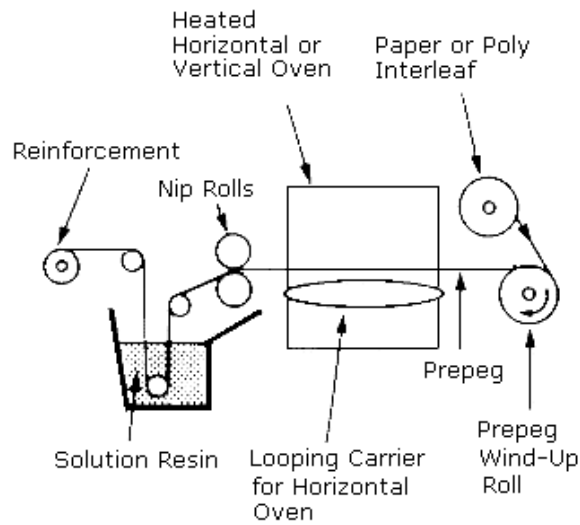


Figure 8 - Prepreg production process [14]

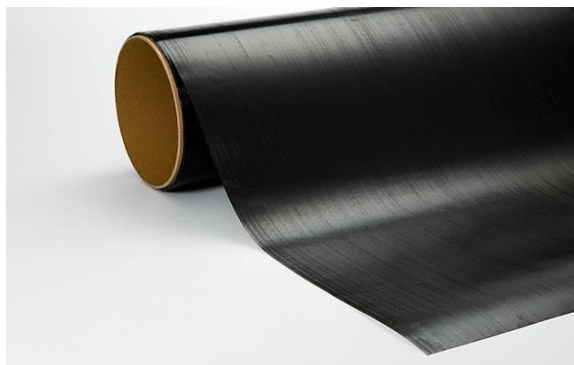


Figure 7 - Carbon fibre reinforced epoxy matrix – prepreg form [15]

According to Adams [16], the continuous bet on carbon fibre composite materials brought various advantages within the automotive industry.

The low density of CFRPs allows the reduction of vehicles total weight, that make possible the production of lighter body components as the driver cabin of some automobiles and chassis mechanisms such as spring rods. Besides those applications, also brake disks and rims in carbon fibre were created. With the advance of high technology in this industry, the presence of carbon fibre composites will be more evident, as presented in Figure 9.

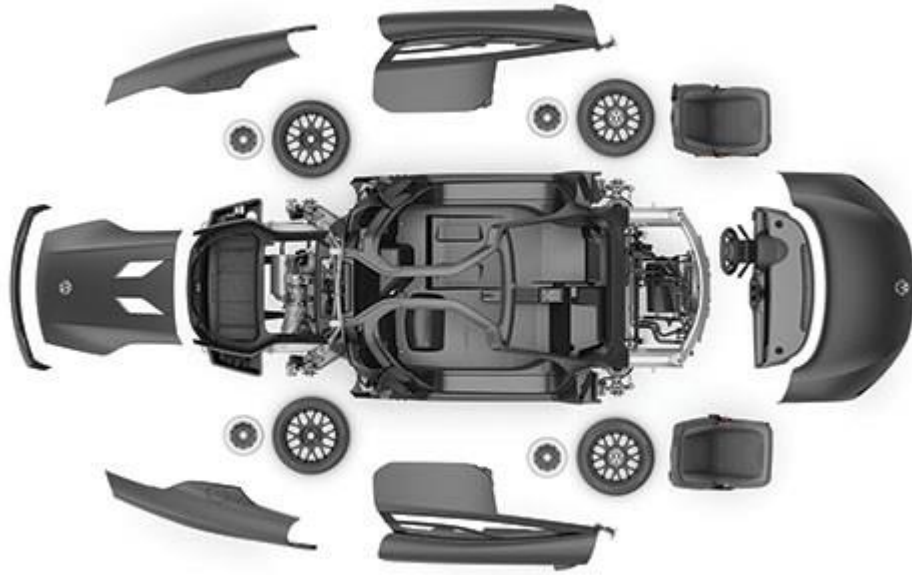


Figure 9 - Automotive CFRP's applications [17]

The use of this composite material as wings and fuselage main component has been increasing with a very high speed, due to the combination of fibres and resin properties: high strength, stiffness, toughness and low density [18]. For instance, analyzing the aircrafts' evolution, the percentage of CFRP has grown through 2 percent in the F15 up to 24 percent in the F22. As have been said before, the use of this kind of material consents the existence of lower weight components which enables a more economic fuel consumption and also lowers operating costs.

Nowadays, it is possible to witness some aircrafts that are made by 50% of composite materials, as Airbus A350, which proves that the constant evolution of these hybrid materials must continue.



### 2.2.2.2. Failure modes and failure mechanics of CFRP's

CFRP's have been chosen for very important and advanced applications such as automotive components or aircrafts mechanisms. Therefore, it is a priority to know how they behave when they work close to failure.

The most common failure loads are presented in Figure 10.

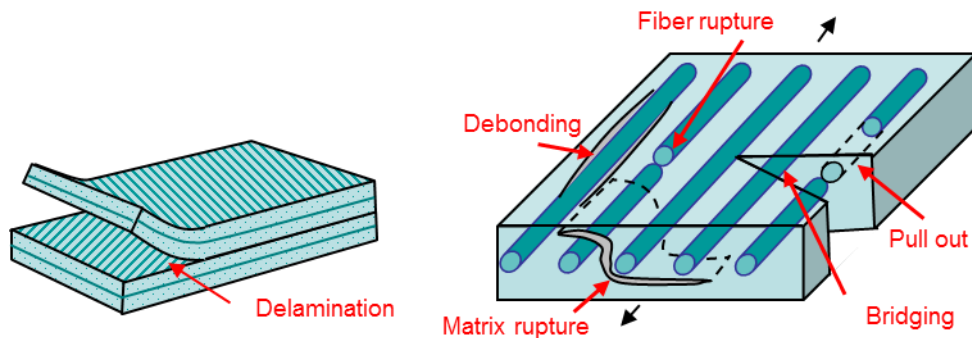


Figure 10 – Failure modes of fibre reinforced polymers [19]

For the aerospace industry, delamination of the composite material is a failure mode that must be avoided at any cost. This kind of failure results from high interlaminar stress, through CFRP's thickness, where the mechanical properties are weaker. Delamination occurs due to the separation of adjacent CFRP's laminates by their interface. There are many causes that may be used to explain delamination such as peel stress, impact or cyclic stress.

There are some techniques used to reduce the peel stress in composite materials and avoid delamination which are described in section 2.3.3.

### 2.3. Adhesive bonding

The constant development and evolution of composite materials in automotive and aerospace industries have shown a lot of benefits. However, these materials, including FMLs, must be bonded in order to achieve a more complex structure as a fuselage or a chassis component. Due to their anisotropy and excellent mechanical properties, this bonding must be done carefully. Some bonding techniques as the use of screws or welding, are not interesting for such applications because both of them affect composite materials in different ways.

The best way to bond composite materials is using adhesive bonding. There are several adhesive's families which present different properties, as shown in Table 1. The aerospace industry is considered one of the pioneers of this technique that starts to be crucial in automotive industry too [20].

The application of adhesive bonding in some industries such as those referred above is absolutely demanding. That is why it is necessary to study the adhesive joint intensely, finding the best joint configuration and predicting the failure load of that joint.

Table 1 – Most important families of adhesives and their properties [21]

Adhesive	Advantages	Disadvantages
Epoxies	High strength, good toughness, temperature resistance and relatively low cost	Short pot life, exothermic reaction, requires precise chemical formulation
Polyurethanes	Good strength and toughness at low temperatures, resistance to fatigue, impact resistance, good durability	Moisture sensitive, poor heat resistance, short pot life
Phenolics	High hardness, excellent thermal stability, cheap	Brittle with low peel strength, requires very high cure pressures
Silicones	Environmental stability, high degree of flexibility, capability to bond materials of various natures, excellent resistant to heat and moisture	High cost, lower mechanical properties at room temperature
Cyanoacrylates	Rapid room-temperature cure, good mechanical strength, long pot life, good adhesion to metal	Expensive, poor durability, poor heat resistance
Modified acrylics	Good peel and shear strengths, does not require an extensive surface treatment, room temperature cure	Limited resistance to thermal chock, difficult to process, toxic and flammable
Aromatics	Very good heat resistance, aerospace applications	Expensive, hard to process, very brittle at room temperature

### 2.3.1. Joint configurations

The conception of an adhesive joint should respect some considerations about this type of bonding process. The majority of the adhesives does not have a good behavior when submitted to peel stresses, because it affects a small adhesive area in a joint. Besides, there are applications which the demand is higher than others. For some of those requests it is enough to use a single lap joint which is the simplest configuration even being efficient for many engineering applications. However, there are many solutions for adhesive bonding joints as shown in Figure 11.

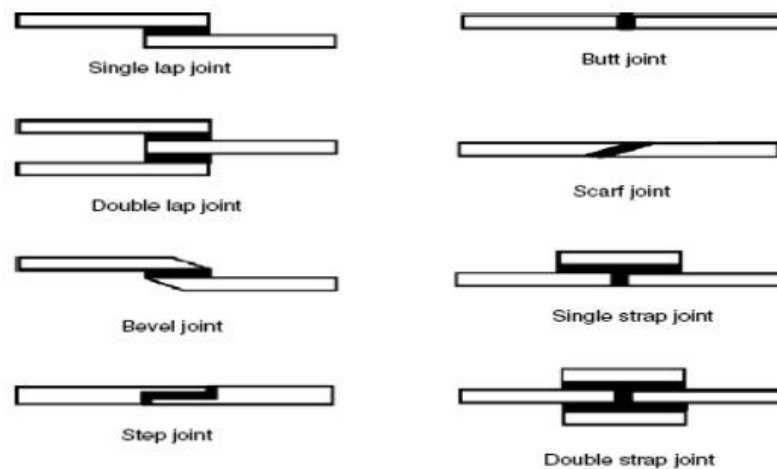


Figure 11 - Adhesive bonded joints [22]

According to Kinloch [21], even existing joint designs more resistant than others, “*the designer should not only attempt to keep stress concentrations to a minimum but also attempt to distribute the imposed loads within the adhesive layer as a combination of compressive and shear stresses; avoiding tensile, cleavage and peel stresses as much possible.*”. To fully understand these typical loads, they are presented in Figure 12.

However, in real situations, it is almost impossible to have just one type of load applied to the adhesive joint. That is why reducing the peel stresses is a matter of extreme importance in aerospace and automotive industries.

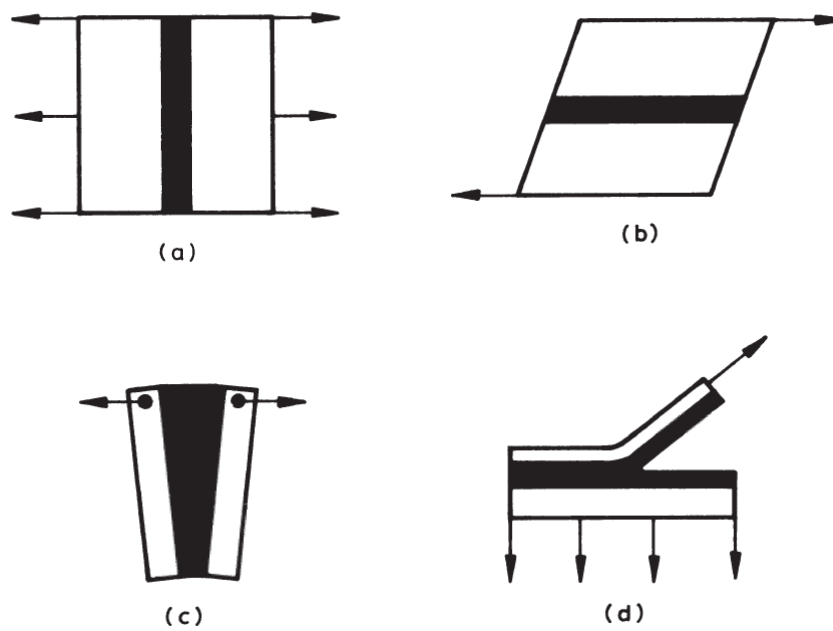


Figure 12 - Typical loads of an adhesive joint: a) Normal stress; b) shear stress; c) cleavage stress; d) peel stress [21]

### 2.3.2. Failure modes in adhesive joints

Once an adhesive joint is created, it is decisive to know how all components, adhesive and adherends, behave when loaded. Sometimes, the stresses concentrated within adhesive joint origin joint's failure. These failure modes may happen in different ways, presented in Figure 13.

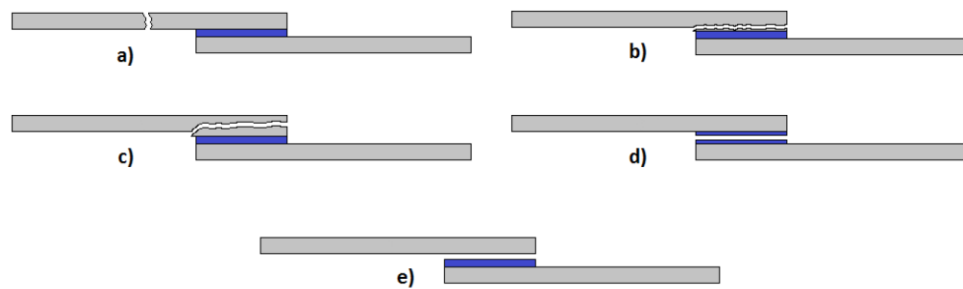


Figure 13 - Failure mode for adhesives joints [23]

There are three typical failure modes in an adhesive bonded joint.

1. Adherend's failure outside the joint (13 a, b, c);
2. Cohesive failure by fracture of the adhesive layer (13 d);
3. Failure at the interface between the adhesive and one adherend, named adhesion failure (13 e).

Evaluating all these failure modes, the one most desirable is the adherend's failure outside the joint. This kind of failure indicates that the adherend chosen fulfilled its structural performance. Therefore, it is only necessary to test the adherends to analyze their structural integrity. When fibre reinforced polymers are used as adherends, this failure is called delamination (Figure 14).

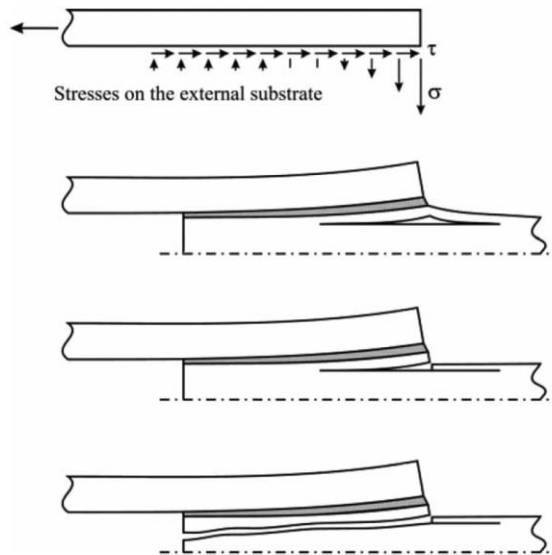


Figure 14 - Delamination of a FRP's adherend [24]

As have been said before, this failure occurs due to peel stresses which affects FRP's poor mechanical strength through thickness. Delamination can be avoided using some techniques that will be described later.

The cohesive failure in the adhesive layer can be identified with the presence of adhesive on both sides of adherend's faces and is a result of a correct surface treatment application. This failure results from shear stresses but a combination of both shear and peel stresses may also cause it. When it occurs during service of an adhesive joint, the responsibility is assigned to the poor design of the joint.

Finally, interface's failure is the worst type of failure, because it is a consequence of a defective manufacturing process including a wrong choice of the surface treatment applied. It is characterized by the absence of adhesive on one of the adherend's surfaces [21, 25].

### 2.3.3. Techniques to reduce the peel stresses in composite materials

Several authors have tried to understand the delamination's phenomenon in order to find solutions. The answer may rely on the way composite materials are bonded. These materials are usually bonded using adhesive joints, because it is a clean bonding without any damage applied in materials bonded, unlike the using of screws for example.

Adams and da Silva [26] studied the influence of an internal taper and adhesive fillet in an adhesive single lap joint, presented in Figure 15.

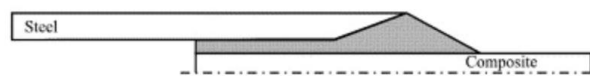


Figure 15 - Internal taper and adhesive fillet [26]

The main objective was not only to reduce the transverse tensile stresses in the composite but also to increase the joint strength at different temperatures. After all experimental tests that were done, the effect of temperature was not investigated but it was shown that this technique is well-succeed and the transverse tensile stresses are reduced as well as delamination avoided, as shown in Figure 16.

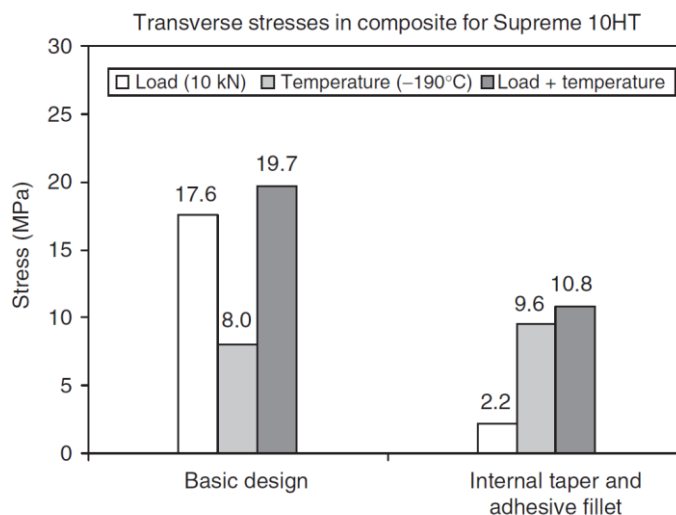


Figure 16 - Reduction of transverse stresses by internal taper and adhesive fillet [26]

Besides working on the adhesive joint, there are other possibilities to explore. One of those possibilities consist in a technique characterized by using carbon nanofibres (CNFs) and carbon fibre z-pins to avoid delamination in CFRPs – Figure 17.

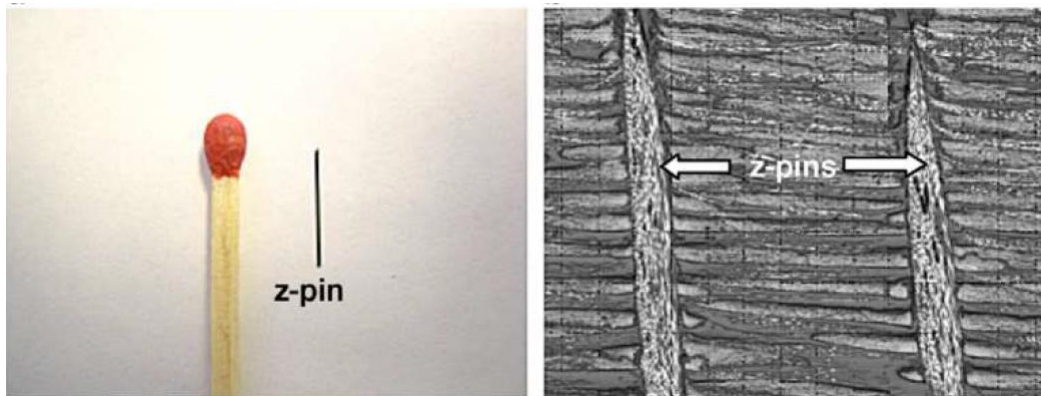


Figure 17 - Z-pins technique [27]

These carbon reinforcements, inserted through thickness, aim to assure that all thin layers of CFRPs are bonded firmly, reducing the risk of delamination. Mouritz et al [28] tested this kind of reinforcement and achieved improved results, presented in Figure 18.

The results show that using both z-pins and CNFs, the composite material needs a higher stress to delaminate, which is a crucial point to several industries as aerospace or automotive.

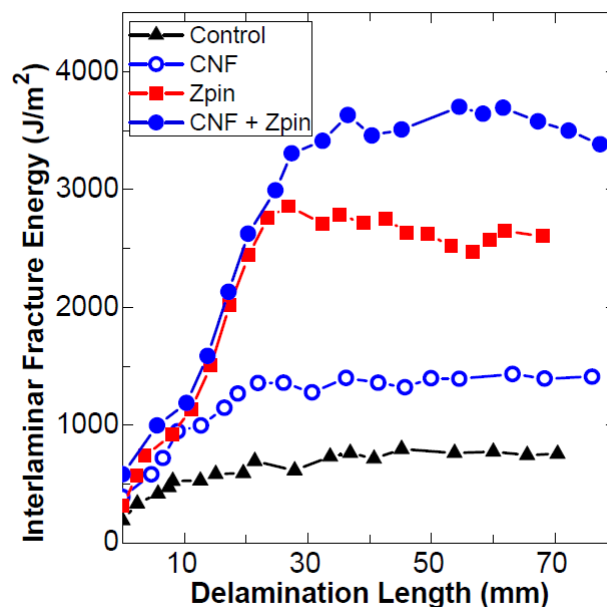


Figure 18 - Crack growth resistance (R-) curves for the unreinforced and through-thickness reinforced laminates containing 0.82 vol% CNFs and/or 0.5 vol% z-pins under quasi-static [28]

A recent technique was developed by Matsuzaki et al [29] that involves using an inter-adherend-fibre joint. This complex term respects to the scheme shown in Figure 19.

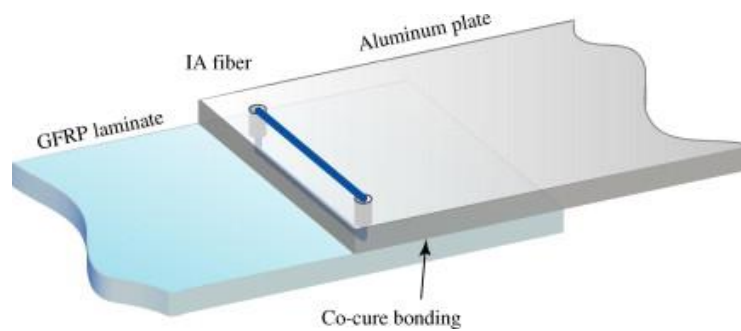


Figure 19 - Inter-adherend-fibre joint [29]

The IA fiber acts as a bridge when a crack occurs, which reduces the driving force of the crack propagation at the crack tip and suppresses or delays the propagation between the adherends [29].

The delamination's issue can be solved with many techniques as have been seen. However, several other options have also been studied due to the difficulties presented by the solutions described above regarding their manufacturing processes. As have been said in chapter 1.1, a FML concept may be used in order to achieve results as good as those accomplished by other techniques, but with significant advantages in terms of production.

#### **2.3.4. Fibre metal laminates**

FML are characterized as hybrid materials constituted by thin sheets of metal and composite material layers, Figure 3. These two different materials are bonded, usually taking advantage of composite's polymer resin cure.

The history of FML have already been enlightened before but it is never too much to refer some important dates in this material progress.

According to Asundi and Choi [30], FMLs were firstly created as a necessity of aerospace industry to find new materials to replace traditional metal components of aircrafts. The main objective was to: *“Develop new aircrafts materials with a better fatigue resistance and preferably a higher specific strength and lower density.”*. Therefore, FML started to be a reality. In 1978, aramid reinforced aluminium laminate, also named ARALL, was introduced at Delft University of Technology. Later, in 1990, emerged an improvement of ARALL in the same place. Instead of aramid fibres, glass fibres with a higher strength were used to create GLARE (glass reinforced).



The evolution of FML has not ended yet. Sinmazçelik et al. [31] made a review about FML's theme. According to these authors, the state of the art about this specific subject can be represented by Figure 16.

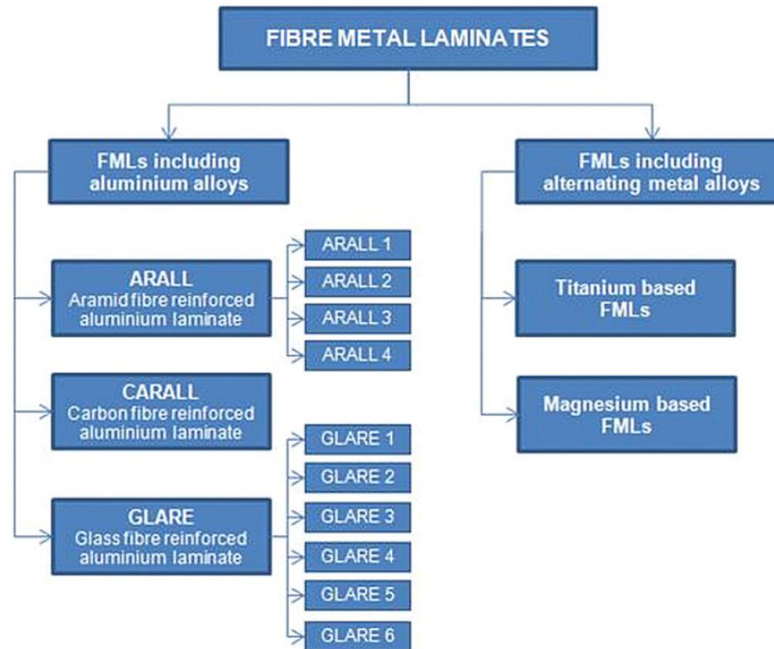


Figure 20 - Classification of FMLs based on metal plies [31]

The key disadvantage of this kind of material is the production cost due to cure's cycle of thermosetting resins used as matrix of composite component. The resin cure delays the whole production chain and decreases productivity.

The applications of FMLs are focused on aerospace requirements. Currently, some structural components that were constituted by aluminium have been replaced by equals made by FML, especially ARALL and GLARE materials. For instance, ARALL are used for wings and cargo doors and GLARE for impact resistant bulk cargo floor.

## **2.4. Strength prediction of adhesively bonded joints**

In order to predict the joint strength of an adhesively bonded joint it is vital to know the stress distribution and to choose an appropriate failure criterion.

There are two main types of failure criteria: the analytical and the numerical ones. The first ones are simpler and offer an approximation of the joint's failure load. However, these solutions obey to some conditions and adhesive's properties and are not suitable for every single case.

On one hand, some of these solutions consider the adhesive's behavior only elastic when submitted to a tensile test, such as the simplest linear analysis [32], Volkersen's analysis [33] or Goland and Reissner analysis [34]. On other hand, there are other solutions more complex that assume the adhesive's behavior as elasto-plastic, such as Hart-Smith analysis [35]. Several authors have tried to develop other analysis considering both elastic and elasto-plastic analysis, such as Chen and Cheng [36], Bigwood and Crocombe [37] or Adams and Mallick [38].

The use of finite element models facilitates the analysis of adherend's plasticity and adhesive's behavior when mathematical formulation is not that simple [39].

### **2.4.1. Numerical solutions**

The analytical analysis to predict the joint's strength is useful to understand the adhesive behavior when submitted to a tensile test. However, this kind of analysis become unachievable in several situations. According to Goglio [40], there are some aspects which turn the numerical solutions more powerful than the analytical ones:

- More complex adhesively bonded joint's geometries;
- Variations of peel and shear stresses through thickness (composite materials) or consideration of other types of stresses;
- Description of local details such as spews of adhesive and adherend's chamfers, which influence significantly the joint strength;
- Consideration of plastic behavior of the adhesive and the adherends.

The Finite Element Method, FEM, can be defined as a "*method to solve a problem in physics or engineering by discretization of the continuum domain in zones of finite size, the finite elements...*" [40]. These elements are joined at their nodes which has a specific number

of degrees of freedom. The FEM allows studying different kind of problems and in terms of adhesive bonding it can be used to study the behavior of several joint's geometries and to calculate all the stress and strain components of any structure obtaining more realistic strength predictions compared with other methods [41]. To succeed using this method it is crucial to know the adhesive and the adherends mechanical properties such as strength and energy parameters. This numerical method is by far the most common one to be used in a context of adhesively bonded joints. The FEM was first used by Adams and Harris [42] to understand the influence of the spew fillet, the joint rotation and the plasticity of the adhesives and the adherends. There are three main approaches using the FEM: continuum mechanics, fracture mechanics and cohesive zone models.

### 1. *Continuum Mechanics*

This approach uses the maximum values of stress, strain or strain energy predicted by FEM and compare them with the experimental data provided about the material's properties. The bond between all joint components, adhesive and both adherends, is considered perfect. This means that any discontinuity or defect within the adhesive joint is not taken into account. Adams and Harris [43] studied the influence of local geometry on the predicted strength and noticed that the stresses were not only dependent on the mesh size used but also on the singular points existent at the corners of the adherends. These authors have demonstrated that the strength of single lap joints with rounded adherends corners was higher than with sharp adherends corners. Nevertheless, this approach has been used with success to predict joint strength [44].

### 2. *Fracture Mechanics*

This criterion differs of the one described above in a crucial aspect: assumes the structure, in this case the single lap joint, as discontinuous. The continuity is no longer a characteristic required and the bond is not perfect. Some defects such as cracks or delamination are points of interest due to stress concentration in those zones which cause failure of the joint. The failure is determined when the material's strength is exceeded for a specific displacement. The main disadvantage of this approach is that it is only used in brittle materials, with no plasticity. However, progresses were made in order to be able to extend fracture mechanics to ductile materials [45, 46].

### 3. Damage Mechanics

To achieve a more reliable prediction to overcome all limitations presented by continuum mechanics and fracture mechanics, a new concept was proposed – damage mechanics. This approach allows the simulation of a gradual damage and fracture following a pre-defined or random crack path until failure is completed [47].

The cohesive zone models are used, combined with FEM, to predict static or fatigue damage in several structures such as adhesively bonded joints. According to Ortiz and Pandolfi [48], the fracture in this cohesive zone is considered to be gradual and controlled by cohesive elements in accordance with an irreversible cohesive traction-separation law responsible for damage's evolution. The cohesive zone elements (CZE) are therefore the cohesive forces between the material layers and are positioned along a specific path and between continuum elements - Figure 21.

There are two main approaches within damage mechanics criteria [49]. The local approach, Figure 21 (a), simulates plastic dissipations of the adhesive bond using solid finite elements, instead of cohesive ones. The last elements are only considered for damage growth simulation [50, 51]. The behavior of adhesive bonds can also be analyzed by the continuum approach, Figure 21 (b). In this case, the whole adhesive layer is composed by cohesive elements [52]. The continuum approach is extensively used in damage mechanics and is dependent on traction-separation laws chosen to govern the comportment of CZEs.

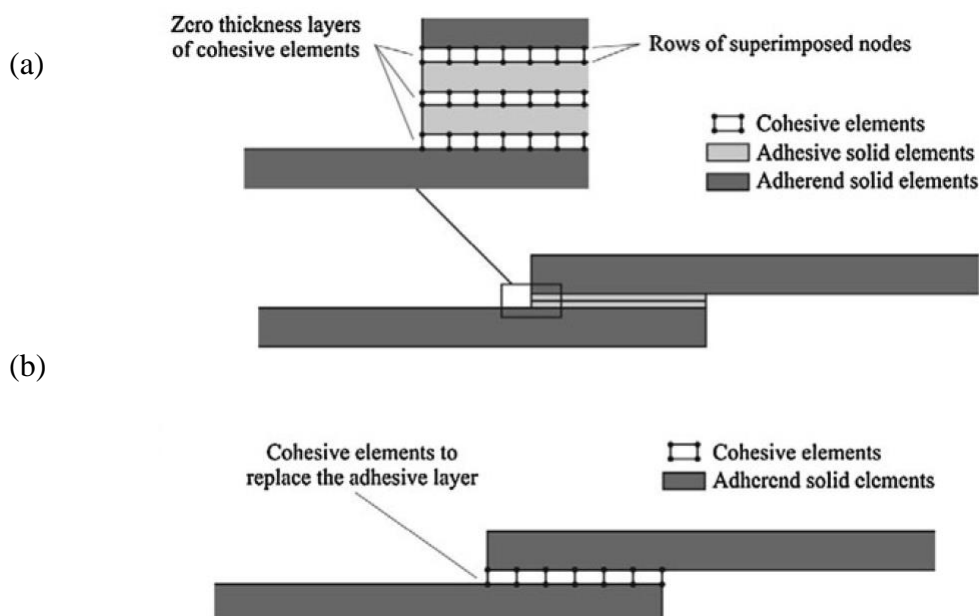


Figure 21 - Cohesive elements to simulate zero thickness failure paths [32]

The damage evolution of CZEs is ruled by traction-separation laws which dictate how the material behaves under mode loads (I or II). Once the material is loaded, the crack will grow and fracture energy ( $G_{I/IIc}$ ) is dissipated. This behavior may be understood while analyzing a traction-separation curve, as shown in Figure 22.

In damage mechanics, there are three key cohesive laws.

- Triangular cohesive law: it is the best law for brittle materials because it does not consider the existence of any ductile behavior. Comparing with other laws, the triangular one is the simplest;
- Trapezoidal cohesive law: it shows a ductile behavior and consists in a better representation of the general material's performance;
- Exponential cohesive law: it is an alternative for the two laws described above. However, when used it shows less accurate results for ductile adhesives than the trapezoidal and for brittle materials than the triangular law [53].

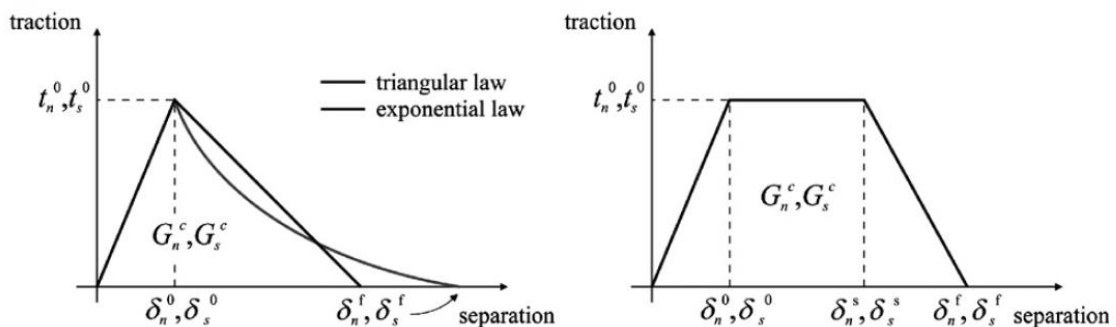


Figure 22 - CZM laws with triangular, exponential and trapezoidal shapes available in Abaqus® [53]

With the analysis of the cohesive laws, it is possible to make some conclusions. The first part of all curves is characterized by a linear elastic behavior of the material. If the exponential or the triangular law are considered, there is a smooth softening after failure. The trapezoidal case is different. There is a plateau before the failure where plastic behavior of the material occurs. After failure, there is a linear softening equal to that existent in the triangular law.

In order to input these laws in a suitable software, it is crucial to know not only how the real material behaves under mode I and mode II in terms of stiffness and strength but also the fracture energy in both modes as well.

### 3. Experimental details

#### 3.1. Adhesive

The adhesive used in this project was a modified epoxy structural adhesive in film form. This adhesive was supplied by 3M Scotch-Weld (Maplewood, Minnesota, USA) [54] and has the commercial reference AF 163-2K. Several aeronautical and aerospace industries use this structural ductile adhesive.

The technical datasheet provided by 3M contains several parameters that were ensured during the experimental procedures. The cure cycle of AF 163-2K is presented in Figure 23 and was respected during whole thesis.

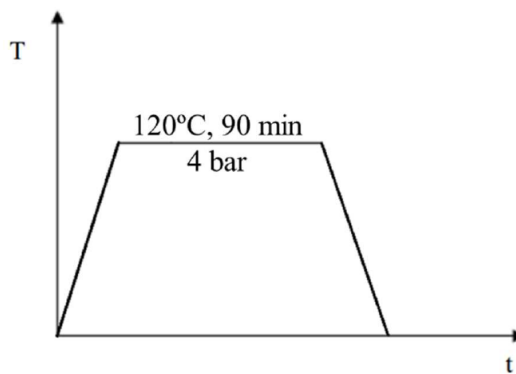


Figure 23 - Cure cycle for the adhesive AF 163-2K [54]

In order to simulate the adhesive behavior during a single lap joint tensile test, it is necessary to understand how the adhesive behaves itself. Therefore, Palmares et al [55] has determined the fracture energy in pure mode I and mode II, performing double cantilever beam (DCB) and end notched flexure (ENF) tests, respectively. Furthermore, the same authors have also performed the Bulk Tensile Test to determine the adhesive's stiffness and tensile strength and the thick adherend Shear test (TAST) to identify its shear strength. The results are shown in Table 2.

The mechanical properties determined allow the definition of the adhesive's cohesive law which will be crucial to implement the numerical models in Abaqus®.

Table 2 – AF 163-2K mechanical properties [55]

Tensile strength [MPa]	$46.93 \pm 0.63$
Young's Modulus [MPa]	$1521.87 \pm 118.29$
Shear strength [MPa]	$46.86 \pm 2.57$
Shear Modulus [MPa]	563.67
$G_{Ic}$ [N/mm]	$4.05 \pm 0.07$
$G_{IIc}$ [N/mm]	$9.77 \pm 0.21$

### 3.2. Adherends

The major objective of this thesis was to study the influence of titanium laminates when placed between CFRP layers in a concept similar to FML, with regard to the composite's peel strength. An improvement of that same property was expected. To achieve this goal, several configurations were studied, experimentally and numerically, to find the optimal solution.

To help define the experimental configurations, some conditions were held constant. The adherend's thickness was 3.2 mm and the proportion of materials was 75% of CFRP and 25% of titanium. The number of configurations chosen was dependent on the stock available for titanium, which is an expensive metal and was only available in 0.8 mm thickness sheets. However, in chapters 7 and 8, several configurations with different material's proportions and thicknesses were numerically analyzed in order to achieve the optimal one.

### 3.2.1. CFRP

The CFRP used was a unidirectional 0° carbon-epoxy composite, HS 160 T700, supplied in a prepreg roll by an Italian company named Composite Materials (Legnano, Italy). For the adherend's preparation, prepreg's sheets of 300 x 300 mm<sup>2</sup> were cut. Each CFRP layer had 0.15 mm of thickness.

The adherends were manufactured using several layers of CFRP that were stacked and, after the introduction of metal laminates, cured in hot plates press machine.

Campilho [56] determined all properties needed to characterize this CFRP. Those properties are presented in Table 3.

Table 3 – Orthotropic components for a unidirectional CFRP ply [56]

$E_x$ [MPa]	$E_y$ [MPa]	$E_z$ [MPa]	$\nu_{zy}$	$\nu_{yz}$	$\nu_{xz}$	$G_{xy}$ [MPa]	$G_{yz}$ [MPa]	$G_{xz}$ [MPa]
109000	8819	8819	0.342	0.342	0.38	4315	4315	3200

### 3.2.2. Titanium alloy

The titanium alloy used to improve the peel strength of CFRP composite was the titanium Ti-6Al-4V alpha-beta (Grade5), annealed [57, 58]. This titanium alloy has been widely used in aerospace's applications such as bolts, seat rails (in airframes) and fan blades (in engines) [59]. Besides, titanium has already been used in fibre metal laminates.

This alloy was supplied in sheets of 300 x 300 mm<sup>2</sup> with a 0.8 mm thickness and was provided by Smiths Metal Centres Ltd (Biggleswade, UK). Only adherends with titanium laminates of 0.8 mm thickness were manufactured. Other thicknesses were tested but only numerically, using Abaqus<sup>®</sup> software.

The mechanical properties of this alloy are presented in Table 4.

Table 4 – Mechanical properties of Ti-6Al-4V alpha-beta, annealed [58]

Young's modulus (GPa)	Yield stress strength (MPa)	Poisson's ratio	Elongation (%)	Coefficient of thermal expansion ( $\mu\text{m}/\text{m}\cdot\text{K}^{-1}$ )
113.8	900	0.342	14	8.6



### 3.3. Specimens configurations

The number of configurations manufactured was mainly dependent on the quantity of titanium available within the adhesive's lab. The only sheets available had 0.8 mm of thickness so, in order to accomplish the conditions of thickness and material proportions and to reduce manufacturing time as much as possible, the configurations chosen are schematically in Figure 24.

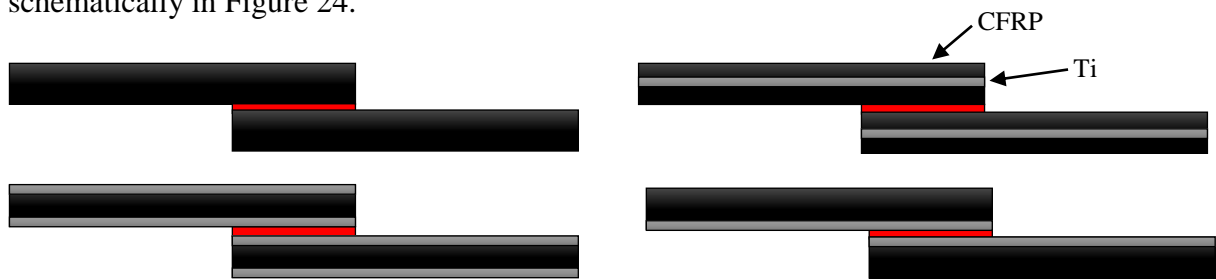


Figure 24 - Selected configurations for FML manufacturing

It was only possible to manufacture four configurations: CFRP standard used to compare with the other three; CFRP with a titanium laminate in the middle; CFRP with a titanium laminate in one extremity; and CFRP with a titanium laminate in both sides. The initial idea was to be able to test other configurations, for instance using two 0.4 mm thickness titanium laminates in the middle or two 0.4 mm thickness titanium laminates in the both sides, as shown in Figure 25.



Figure 25 - Other possible FML configurations

Nevertheless, these thicknesses were not available and ordering would not be possible within the time range of this thesis. Other possibility was to machine part of the 0.8 mm thickness sheet into a smaller thickness, such as 0.4 mm. Rolling a titanium sheet was attempted, but due to its high strength the attempt was not successful.

### 3.4. Specimens manufacture

#### 3.4.1. CFRP plates

The CFRP plates were manufactured from several 300 x 300 mm<sup>2</sup> composite sheets, that were cut from the prepreg roll. Each sheet had a 0.15 mm thickness thus it was needed to stack those sheets so that compact laminates with the intended thickness could be created.

The whole manufacturing process is described below, following five major steps.

- I. The prepreg roll is removed from the freezer and left to warm until it reaches the room temperature (about 26°C);
- II. While the prepreg is defrosting, the mould components which will be used to manufacture the CFRP laminates are cleaned and degreased. This cleaning and degreasing is done using a sandpaper, in a first approach to remove the solid impurities, and then with an organic solvent such as acetone. After this, it is crucial to apply a release agent to the mould components (Figure 26) so that the plate's removal may be easier at the end of the CFRP cure cycle. Two coats of release agent are applied in each side of the components. The product used for this purpose was Loctite® Frekote 770-NC, provided by Henkel (Dusseldorf, Germany);



Figure 26 - Application of releasing agent to the mould components

- III. When the prepreg reaches the room temperature, several 300 x 300 mm<sup>2</sup> sheets are cut to use in different configurations and the roll is stored in the freezer. Then, using a hand lay-up method, several CFRP layers are stacked. To achieve a value close to 3.2 mm of thickness, it is necessary to stack 21 CFRP layers. The stacking process is made carefully because every single layer must have the fibres in the same direction than the previous one. To improve the bond between the CFRP a hot air gun is used (Figure 27), applying heat to make the material more malleable and tacky. Layer by layer, the stacking is made applying pressure with a scraper to release any air bubbles existing between the bonding interface. The protective wax paper coating of every layer is removed and the next layer is applied to continue the process;

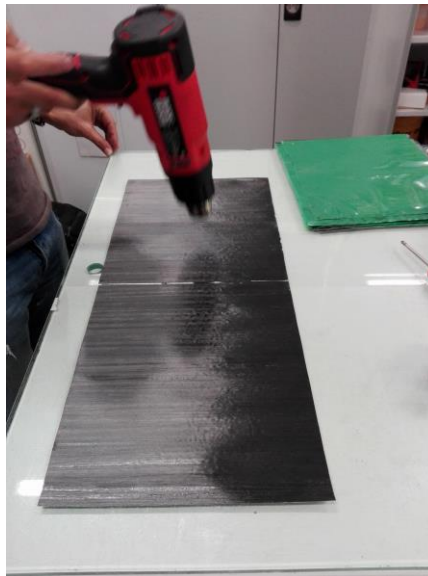


Figure 27 - Pre-heating of the CFRP layers with a hot air gun

- IV. After the stacking process is completed, a CFRP plate with the desired thickness is obtained. In a first approach, the plate is cooled until it reaches room temperature. Afterwards, the plate is placed in the mould and transported to the hot plates press machine (Figure 29) in order to initiate the cure cycle (Figure 28). The cure of the prepreg follows all the recommendations of the supplier including a heating rate of 4°C/min until the temperature of 130°C is achieved. Once the cure cycle is completed and the plate is already at room temperature, it is removed from the press and is ready to be machined;

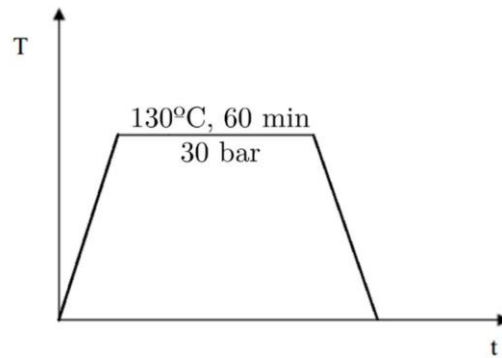


Figure 28 - Cure cycle for CFRP plates



Figure 29 - Hot plates press machine *INTOCO*

- V. At the end of the cure cycle, the plates have 300 x 300 mm<sup>2</sup>. Thus, it is necessary to cut the plates into the desired shape using an appropriate machine with high strength tools due to the mechanical properties of CFRP in the fibre's direction. The machine used was the model DV 25 Batisti Meccanica, made in Italy, with a diamond disc as the cutting tool, as shown in Figure 30.



Figure 30 - Diamond disc cutting from model DV 25 Batisti Meccanica

### ***3.4.2. Surface treatment of the titanium alloy***

Once the standard configuration of only CFRP was manufactured, the manufacturing of other specimens, CFRP-titanium laminates, was carried out. It is for these configurations, where one of the main problems associated to this kind of material appears, which is the lack of bonding between both materials.

In this case, two surface treatments for the titanium alloy were evaluated: as supplied with a light use of a sandpaper and grit-blasting. A third surface treatment, named alkaline peroxide etch [60], was taken into account but unfortunately it was not applied due to the unavailability of the chemical products needed to complete such process. However, this chemical surface treatment will be also described.

#### ***1. As supplied***

As supplied state is not properly a surface treatment. This state respects to the utilization of the material as it is provided by the supplier. No surface treatment was, consequently, applied to the titanium's surface.

#### ***2. Grit-blasting***

Grit-blasting is a mechanical surface treatment that is used to produce a clean macroscopically rough surface and to remove surface contaminants. This mechanical process uses a machine that projects an abrasive material, such as alumina for instance, against the surface, under high pressure [61]. The surface should be maintained at a certain distance, and blasted on both sides, in order to prevent the titanium's bending.

For this project, the grit-blasting was performed using the machine model 705 GM produced by de Laurentiis. Afterwards, the surface was degreased with acetone to remove the last impurities and the titanium laminate was soon placed in the mould to manufacture the specimen to avoid any kind of contamination.

According to Clearfield et al [62], grit-blasted titanium presents a poor durability. Therefore, a chemical surface treatment is more indicated for this kind of material. Though, in some cases where durability is not a crucial condition to be taken into consideration, grit-blasting should offer reasonable results [63]. That is the key motive why grit-blasting was

used instead of a chemical treatment – the main purpose was to improve the bond strength and not the bond durability.

### ***3. Peroxide Alkaline Etch***

The peroxide alkaline etch is a chemical surface treatment currently used in titanium alloys and that provides very good results in terms of bond strength and durability when joined with composite materials. The process follows five major steps [44, 64].

- I. Vapor degreasing and wet-blasting with alumina;
- II. Immersion for 20 minutes at 65-70°C in sodium hydroxide 20 g, hydrogen peroxide (100vol) 22.5 ml, water to 1 liter. The sodium hydroxide is dissolved in water and, when the target temperature is reached, the metallic laminates are added and are only removed when the surface almost appears black (taking about 20 minutes);
- III. Rinsing in hot water for at least 10 min;
- IV. Drying in warm air;
- V. Preferably, primer coating should be applied immediately.

### 3.4.3. Surface treatment influence

Before initiating the manufacture of CFRP-titanium laminates, it was necessary to evaluate the influence of different surface treatments in metal-composite bonding. The two treatments analyzed were, as said above, as supplied and the grit-blasting. The chemical treatment described in the previous section was not evaluated due to the impossibility of accomplishing it.

The test used to evaluate both surface treatments was the traction test in mode I. This test consisted in loading in mode I (tensile stresses) two steel blocks that were bonded to the  $25 \times 25 \text{ mm}^2$  specimen with the configuration CFRP-Ti-CFRP, as shown in Figure 31.



Figure 31 - Bonding between the steel blocks and the specimen CFRP-Ti-CFRP

The steel blocks had a hole with a 5mm diameter through which a steel pin was introduced connecting the sample to the testing machine's grips. A loading scheme is presented in Figure 32.

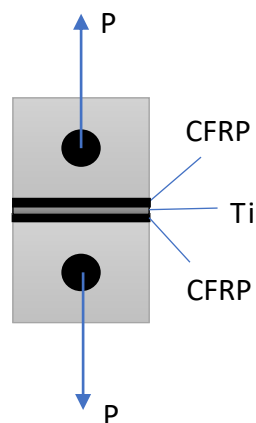


Figure 32 - Loading scheme of traction test in mode I

The test was performed with two different surface treatments and the results were completely dissimilar. When the CFRP was bonded to a titanium sheet without any surface treatment, the average failure load was  $1.69 \pm 1.28$  kN. Nevertheless, when the composite was bonded to a titanium sheet that was grit-blasted the results were extremely better and the average failure load was  $11.40 \pm 1.56$  kN. These results shown in Figure 33 and the typical failure of the sample for each test pictured in Figure 34 a) and b).

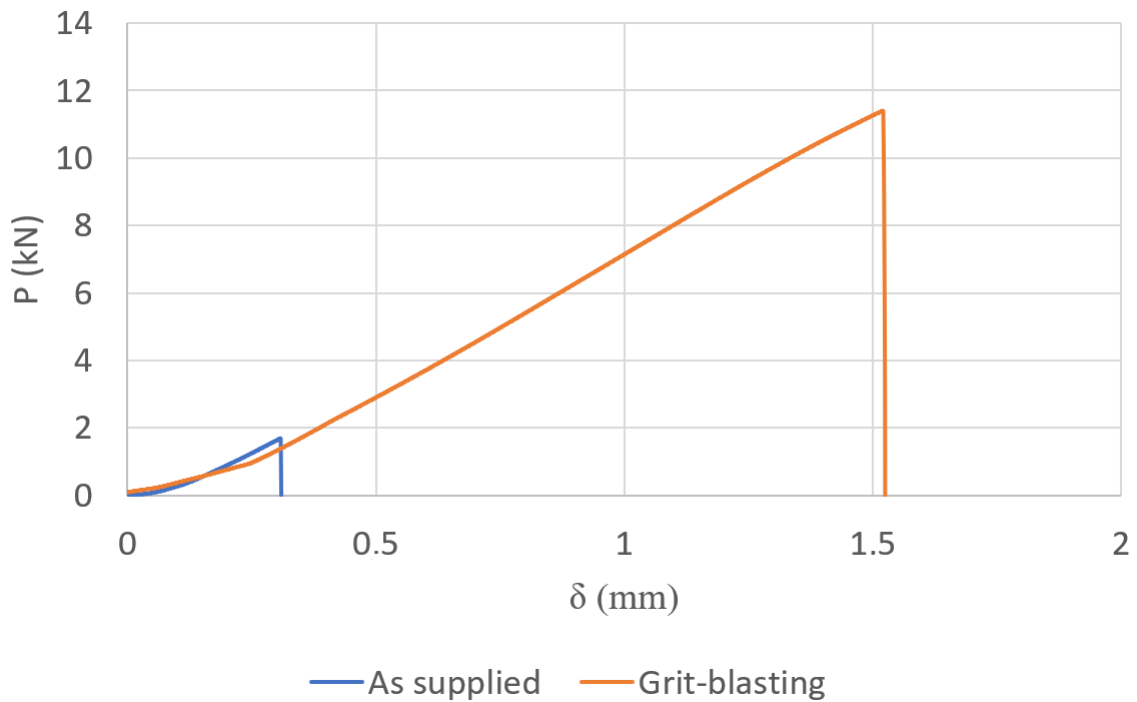


Figure 33 – Most representative curve for Mode I traction test

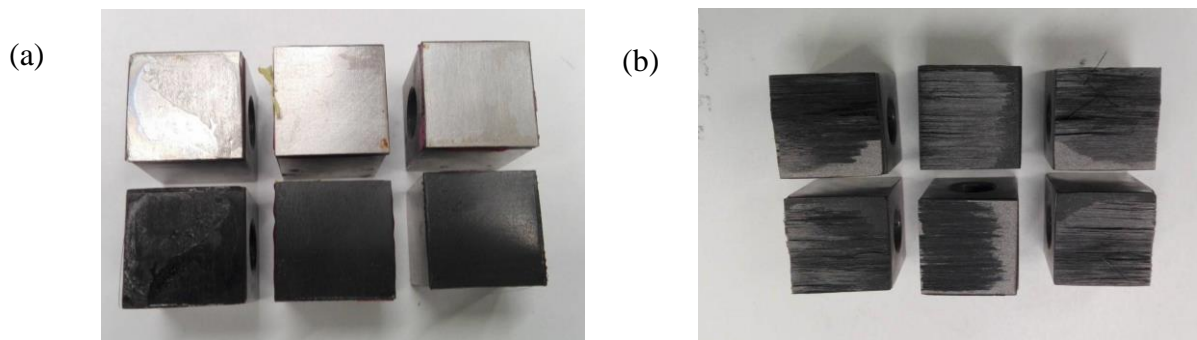


Figure 34 - Typical failure of the samples in mode I traction test: (a) adhesive failure in Ti-CFRP interface; (b) cohesive failure in CFRP (delamination)



The typical failures in the samples tested were different depending on which surface treatment was applied. In the case where titanium was used as supplied, the failure was adhesive in the interface between the titanium sheet and the CFRP plate. This happened due to the poor adhesion between those materials, which led to the conclusion that using the titanium as supplied was not a possibility. When the mechanical surface treatment was applied, the failure was completely dissimilar. The composite suffered delamination near the interface between the CFRP plate and the steel block. These results showed that the adhesion between the CFRP and the treated titanium was stronger than the one between the composite and the steel. Therefore, the grit-blasting was proven to be a surface treatment that offers satisfactory results and it was chosen to be applied to all titanium sheets.

It was expected that, using the peroxide alkaline etch, the results would be even better than those achieved using the grit-blasting. However, the purpose was to reach a reasonable bond strength between the CFRP and the titanium and not to improve the bond durability. Thus, it was considered that the grit-blasting should be the one chosen for this work.

#### 3.4.4. Manufacture of CFRP-Titanium laminates

The manufacture of the CFRP-Titanium laminates followed the same basic principles than the manufacturing of the CFRP plates described in section 3.4.1. The major difference between the two manufacturing processes is the presence of metal laminates that must be interleaved according to their position within the specimen configuration.

All of titanium laminates used had a 0.8 mm thickness, so to achieve a 3.2 mm of total thickness, it was necessary to stack 16 CFRP layers together for the Ti-CFRP configuration and 8 plus other 8 layers for the CFRP-Ti-CFRP configuration.

In order to understand this procedure, a brief description is done following the main steps to manufacture the CFRP-Ti-CFRP configuration.

- I. The first three steps described in section 3.4.1 are followed. However, the number of CFRP layers stacked are not 21 but only 8. At the end there are plates with a 1.2 mm thickness;
- II. The titanium's surface is degreased with acetone, to remove contaminants present;

- III. The chosen surface treatment is applied to the titanium laminate, in this case the grit-blasting treatment. After this mechanical treatment is completed, the surface should be degreased again using acetone until it is completely clean;
- IV. Subsequently, the protective wax paper coating is removed from the last CFRP layer, and the plate is heated using a hot air gun to improve bonding with the metal laminate. The titanium laminate should be applied, as shown in Figure 35.

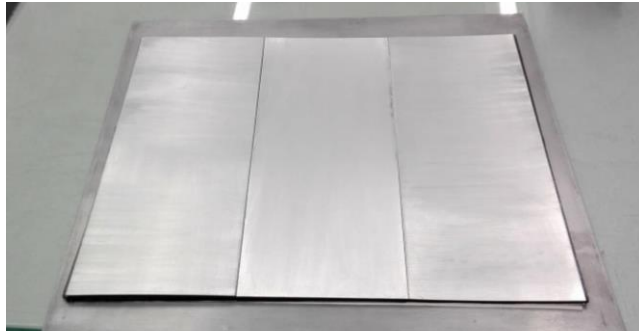


Figure 35 - Stacking of the titanium laminates over the CFRP plate

- V. The remaining CFRP plate are stacked on the top the titanium sheets, with 1.2 mm thickness to complete the specimen configuration;
- VI. Once the configuration is completed, the FML is placed in the hot plate press machine and the CFRP cure cycle is carried out. This step is similar to the one described in point IV for the CFRP plates. The mould is prepared in the same way;
- VII. Using the model DV 25 Batisti Meccanica, the specimen is cut into the desired shape.

For the remaining configuration, Ti-CFRP, the procedure is the same, but the titanium sheet is placed over the 2.4 mm thick CFRP plate (16 layers stacked) and, then transported to the hot plate press for curing.

#### 3.4.5. Manufacture of single lap joints

The manufacture of the adherends was the first stage in the experimental component of this thesis. Subsequently, the single lap joints were manufactured in order to be tested later.

These single lap joints were produced with a specific geometry. However, two overlaps were chosen: 12.5 mm and 50 mm. The width of the SLJs was 25 mm. The geometries are presented in Figure 36.

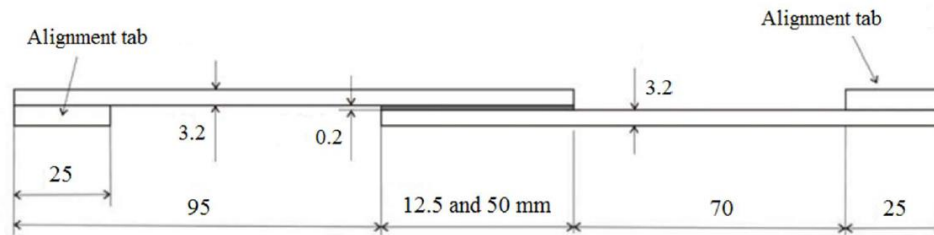


Figure 36 - SLJs geometry (mm) [55]

The manufacture of the complete SLJs followed the procedure described below.

- I. Using the model DV 25 Batisti Meccanica, the adherends and the alignment tabs of the same material are cut and treated superficially using sandpaper (in a 45° direction to avoid damaging the fibres) and degreased with acetone. In the case of Ti-CFRP, the metallic surface is grit-blasted to a better application of the adhesive and then degreased with acetone.
- II. The adhesive in film form, AF 163-2K, is defrosted and cut according to the overlap dimensions, 12.5 and 50 mm, and the dimensions of the alignment tabs, 25 mm. Later, the adhesive is applied in one of the adherends, as shown in Figure 37;

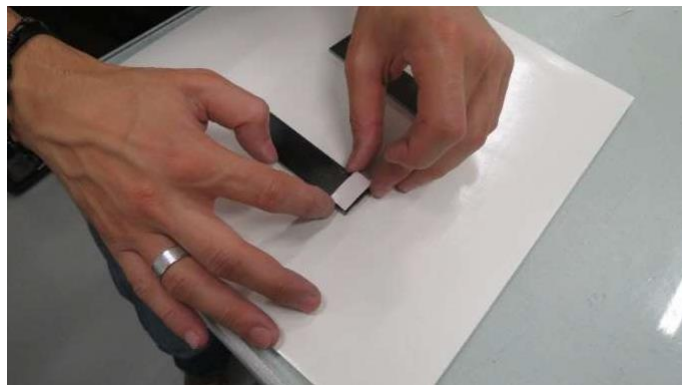


Figure 37 - Adhesive in film placed on one adherend

- III. The SLJ mould is cleaned and degreased to remove any solid contaminant. Two layers of Loctite® Frekote 770-NC, a release agent, are then applied to facilitate the SLJs' removal after the adhesive cure. The CFRP's spacers also receive two layers of the release agent as to be easier to remove;

- IV. The alignment tabs are bonded on the end of each adherend with the same adhesive. Several substrates are positioned in the SLJ mould, followed by the spacers. The two adherends are then bonded carefully so that the single lap joint may be obtained, as shown in Figure 38;



Figure 38 - SLJs bonding

- V. The closed mould is transported to the hot plate press and apply the adhesive's cure cycle is followed;
- VI. Afterwards, when the cure is already done, the excess of adhesive is carefully removed using an iron file so that the fibres are not damaged. Then, a sandpaper is applied to finish the cleaning process;
- VII. To finish the manufacturing process, the free end of each substrate is drilled slowly, where the alignment tabs are placed in order to make a hole for inserting the dowel pins for gripping purposes. This procedure is done carefully and using a lubricant to avoid high temperatures due to the differences in the thermal expansion coefficient that may cause tension concentrations. The impurities are removed by using acetone degreasing one last time.

### **3.4.6. Testing conditions**

The SLJs were tensile tested in a servohydraulic machine, MTS® model 810 with a load cell of 100 kN, presented in Figure 39.

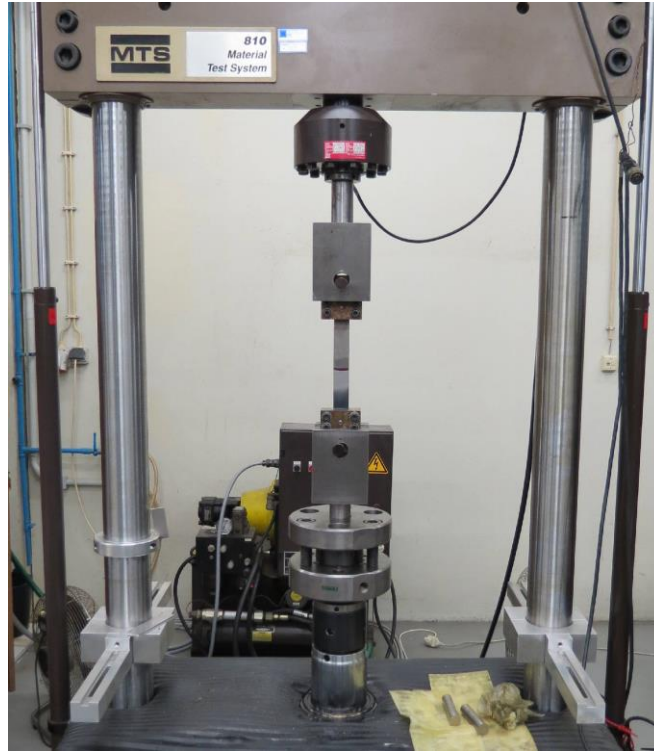


Figure 39 - MTS® model 810

The SLJs were fixed using clamps placed in the free extremities of each specimen. Dowel pins were also used, which trespassed the sample and the holes presented in clamps maintaining the SLJs aligned. The bolts that held the two parts of the clamps were tightened using a torque wrench. The torque applied were dependent on the overlap length of the SLJs. For an overlap of 12.5 mm a torque of 20 N.m was applied. For an overlap of 50 mm, a torque of 40 N.m was used. Three samples of each design were tested.

Additionally, a video system was set up to identify the origin of the delamination in the cases of CFRP-only and CFRP-Ti-CFRP configurations. These videos had the purpose of identifying the beginning of CFRP delamination, to later compare, with the delamination obtained numerically using Abaqus® software. The established system is shown in Figure 40.



Figure 40 - Video system setup to observe the delamination phenomenon

## 4. Experimental Results

### 4.1. CFRP-only SLJs

The CFRP-only SLJs were manufactured to compare with the hybrid configurations. The main objective of this thesis was to find the best FML configuration that offers the optimal improvement related to the peel strength of the composite and also the joint strength of composite adhesive joints. In order to evaluate such influence, a reference value for each overlap length used was needed. Thus, CFRP-only adherends were produced and tensile tested in SLJs.

#### 4.1.1. 12.5 mm overlap length

A typical  $P$ - $\delta$  curve (load versus displacement) of a CFRP-only SLJ with a 12.5 mm overlap tested is shown in Figure 41.

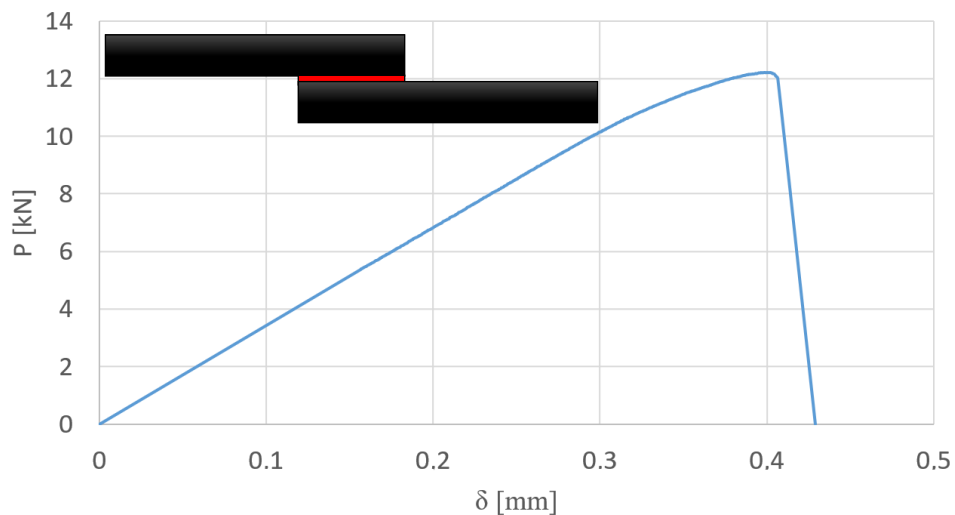


Figure 41 - Load vs displacement typical curve of a CFRP-only SLJ with a 12.5 mm overlap

The type of failure of the tested specimens was cohesive in the adhesive, as shown in Figure 42. The average failure load for CFRP-only SLJs was  $11.76 \pm 0.90$  kN, in terms of 12.5 mm overlap.



Figure 42 - Typical failure surface of 12.5 mm overlap CFRP-only SLJs

#### 4.1.2. 50 mm overlap length

For the SLJs with CFRP-only adherends and a 50 mm overlap, the results were different in terms of failure load and type of failure when compared with those obtained for an overlap of 12.5 mm. A typical  $P$ - $\delta$  curve is shown below in Figure 43.

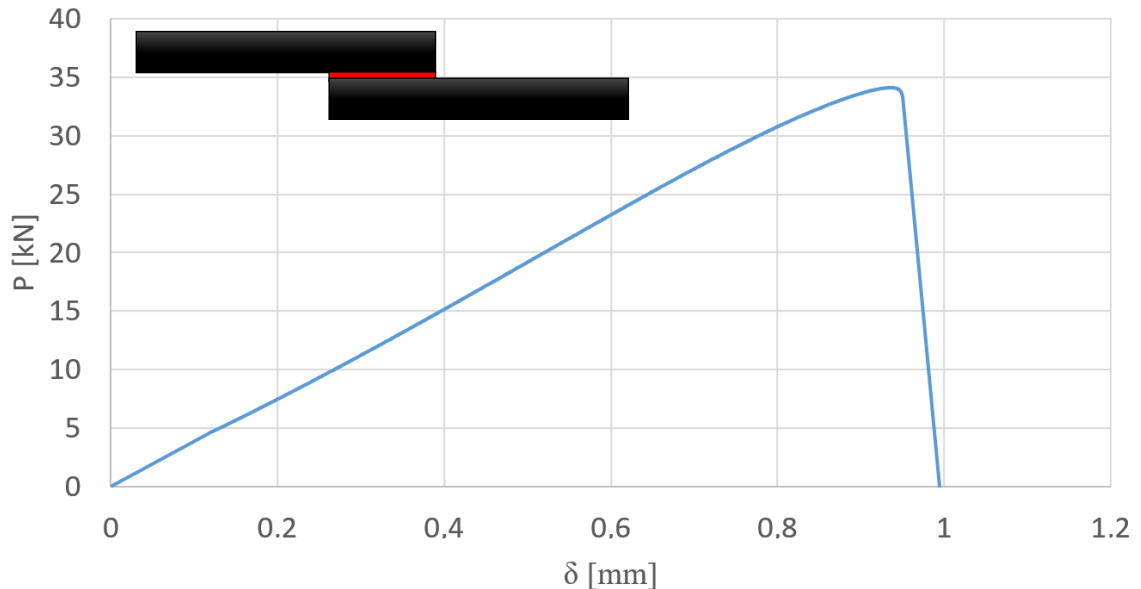


Figure 43 - Load vs displacement typical curve of a CFRP-only SLJ with a 50 mm overlap

The typical failure surface linked to this kind of SLJ was cohesive in the adherend, more specifically, in the CFRP (Figure 44). Therefore, delamination of the composite was clear, which meant that the adhesive did not fulfill its service. It was thus necessary to improve the peel strength of the CFRP-only adherend. Consequently, titanium reinforcement sheets were included between CFRP layers in various configurations, as shown later.



Figure 44 - Typical failure surface of 50 mm overlap CFRP-only SLJs



The average failure load for CFRP-only SLJs was  $33.40 \pm 1.27$  kN for the 50 mm overlap.

## 4.2. CFRP-Ti-CFRP SLJs

The CFRP-Ti-CFRP configuration was the first to be tested as a FML concept in order to improve the peel strength of CFRP composite and also the joint strength of single lap joints.

Both 12.5 mm and 50 mm overlap configurations were studied.

### 4.2.1. 12.5 mm overlap length

The  $P$ - $\delta$  typical curve associated to the three CFRP-Ti-CFRP specimens with a 12.5 mm overlap is presented in Figure 45.

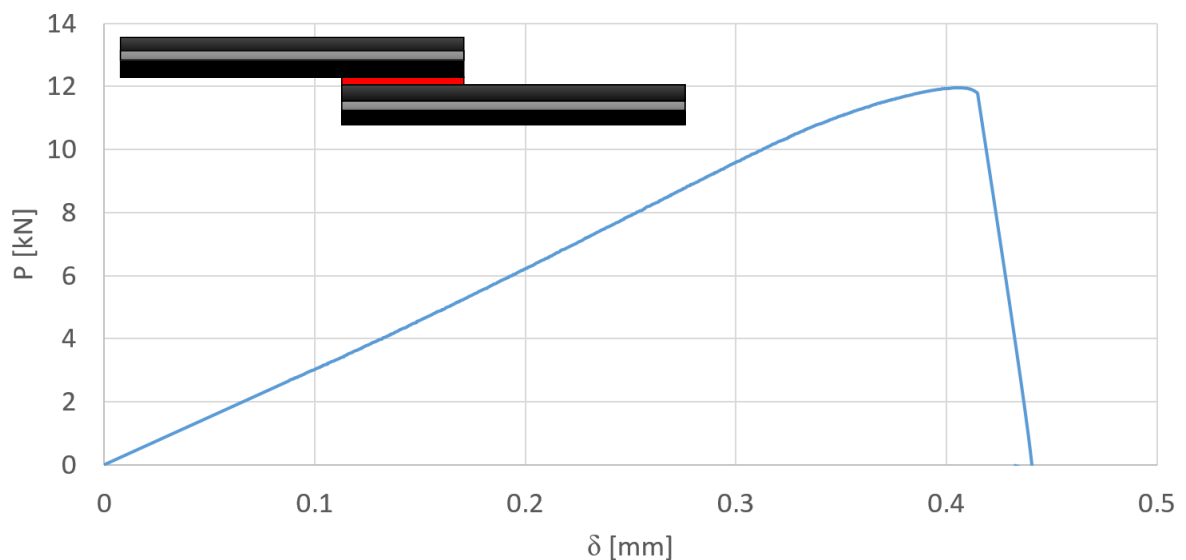


Figure 45 - Load vs Displacement typical curve of a CFRP-Ti-CFRP SLJ with a 12.5 mm overlap

After analyzing the overlap surfaces, it was possible to observe that the failure was cohesive in the adhesive, as had already occurred for CFRP-only SLJ with an overlap of 12.5 mm. Thus, the adhesive reached its maximum resistance. The typical failure surface is shown in Figure 46.

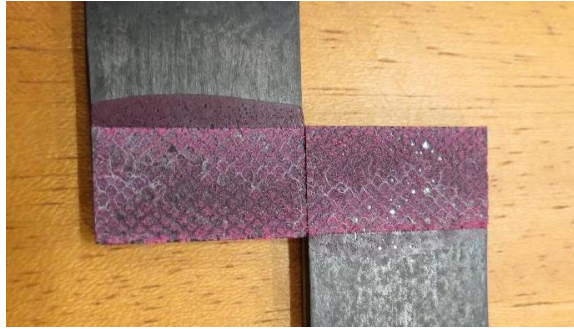


Figure 46 - Typical failure surface of 12.5 mm overlap CFRP-Ti-CFRP SLJs

The average failure load for CFRP-Ti-CFRP SLJs with a 12.5 mm overlap was  $11.94 \pm 0.41$  kN.

#### **4.2.2. 50 mm overlap length**

For the SLJs with a 50 mm overlap, it was expected the joints would reach higher levels for failure load than the ones obtained using CFRP-only substrates. In such case, the use of titanium laminates would be considered a success as a reinforcement. The load as a function of the displacement is presented as a typical curve in Figure 47.

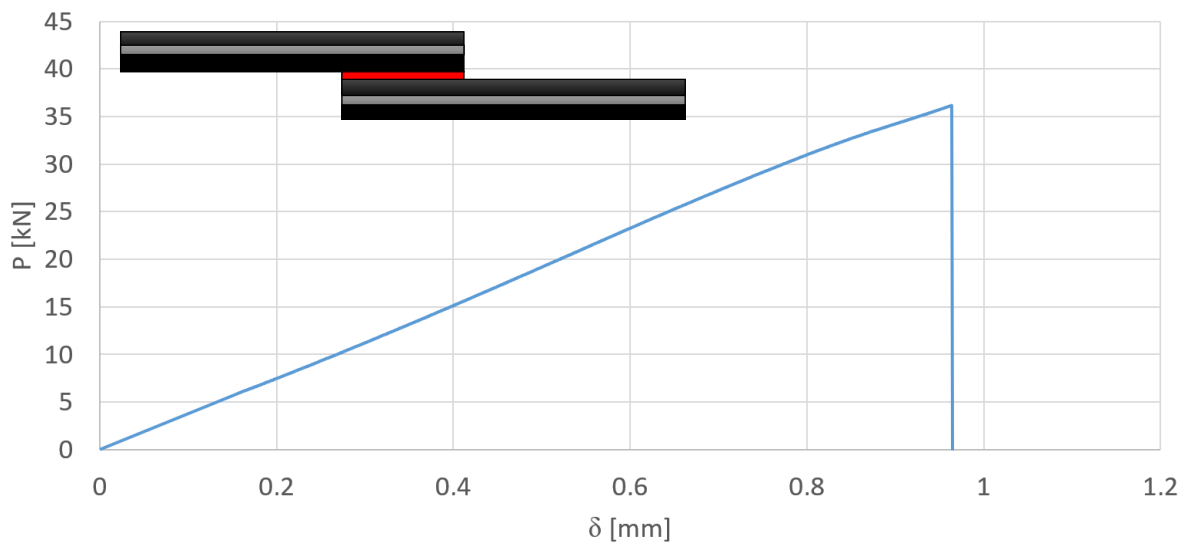


Figure 47 - Load vs displacement typical curve of a CFRP-Ti-CFRP SLJ with a 50 mm overlap

The failure surface for this configuration was the same as observed for CFRP-only SLJs with a 50 mm overlap – composite delamination (Figure 48). However, the average failure load was higher than the one achieved for CFRP-only adherends, a consequence of the improvement of CFRP's peel strength by the introduction of a 0.8 mm thickness titanium laminate.



Figure 48 - Typical failure surface of 50 mm overlap CFRP-Ti-CFRP SLJs

The average failure load for CFRP-Ti-CFRP SLJs was  $33.92 \pm 2.27$  kN, for the 50 mm overlap situation.

### **4.3. Ti-CFRP SLJs**

The second configuration tested, was Ti-CFRP. It was expected that, because the adhesive would bond the two titanium laminates directly, the results obtained for the 50 mm overlap would be better than those achieved with the other configurations.

#### **4.3.1. 12.5 mm overlap length**

The  $P-\delta$  typical curve of a Ti-CFRP joint with a 12.5 mm overlap tested is presented in Figure 49.

After evaluating the overlap surfaces, it was possible to witness that the failure was cohesive in the adhesive again. The typical failure surface is shown in Figure 50.

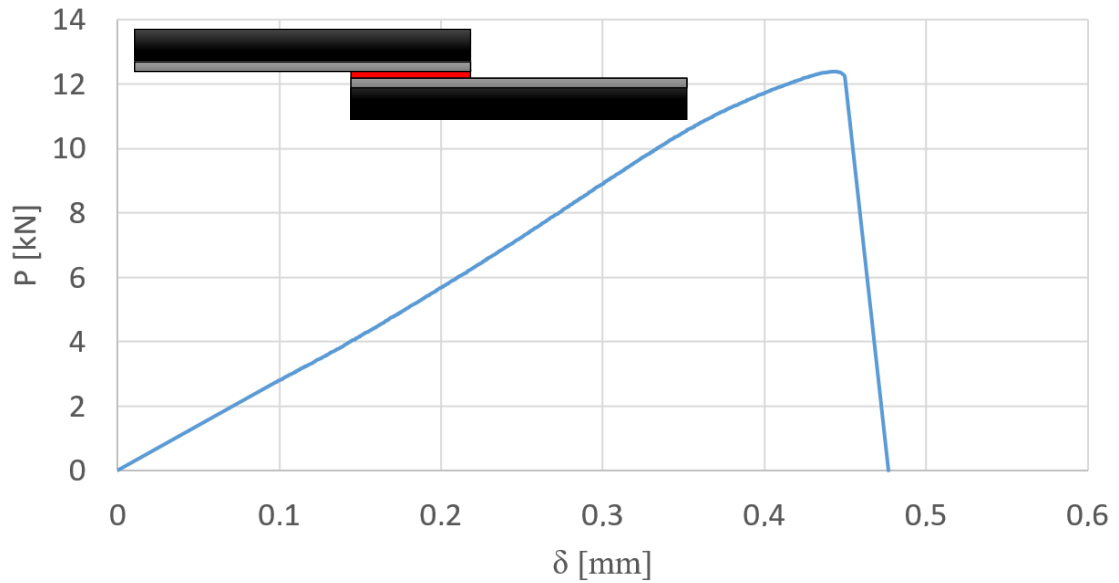


Figure 49 - Load vs Displacement typical curve of a Ti-CFRP SLJ with a 12.5 mm overlap



Figure 50 - Typical failure surface of 12.5 mm overlap Ti-CFRP SLJs

The average failure load for Ti-CFRP SLJs was  $12.82 \pm 0.22$  kN, for the 12.5 mm overlap.

#### **4.3.2. 50 mm overlap length**

It was expected that, due to metal-metal adhesive bonding, the failure surface could be different than the ones accomplished with the configurations CFRP-only and CFRP-Ti-CFRP (50 mm overlaps), thus the failure was expected to be cohesive within the adhesive, which did not occur.

The P- $\delta$  typical curve is shown in Figure 51.

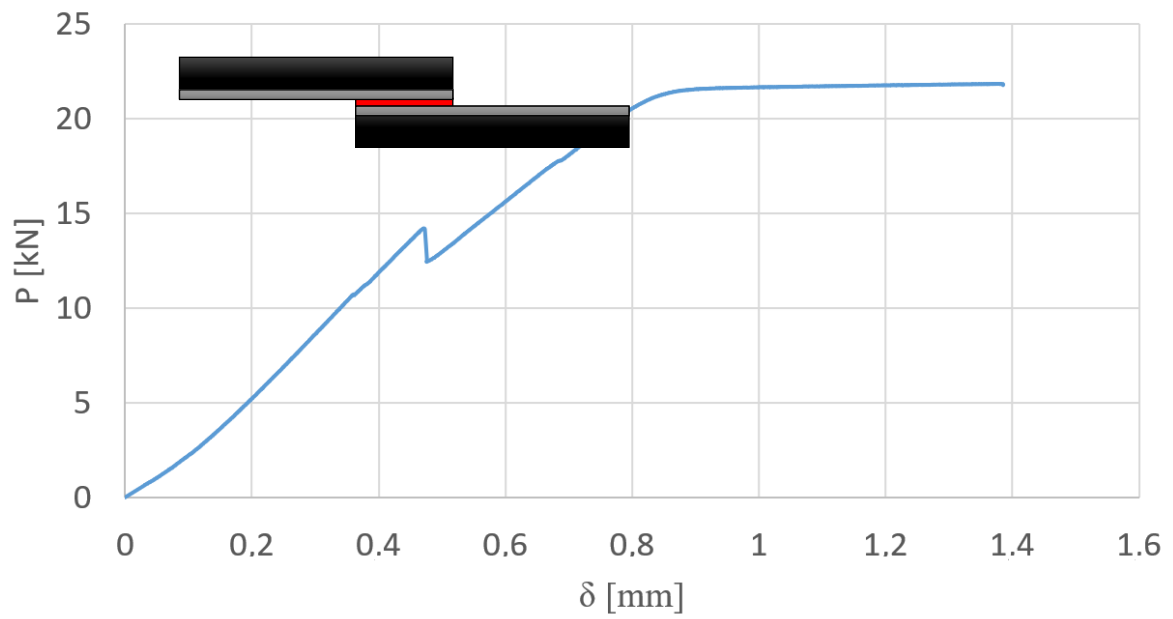


Figure 51 - Load vs displacement typical curve of a Ti-CFRP SLJ with a 50 mm overlap

The type of failure is presented in Figure 52. It was an adhesive failure at the interface Ti-CFRP.

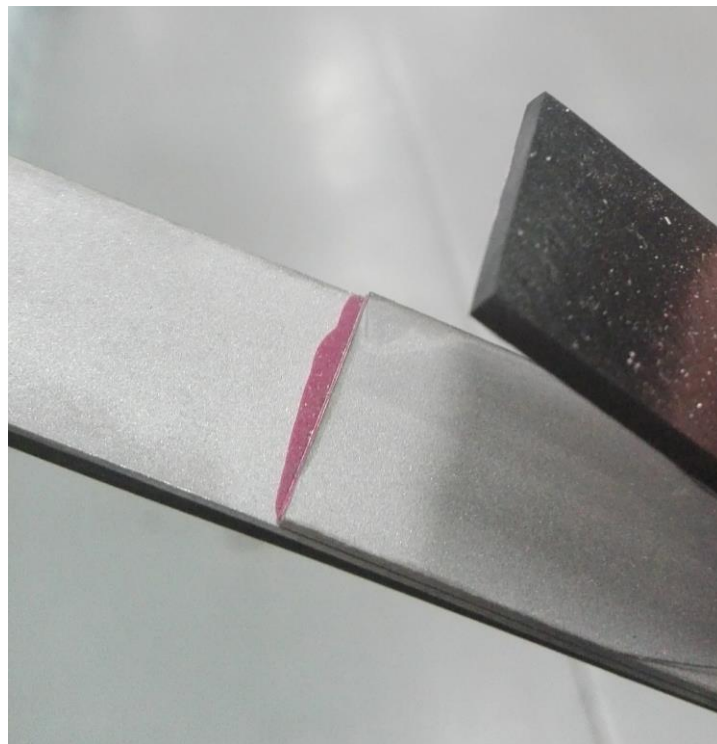


Figure 52 - Failure surface of a 50 mm overlap Ti-CFRP SLJ

The average failure load for 50 mm overlap Ti-CFRP SLJs was  $22.07 \pm 0.38$  kN.

#### 4.4. Ti-CFRP-Ti SLJs

In order to achieve better results than the ones given by the 50 mm overlap Ti-CFRP SLJs, some new SLJs with the configuration Ti-CFRP-Ti were manufactured, which were expected to offer the best results in terms of failure load and surface failure type for this overlap. Due to material limitations respecting the titanium laminates, only two joints were produced with a titanium laminate with 0.8 mm of thickness in both extremities of the adherends. The global adherend thickness was maintained in 3.2 mm, so the proportion of materials was changed from 25% to 50% of metal laminates.

The two SLJs with this configuration were tested in the same conditions than all others and the typical  $P$ - $\delta$  curve is shown in Figure 53.

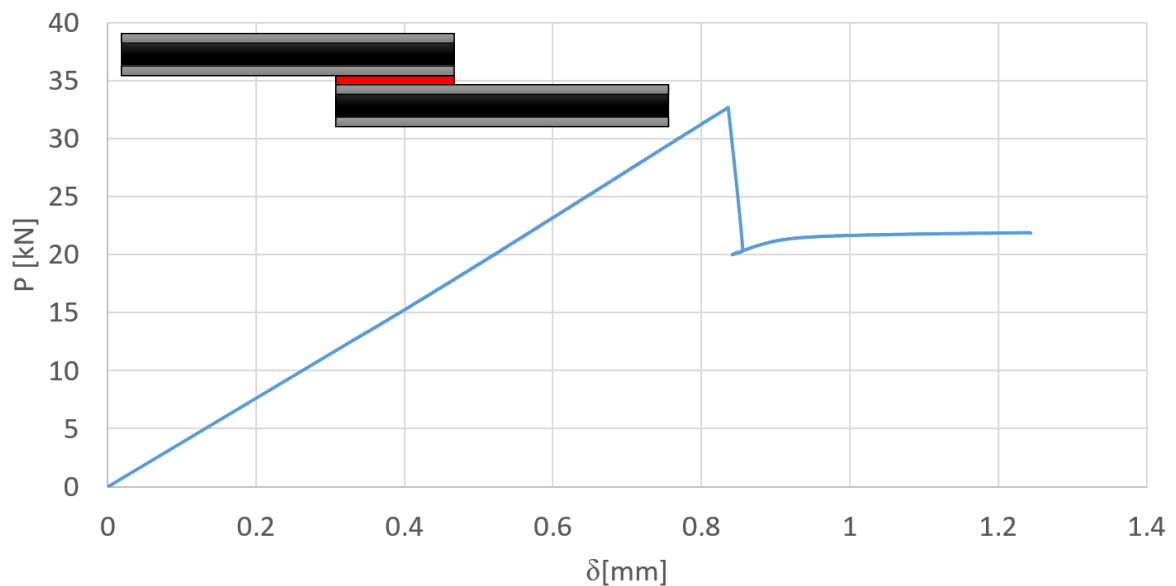


Figure 53 - Load vs displacement typical curve of a Ti-CFRP-Ti SLJ with a 50 mm overlap

It is possible, with the analysis of Figure 53, to witness that the results exhibited a behavior similar to the one exposed by the joints with the configuration T-CFRP. However, the reached failure load was higher than the one presented in Figure 51. The failure surface is shown in Figure 54 and it is also possible to watch some resemblances between both Ti-CFRP and Ti-CFRP-Ti surface failures. The failure surface is a combination of CFRP delamination and adhesive failure in the Ti-CFRP interface, with the second type being more obvious.

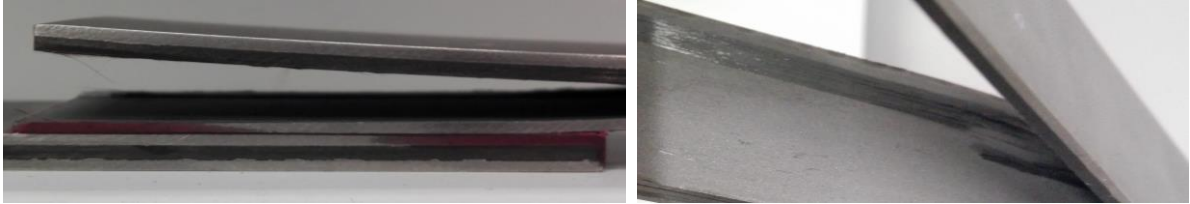


Figure 54 - Failure surface of a 50 mm overlap Ti-CFRP-Ti SLJ




The average failure load for 50 mm overlap Ti-CFRP-Ti SLJs was  $32.27 \pm 0.57$  kN.

#### 4.5. Comparison of SLJs' results

In order to better understand the real influence of a titanium laminate in the peel strength of a composite adherend and also in the joint's shear strength, both are presented in two different tables: one for all 12.5 mm overlap SLJs' configurations and another related to the 50 mm overlap SLJs' configurations.

##### 4.5.1. 12.5 mm overlap SLJs

Table 5 – Failure load and type of failure for joints with a 12.5 mm overlap

Configuration	Average failure load [kN]	Shear joint strength [MPa]	Failure type
	11.76 ± 0.90	37.63 ± 1.50	Cohesive in the adhesive
	11.94 ± 0.41	38.21 ± 1.22	Cohesive in the adhesive
	12.82 ± 0.71	41.02 ± 0.64	Cohesive in the adhesive





For all the configurations with an overlap of 12.5 mm, it may be considered that the results are what were expected. In this case, it was predicted that the failure surface would be cohesive within the adhesive, which happened for all cases. Nonetheless, some conclusions about the influence of the metal sheet used as a reinforcement of CFRP plate could be drawn. Firstly, the configurations with a titanium laminate presented a higher average failure load than the reference configuration (CFRP-only). Secondly, the joint strength was also improved as is shown in Table 5. It is clear, by the comparison between the CFRP-Ti-CFRP and the Ti-CFRP configurations, that the adhesive prefers a metallic bonding than a composite one, evident by the fact that the experimental failure was slightly higher for the Ti-CFRP configuration.

Due to material limitations, regarding the titanium laminates, only three specimens could be produced. However, the results for this overlap type were extremely satisfactory and were similar to the ones obtained numerically.



4.5.2. 50 mm overlap SLJs

Table 6 - Failure load and type of failure for joints with a 50 mm overlap

Configuration	Average failure load [kN]	Shear joint strength [MPa]	Failure type
	$33.40 \pm 1.27$	$26.42 \pm 1.47$	Delamination
	$33.92 \pm 2.27$	$26.78 \pm 1.38$	Delamination
	$22.07 \pm 0.38$	$17.66 \pm 0.87$	Adhesive in the interface Ti-CFRP
	$32.27 \pm 0.57$	$25.82 \pm 0.92$	Adhesive in the interface Ti-CFRP

Regarding to the 50 mm overlap, the results achieved were in line with those expected for the reference configuration and the CFRP-Ti-CFRP one. The failure surface exposed by both configurations was cohesive within the adherend (delamination). However, the peel strength of CFRP-Ti-CFRP substrate was slightly higher than the one of CFRP adherend. This could be witnessed by a detailed analysis of the surface failure of both configurations SLJs. The delamination was less obvious within the CFRP-Ti-CFRP adherends. It may also be explained by the average failure load and the shear joint strength presented in Table 6. These values were higher for CFRP-Ti-CFRP configuration, suggesting that the titanium laminate improved the global joint. The increase in these parameters were more noteworthy for this overlap than for 12.5 mm. For this overlap, two additional conclusions may be drawn. Primarily, the adhesive did not fulfill its service because the shear joint strength was lower than for the overlap of 12.5 mm, explained by the delamination occurred. Furthermore, if another surface treatment had been applied, for instance the peroxide alkaline etch, the average failure load could be higher due to a stronger metal-composite bonding and, consequently, the shear joint strength could also be higher.

Concerning the 50 mm overlap Ti-CFRP and Ti-CFRP-Ti configurations, the results were different than those expected. It was expected that the average failure load would be higher than the one for the CFRP-Ti-CFRP configuration with a 50 mm overlap, which did not happen. Instead, the average failure load was much lower than the others presented in Table 6 for the Ti-CFRP configuration and also inferior for the Ti-CFRP-Ti one. The failure

surface was not as anticipated, as it was not cohesive within the adhesive but adhesive in the metal-composite interface. The explanation for these results may be found in experimental conditions and manufacturing decisions. On one hand, if a chemical surface treatment had been applied, the bonding between Ti-CFRP could be stronger for both configurations, as was already mentioned. On the other hand, the thermal stresses that occurred during the CFRP's cure cycle caused some bending to the substrate, which may be the main reason for these results. Furthermore, when the SLJs were produced and the adhesive cured, additional stresses were added.

Analyzing and comparing both adherends, it is perceptible that using titanium laminates in both sides brought improved results in terms of failure load, almost reaching the value obtained by the CFRP-Ti-CFRP configuration. Nonetheless, the failure surface revealed insufficient adhesion between the composite and the metal as well. The higher failure load could be explained by the reduction of thermal stresses during the CFRP cure cycle, due to a neutralization of those stresses when using a titanium laminate in both extremities.

After evaluating all the results, it was evident that a chemical surface treatment could be enough to obtain better results, regarding the Ti-CFRP-Ti configuration. Furthermore, other adherends combinations might lead to better results as well, but as has already been mentioned the limitations in terms of titanium laminates forced the manufacturing of a restrict number of joints and, therefore, only those described above were produced.

Although it was predictable that the failure mode would be cohesive in the adhesive for the Ti-CFRP-Ti design, the failure mode obtained experimentally was quite interesting in terms of safety conditions that must be provided by an aircraft to its passengers. The progressive failure witnessed for this configuration in the Ti-CFRP interface allows the joint to gradually fail instead of a sudden failure. Firstly, the CFRP starts to unstick from the metallic laminates. Then, the titanium bonded by the adhesive initiates its deformation until the adhesive completes its service. Therefore, there is no abrupt failure of the joint.

A numerical procedure was defined in order to create a model that could characterize the different tensile tests made experimentally and to understand if there was any configuration that, in perfect manufacturing conditions, could lead to better results than all those obtained in practice. This numerical analysis is fully described in chapter 5.

## 5. Numerical Analysis

This kind of simulation allows studying a material under several conditions and understanding how it behaves and fails without resorting to destructive tests such as the tensile tests made. Furthermore, this software may be also used to model a structure and evaluate it before producing a prototype by expensive manufacturing processes.

### 5.1. Model description

In order to simulate a tensile test of a single lap joint, a 2D planar deformable shell model was developed using Abaqus®. The final objective was to numerically confirm all the results obtained experimentally (both the failure load and failure type).

After designing the single lap joint according to the dimensions presented in Figure 36 the mechanical properties of the material that composed each SLJ section were introduced. The adhesive was evaluated using a traction-separation law, to simulate the damage evolution of the adhesive and the results are presented in section 5.2. Besides, the CFRP also had to be sectioned in order to include a cohesive zone to replicate the delamination that might occur. The cohesive layer was 0.02 mm thick and was placed 0.15 mm from the adhesive, which is equal to one single CFRP prepreg layer, as shown in Figure 55. When a titanium laminate was used on the extremity, the cohesive zone related to the CFRP was placed 0.15 mm from the titanium face in contact with the composite.

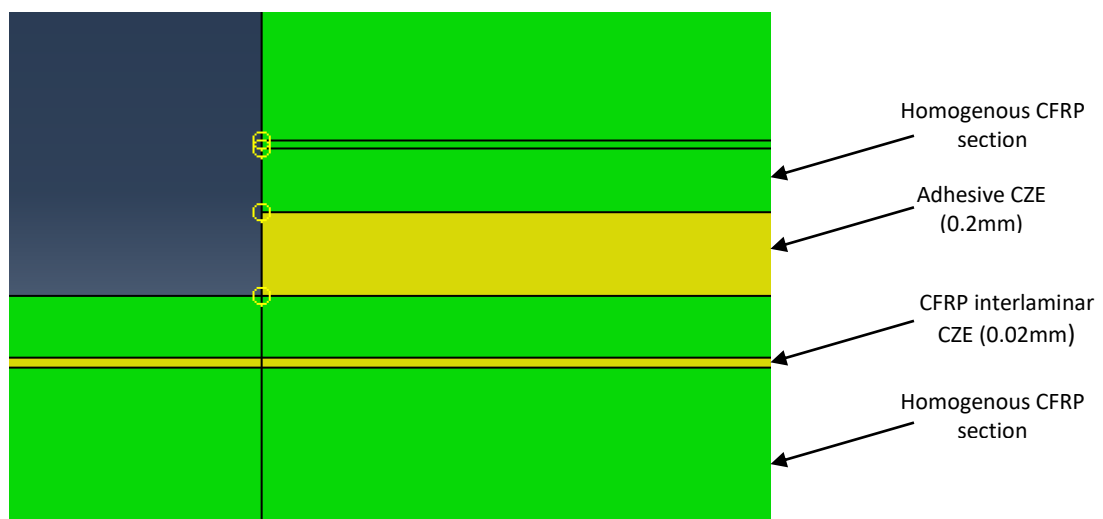


Figure 55 - Distribution of CZE layers throughout the SLJ

The cohesive parameters were defined within the properties of each material. For the adhesive, the parameters used have been already presented in Table 2. Concerning the CFRP, the cohesive parameters chosen to represent the interlaminar failure are presented in Table 7.

Table 7 – Cohesive parameters for CFRP interlaminar failure [55]

	Mode I	Mode II
$\sigma_R$ [MPa]	32	30
$G_c$ [N/mm]	0.66	1.13

The following step to create a SLJ model capable of simulating a tensile test was to assemble all different components that constitute the joint. Then, two different steps were established: one to simulate the tensile test itself and another intermediate to represent the cure cycle of CFRP that every single adherend suffered before SLJs' manufacture.

The boundary conditions were crucial to correctly simulate both steps. For the first one, the physical boundary conditions are shown in Figure 56. At the end of the left extremity, displacement and rotation restrictions were imposed to fix the joint in every direction (vertical and horizontal) simulating the gripping system job. At the opposite extremity, the joint was also fixed in the vertical direction and a constant displacement representing the tensile test itself was applied horizontally.

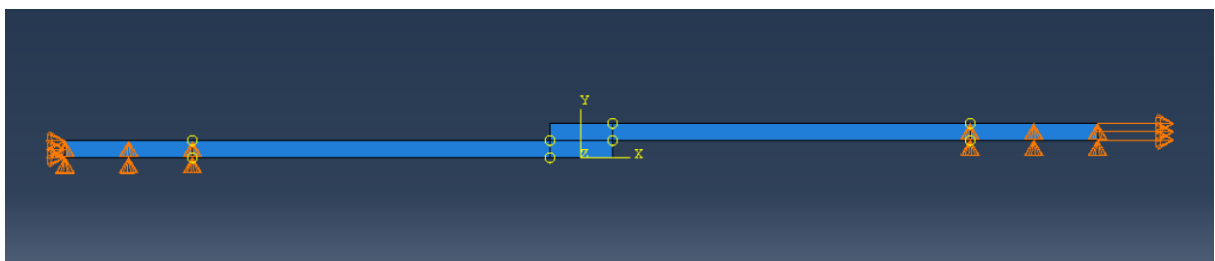


Figure 56 - Schematic view of the physical boundary conditions in Abaqus®

The thermal boundary condition was conceived predefining a thermal field that represented the cure cycle of CFRP, as shown in Figure 57.

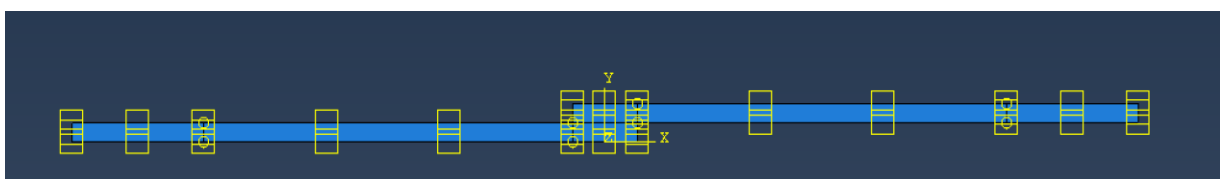


Figure 57 - Schematic view of the thermal predefined field

One of the major problems regarding this kind of adherend configuration, is the thermal stresses due to the CFRP cure cycle, which was witnessed experimentally when the configuration Ti-CFRP was used, as presented in Figure 58 a). Nevertheless, a numerical model was performed just to simulate the thermal effect evident in all SLJ models and to compare with the results achieved experimentally. Every stage was developed in the same way as described above, only changing the part's geometric design. The result may be observed in Figure 58 b).

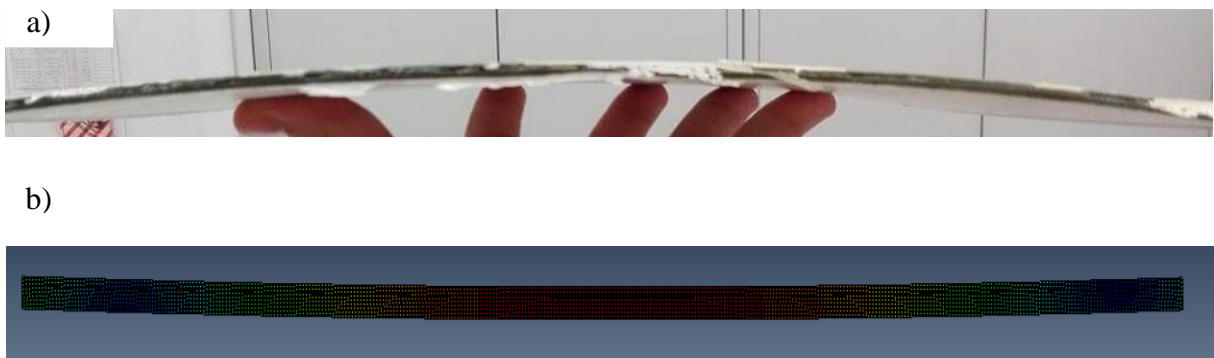


Figure 58 - Ti-CFRP adherend's bending due to thermal stresses: a) Experimentally; b) Numerically

These results were also compared with the ones reached for the Al-CFRP adherend by Palmares [55]. The titanium CTE is  $8.6 \mu\text{m}/\text{m}\cdot\text{K}^{-1}$  which is almost three times less than the one verified for the aluminium alloy ( $23.22\mu\text{m}/\text{m}\cdot\text{K}^{-1}$ ). However, the bending occurred for both configurations, even being much lower for the Ti-CFRP adherend, as shown in Figure 59. For the Al-CFRP adherend the displacement was 2.26 mm and for the Ti-CFRP one was 0.73 mm. The CTE for CFRP was considered  $0 \mu\text{m}/\text{m}\cdot\text{K}^{-1}$ . Besides the lower CTE, titanium is more resistant to corrosion than the aluminium which makes a titanium laminate an interesting composite reinforcement.

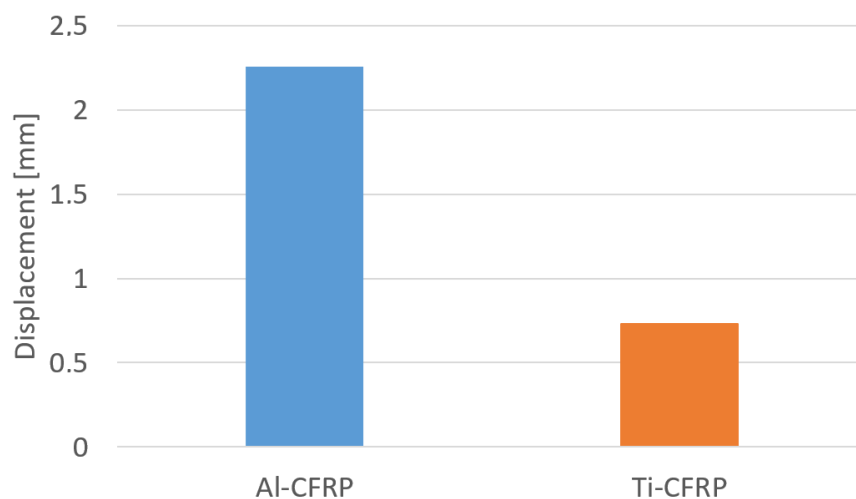


Figure 59 - Vertical displacement suffered by both adherends

The mesh was refined until the 0.2 mm that corresponded to the adhesive layer thickness, producing a constant square mesh with all the elements being  $0.2 \times 0.2 \text{ mm}^2$ , as presented in Figure 60.

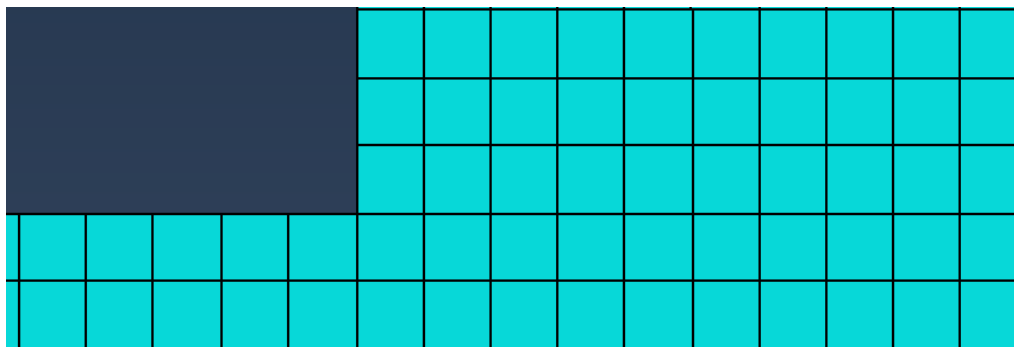


Figure 60 - SLJ square mesh with 0.2 mm refinement

Regarding the elements type, two different kind of elements were used to represent the continuous and the cohesive elements:

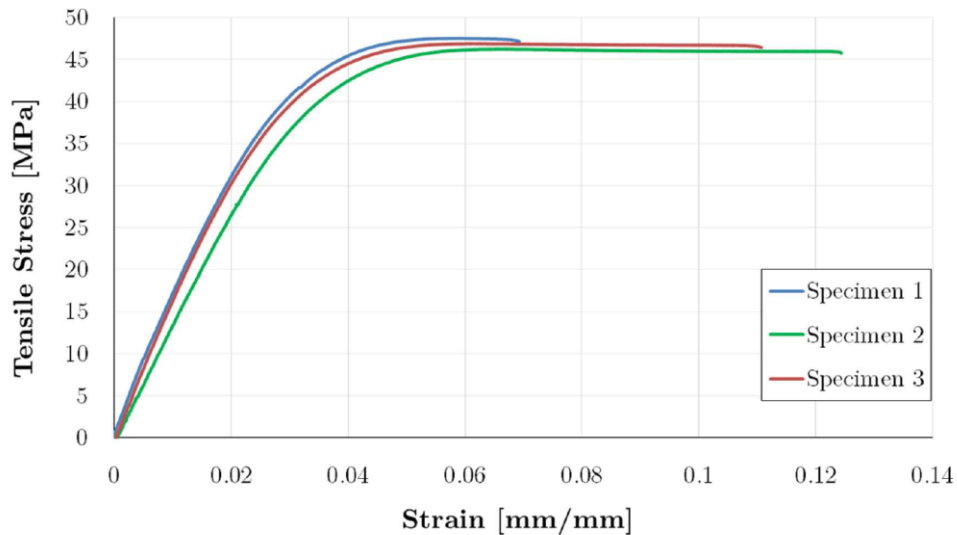
- 8-node biquadratic plane stress quadrilateral, reduced integration elements;
- 4-node two-dimensional cohesive elements.

## 5.2. Triangular cohesive law vs Trapezoidal cohesive law

The traction-separation law is an important component of a numerical model. It will be responsible for the damage evolution through all cohesive zone elements, in this case in both CFRP and adhesive. So, it is crucial to evaluate which law will better simulate both cases.

For the CFRP cohesive elements, a triangular law, using the cohesive parameters presented in Table 7, was used. This cohesive law is widely used to simulate the damage of brittle materials; thus, it was chosen for the composite as it presents a stiff behavior.

On the other hand, the AF 163-2K is an adhesive in film extensively used in aerospace industry due to its mechanical properties. The  $P-\delta$  curves (Figure 61) obtained by Palmares [55], show that the adhesive is ductile, due to its failure strain of approximately 10%.

Figure 61 – AF 163-2K P- $\delta$  curves [55]

Two different numerical models were created in Abaqus<sup>®</sup> using the data provided by Table 2: one with a triangular cohesive law, and another with a trapezoidal law. Then, from the experimental results obtained with DCB, ENF [55] and tensile tests made using hard steel samples with the adhesive in study, it was possible, comparing with the results from both numerical models, to conclude which cohesive law was ideal for this adhesive.

#### ✓ *DCB tests*

The DCB test simulation model was accomplished in the same way than the SLJ tensile test one. However, the specimen design and the boundary conditions were completely different, as shown Figure 62.



Figure 62 - DCB test specimen's model

After the model's creation, implementing both laws, it was possible to compare the experimental results with those achieved numerically. This comparison is presented in Figure 63.

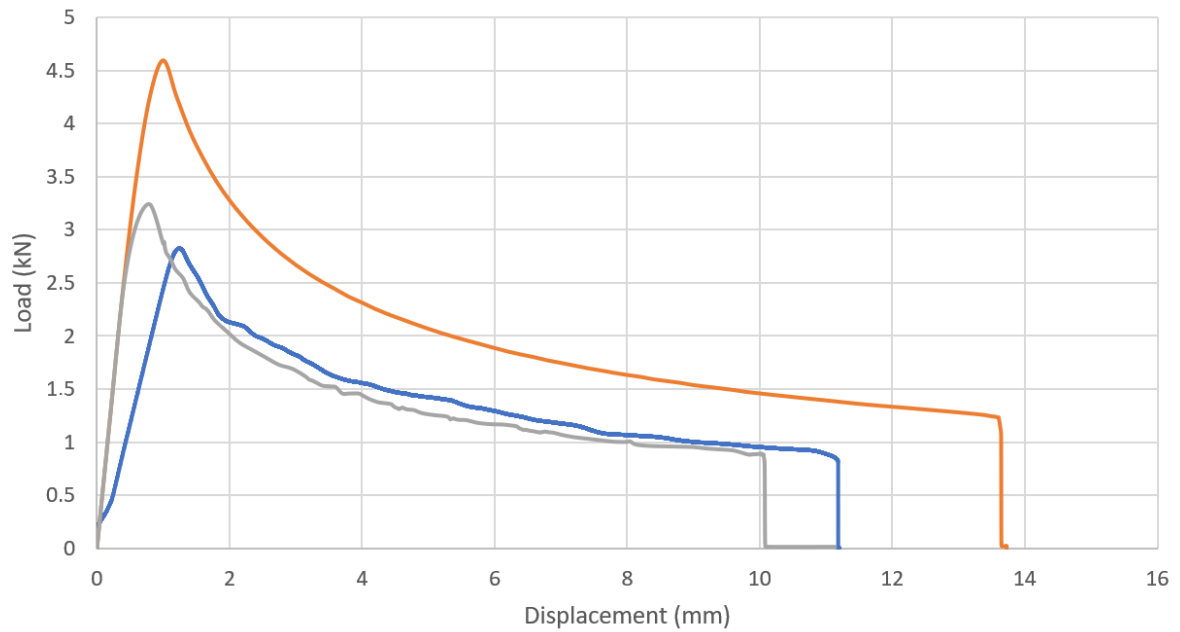


Figure 63 - Comparison between DCB experimental and numerical results

It is noticeable from Figure 63 that the trapezoidal cohesive law better simulates the mode I DCB test than the triangular cohesive law.

#### ✓ *ENF tests*

The ENF test model was implemented similarly to the DCB test. The boundary conditions and the design were different, although everything else was preserved, as presented in Figure 64.

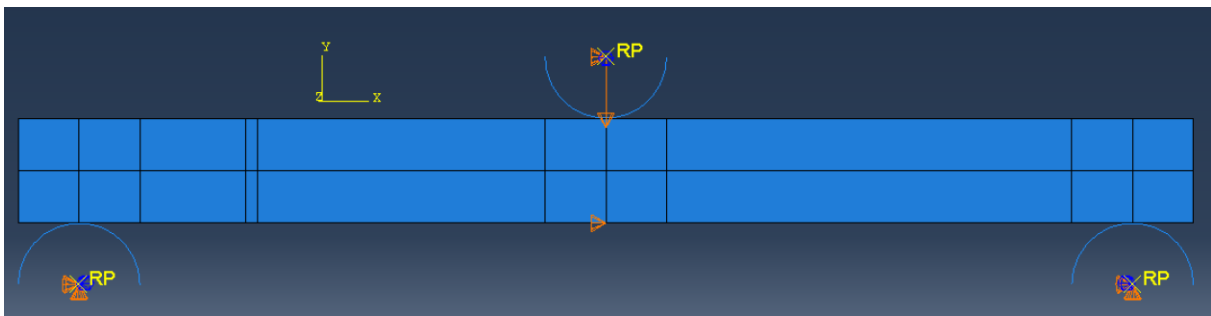


Figure 64 – ENF test specimen's model

The trapezoidal law proved to be the best one to correctly simulate this mode II fracture mechanic test, as shown in Figure 65.



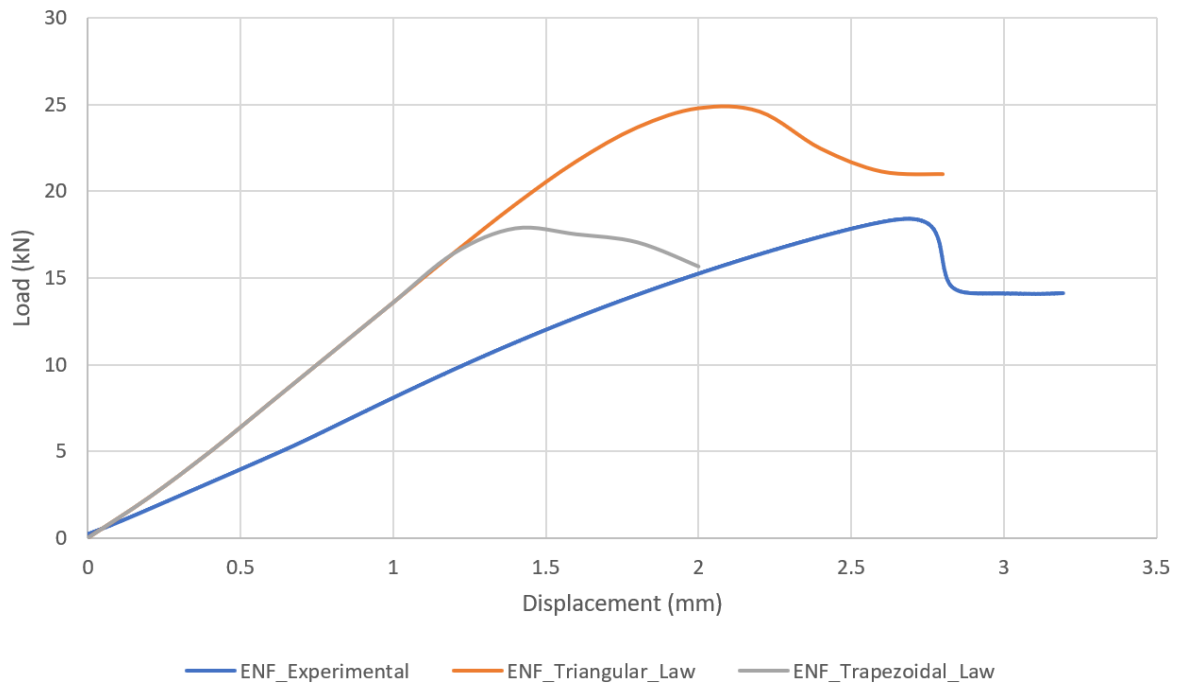


Figure 65 - Comparison between ENF experimental and numerical results

#### ✓ *SLJ tests*

Despite the results accomplished for mode I and mode II have been good enough to confirm that the trapezoidal law is the one that correctly simulates what happens experimentally, tensile SLJs tests were performed using hard steel bonded with the AF 163-2K adhesive. They have showed that in a mixed mode test, the trapezoidal cohesive law is the one that better represents the experimental behavior of the adhesive. The model was similar to those made for the various SLJ adherend configurations, but instead of titanium or CFRP, the hard steel properties were used.

The comparison between the experimental and the numerical results is characterized in Figure 66.

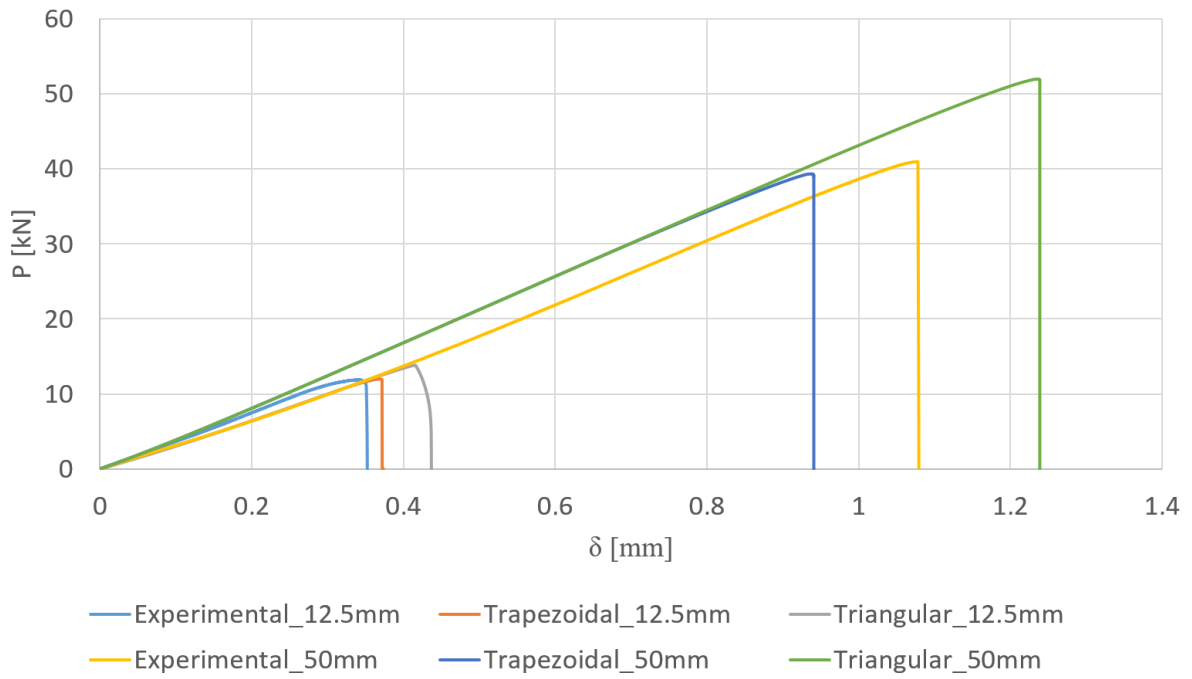


Figure 66 - Comparison between the SLJs tests experimental and numerical results

## Numerical results

As have already been discussed in section 5.1, the numerical models had the objective of simulating the tensile tests performed experimentally. Then, it would be possible to compare the different results reached numerically with those achieved experimentally in order to validate the models created in Abaqus<sup>®</sup>. Afterwards, these models would be available for different configurations and materials, if their validation was considered successful.

The different  $P$ - $\delta$  curves and failure surfaces obtained numerically for each type of SLJ manufactured will be presented here and also compared with the experimental results which were exposed throughout chapter 4.

### 5.3.1. CFRP-only SLJs

#### 5.3.1.1. 12.5 mm overlap length

The numerical  $P$ - $\delta$  curve of a CFRP-only SLJ with a 12.5 mm overlap obtained from Abaqus<sup>®</sup>, using a trapezoidal traction-separation law for the adhesive CZE, is presented in Figure 67. The experimental characteristic  $P$ - $\delta$  curve for the same SLJ tested is shown as well with the purpose of comparing both curves.

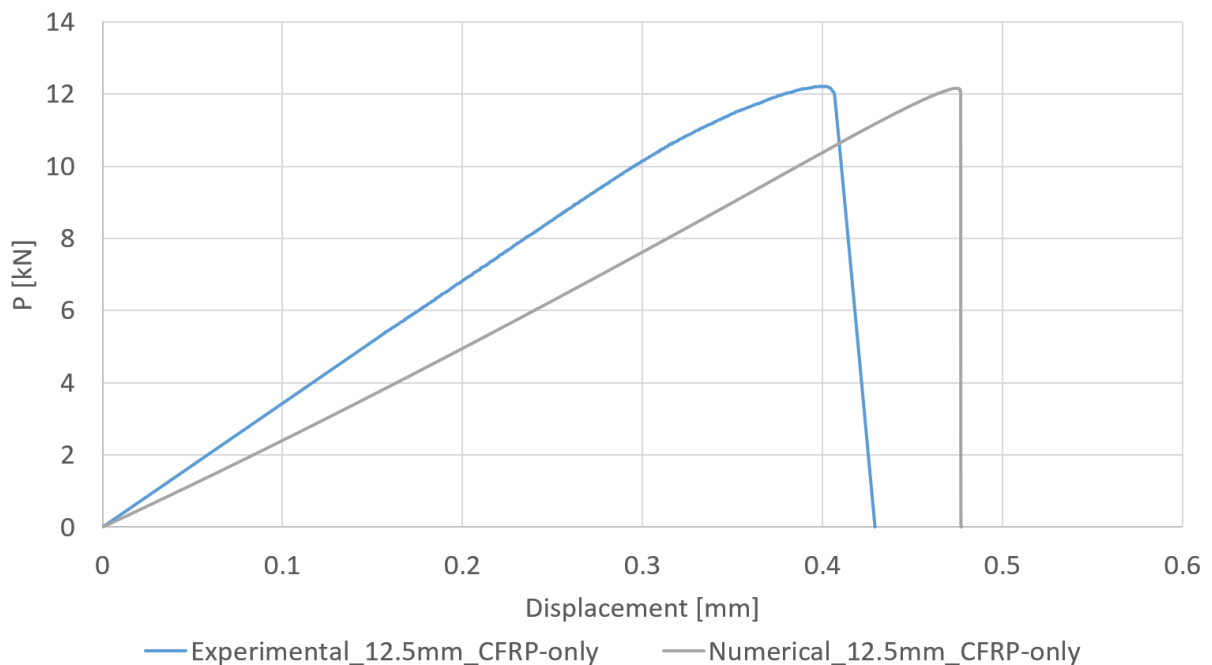


Figure 67 – Numerical  $P$ - $\delta$  curve vs experimental  $P$ - $\delta$  curve for a 12.5 mm overlap CFRP-only SLJ

The failure that occurred at the end of the simulation was cohesive in the adhesive, as shown in Figure 68. The numerical failure surface was equivalent to the one achieved experimentally.

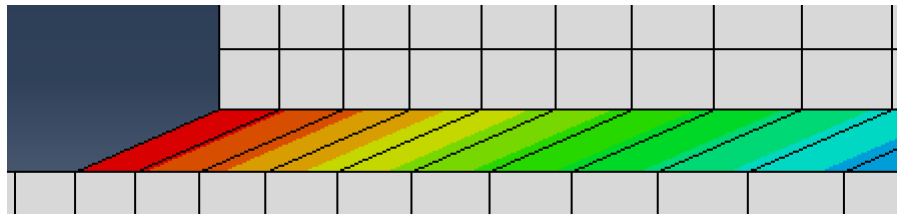


Figure 68 - Numerical failure surface of 12.5 mm overlap CFRP-only SLJ

### 5.3.1.2. 50 mm overlap length

For the SLJ with CFRP-only adherends and a 50 mm overlap, the failure load was much higher comparing with the one obtained for an overlap of 12.5 mm. The numerical  $P$ - $\delta$  curve is shown below in Figure 69.

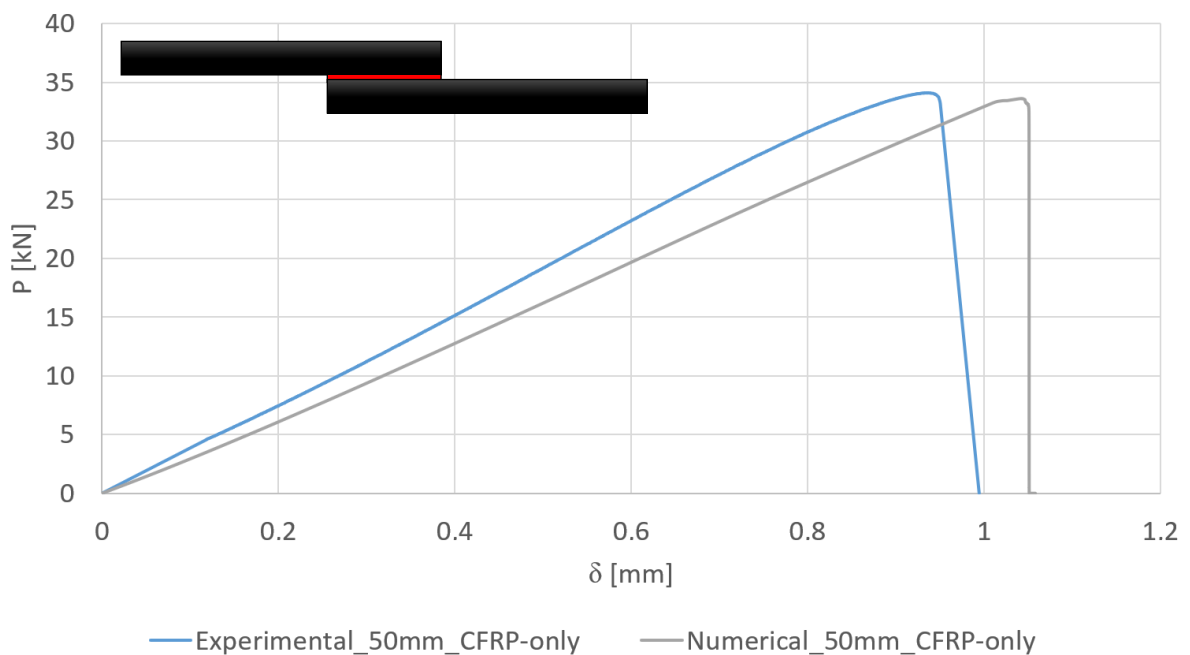


Figure 69 - Numerical  $P$ - $\delta$  curve vs experimental  $P$ - $\delta$  curve for a 50 mm overlap CFRP-only SLJ

Analyzing the failure surface, it was possible to detect similarities between it and the experimental failure. Delamination of the composite within the CFRP layers was perceptible, as shown in Figure 70.

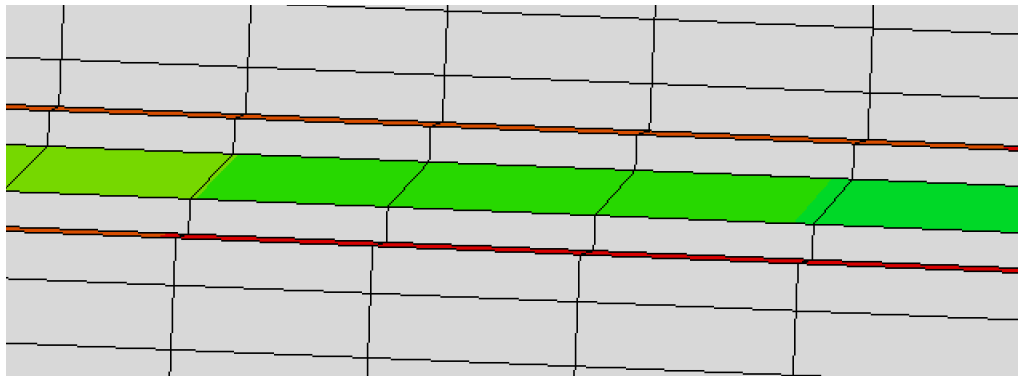


Figure 70 - Numerical failure surface of 50 mm overlap CFRP-only SLJ

### ***5.3.2. CFRP-Ti-CFRP SLJs***

The CFRP-Ti-CFRP configuration was the first being studied numerically, in order to evaluate the influence of titanium laminates as a reinforcement with the objective of improving the peel strength of the composite and also the global strength of the joint. The experimental results have revealed that introducing titanium laminates had more noticeable consequences for the SLJs with a 50 mm overlap than for the ones with 12.5 mm. Numerically, the same outcome was expected.

#### ***5.3.2.1. 12.5 mm overlap length***

The numerical  $P-\delta$  curve for a 12.5 mm CFRP-Ti-CFRP SLJ is shown below in Figure 71. Once again, the trapezoidal cohesive law has demonstrated to correctly simulate the experimental behavior of this type of SLJ.

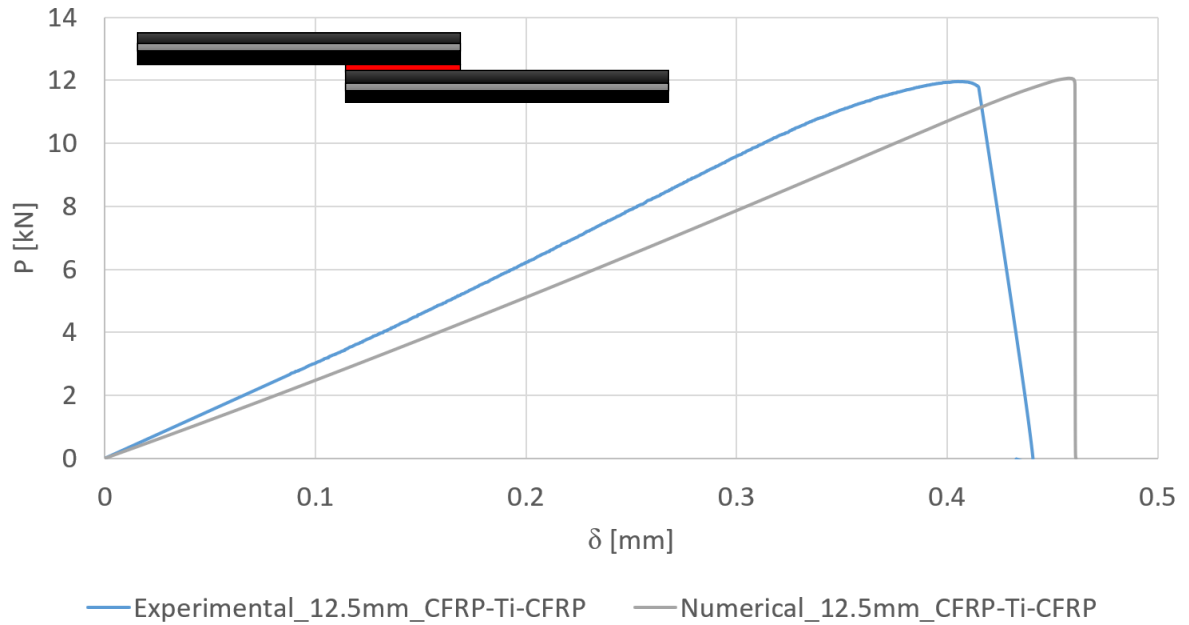


Figure 71 - Numerical P- $\delta$  curve vs experimental P- $\delta$  curve for a 12.5 mm overlap CFRP-Ti-CFRP SLJ

The failure surface found for this SLJ was the same as observed for CFRP-only SLJ with a 12.5 mm overlap – cohesive in the adhesive (Figure 72).

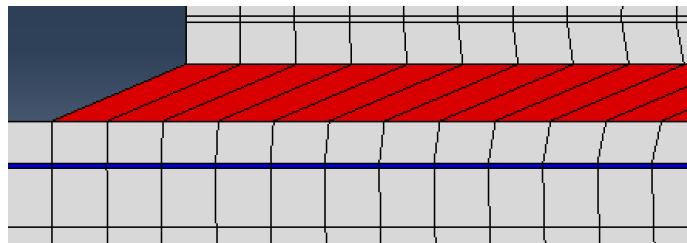


Figure 72 - Numerical failure surface of 12.5 mm overlap CFRP-Ti-CFRP SLJ

### 5.3.2.2. 50 mm overlap length

The numerical  $P-\delta$  curve for a 50 mm CFRP-Ti-CFRP SLJ is shown below in Figure 73. The failure load is expected to be slightly higher than the one reached for the CFRP-only configuration with the same overlap, due to the same failure surface achieved by both, as presented in Figure 74.

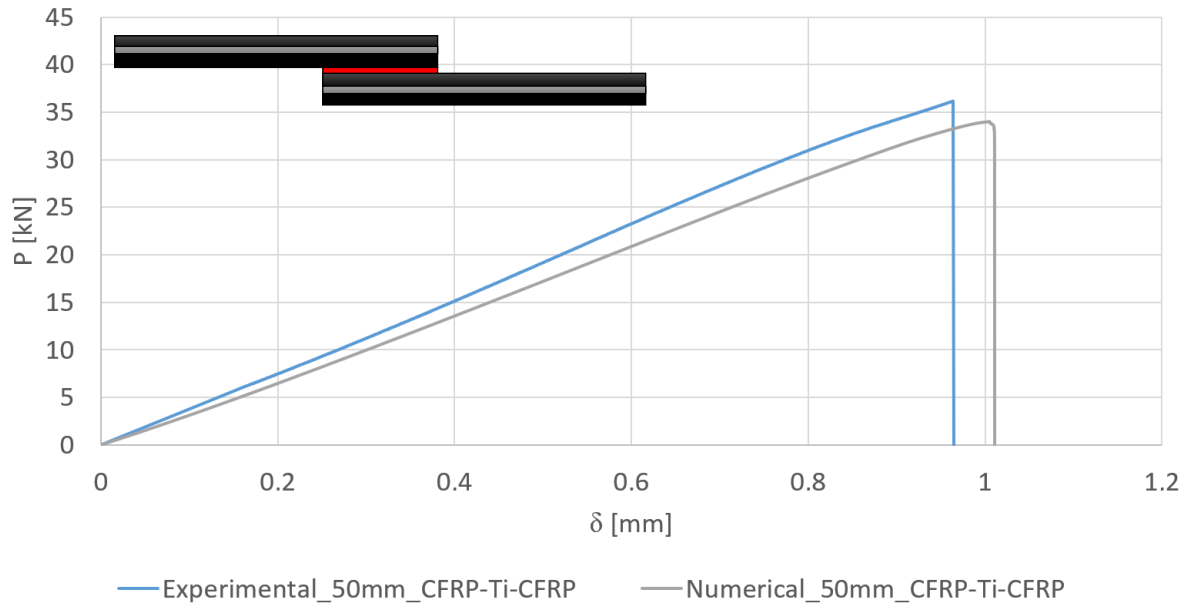


Figure 73 - Numerical  $P-\delta$  curve vs experimental  $P-\delta$  curve for a 50 mm overlap CFRP-Ti-CFRP SLJ

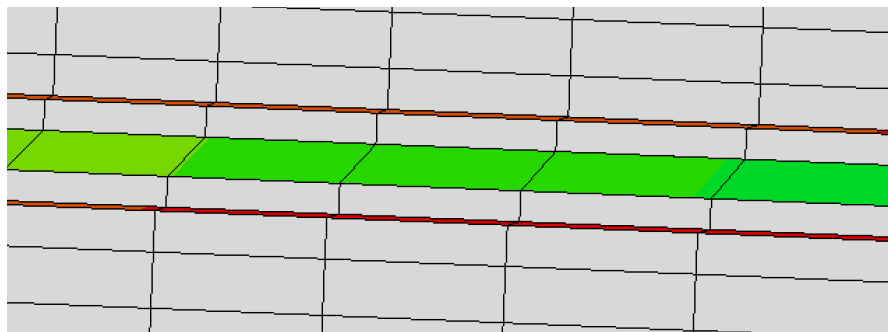


Figure 74 - Numerical failure surface of 50 mm overlap CFRP-Ti-CFRP SLJ

### 5.3.3. Ti-CFRP SLJs

The second configuration numerically studied was Ti-CFRP. However, analyzing the experimental results obtained for all the joints with this configuration, it was possible to recognize that for an overlap of 50 mm, the bending caused by thermal stresses due to the CFRP cure cycle had a negative influence in the achieved results. For that reason, a numerical model was created to simulate the behavior of the Ti-CFRP joints only for the overlap of 12.5 mm. Later, an additional finite element analysis was accomplished for the Ti-CFRP-Ti design, only for an overlap of 50 mm.

#### 5.3.3.1. 12.5 mm overlap length

The numerical  $P$ - $\delta$  curve for a 12.5 mm Ti-CFRP SLJ is shown below in Figure 75.

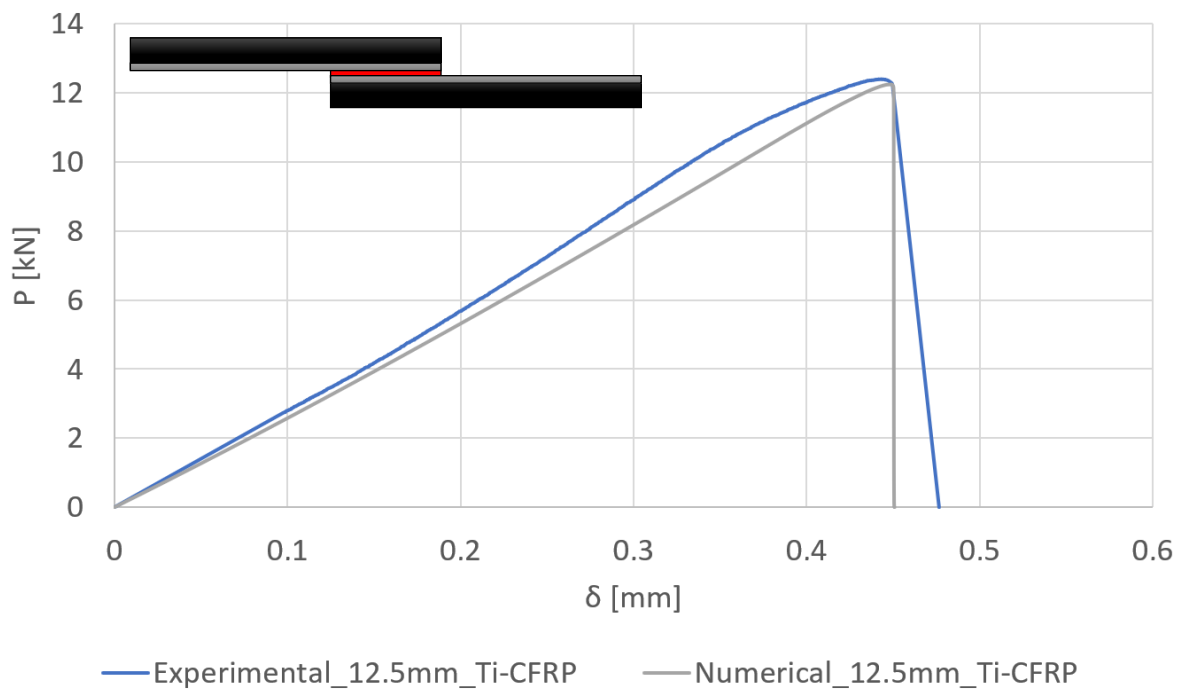


Figura 75 - Numerical  $P$ - $\delta$  curve vs experimental  $P$ - $\delta$  curve for a 12.5 mm overlap Ti-CFRP SLJ



The failure surface witnessed for this SLJ was the same observed for CFRP-only and CFRP-Ti-CFRP SLJs with a 12.5 mm overlap – cohesive in the adhesive – as shown in Figure 76.

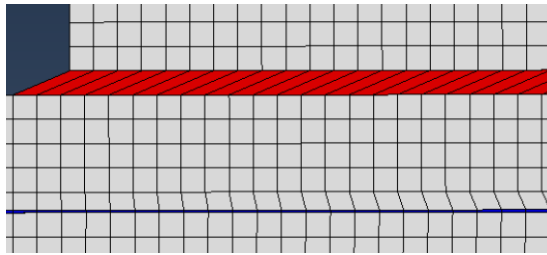


Figure 76 - Numerical failure surface of 12.5 mm overlap Ti-CFRP SLJ

#### **5.3.4. Ti-CFRP-Ti SLJs**

Following the analysis of the experimental results for Ti-CFRP-Ti, a numerical model was created to simulate their mechanical behavior. However, the model assumed that the metal-composite interface would be optimal, which was not experimentally witnessed. Consequently, some differences between the experimental  $P-\delta$  curve and the numerical curve were expected. Only a model for the 50 mm overlap configuration was created because it was the overlap tested in practice.

##### ***5.3.4.1. 50 mm overlap length***

The numerical  $P-\delta$  curve for a 50 mm Ti-CFRP-Ti SLJ is shown in Figure 77. As have already stated, some differences were anticipated due to the weak adhesion between the titanium laminates and the CFRP plates. These details may be detected in Figure 77.

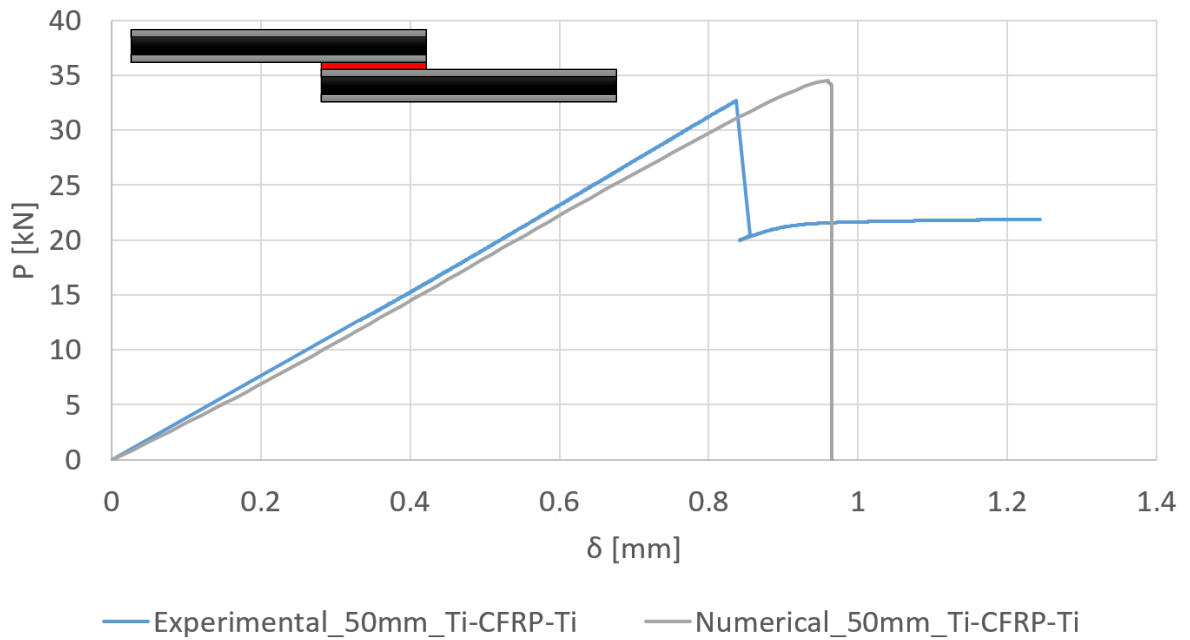


Figure 77 - Numerical  $P$ - $\delta$  curve vs Experimental  $P$ - $\delta$  curve for a 50 mm overlap Ti-CFRP-Ti SLJ

Examining the numerical  $P$ - $\delta$  curve, it is evident that the adhesion of the metal-composite interface was considered perfect in Abaqus®. That situation was not verified in practice and, therefore, the failure surface achieved by the FEM software was different from the one witnessed from the lab tests, shown in Figure 78. The obtained failure load was higher than the experimental one and its value reached the 35 kN.

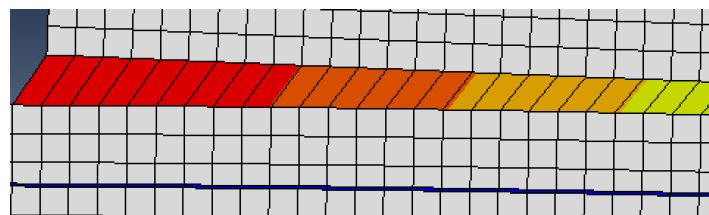


Figure 78 - Numerical failure surface of 50 mm overlap Ti-CFRP-Ti SLJ

## 6. Discussion

By having both experimental and numerical results the comparison between them can be performed in order to conclude if the numerical models properly predict the failure load and the type of failure occurred during each SLJs tests.

The various types of SLJs with 12.5 mm overlap tested experimentally reached a similar failure load value, despite their different configuration. Furthermore, comparing both traction-separation laws, it was clear that the trapezoidal cohesive law was the one that better replicates what happened experimentally. In Figure 79, the failure load obtained numerically was compared to the values achieved in practice.

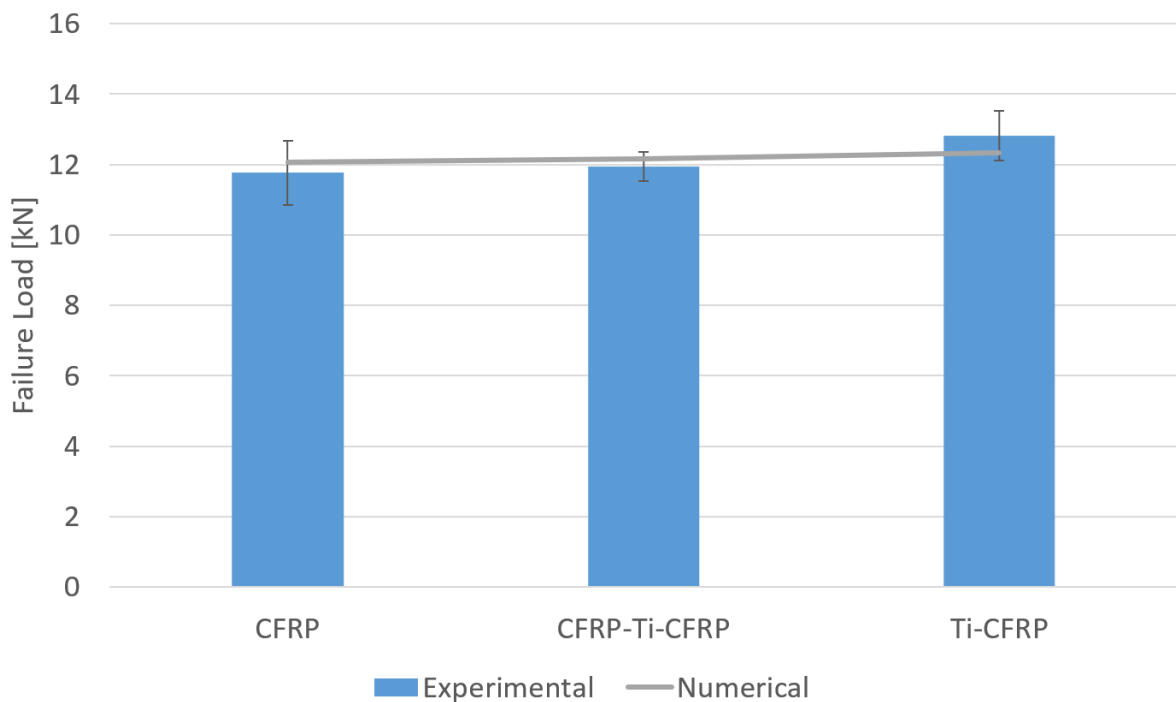

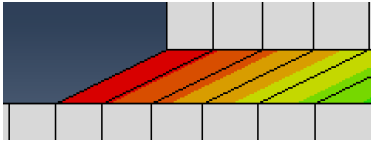


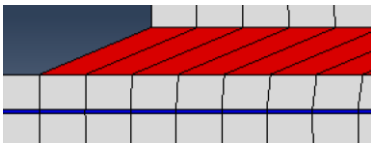


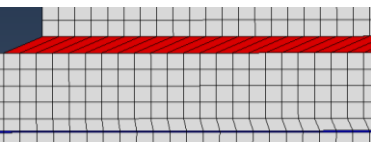



Figure 79 - Comparison between FEA predictions and experimental results for the failure load of 12.5 mm overlap SLJs

Regarding the failure modes of the 12.5 mm overlap specimens, they are compared in Table 9. The failure mode was equal for all the specimens tested, cohesive in the adhesive, and the same surface failure was obtained by 12.5 mm overlap SLJs numerical models.

Table 8 – Failure type obtained experimentally and numerically for the 12.5 mm overlap joints

Configuration	Numerical	Experimental
		
		
		

For the 50 mm overlap length, the numerical predictions matched perfectly the experimental results achieved for the CFRP-only and the CFRP-Ti-CFRP configurations, as shown in Figure 80. Once again, the trapezoidal traction-separation law has proved to be the one that better represents the experimental tests. Nevertheless, the prediction of the failure load for the 50 mm overlap Ti-CFRP-Ti SLJs was slightly different than the value obtained in practice. In fact, the difference between the numerical and experimental values was not that significant even though the failure mode was completely different, as presented in Table 10.

As mentioned before, this configuration was manufactured due to the damage suffered by Ti-CFRP adherends, which numerical results were not taken into account because they were completely influenced by the bending occurred during the CFRP cure cycle. Only the 12.5 mm overlap SLJs were tested successfully. Analyzing Figure 81 and Table 10, it is possible to confirm that the failure load associated with the adhesive maximum contribution was almost reached experimentally by the Ti-CFRP-Ti joints, despite the adhesive failure in the Ti-CFRP interface. This failure mode witnessed in practice was not coherent with the one simulated in Abaqus®. The main reason for this occurrence was the weak adhesion between the grit-blasted titanium and the CFRP. One way to improve adhesion was treating the titanium laminates chemically, for instance recurring to the peroxide alkaline etch. However, the practical results led to some interesting ideas that could be worth further study. Although

the numerical failure mode was cohesive in the adhesive for the Ti-CFRP-Ti configuration and it was expected for the experimental results that the same would occur, it might not be as interesting for the aerospace industry as the experimental failure mode obtained. The failure within the adhesive layer is characterized as an abrupt failure where the adherends are suddenly detached from each other and, as a structural component of an aircraft, it is not the ideal in terms of the passengers' security. On the contrary, the witnessed experimental progressive failure could be important regarding the safety of aircrafts, as the bonding of a structural component, such as the fuselage or the empennage, would not fail entirely at the same time. Originally, it would fail adhesively in the interface of metal-composite bonding and, then, the titanium joint would deform until the rupture of the joint.

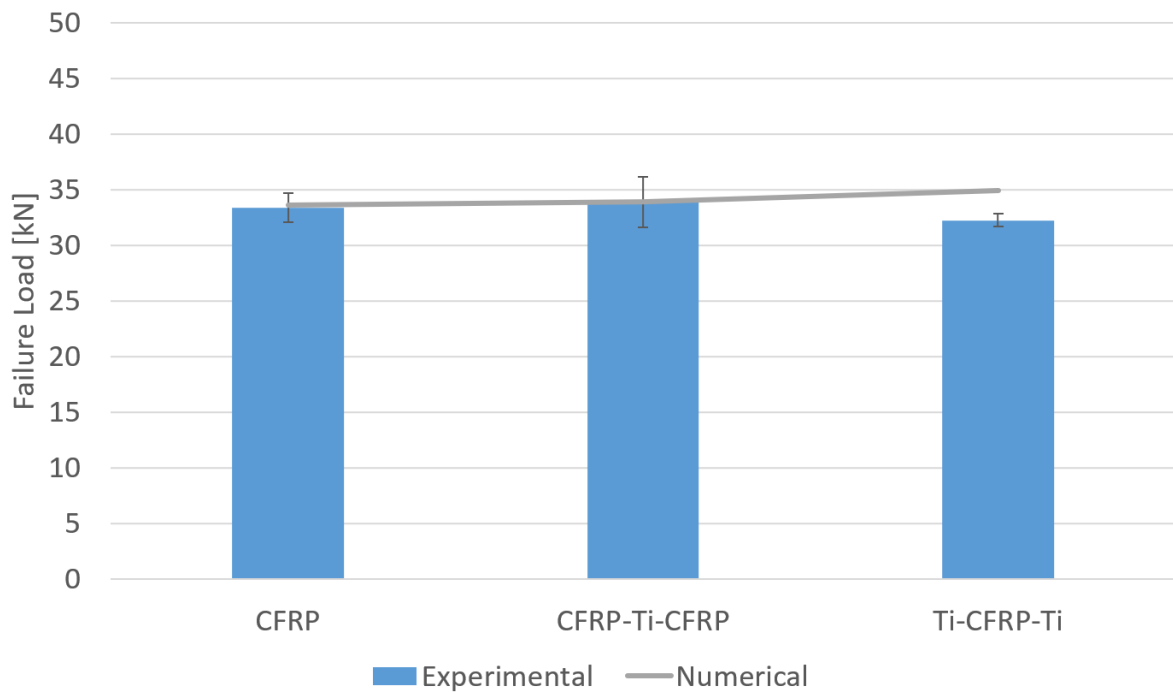

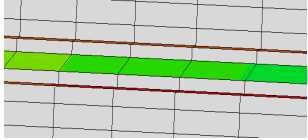


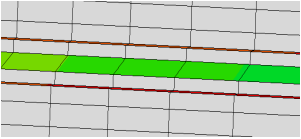
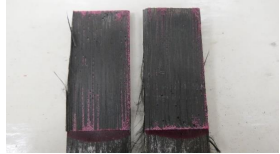

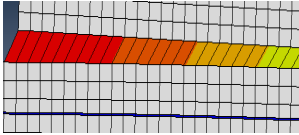



Figure 80 - Comparison between FEA predictions and experimental results for the failure load of 50 mm overlap SLJs

Table 9 - Failure type obtained experimentally and numerically for the 50 mm overlap joints

Configuration	Numerical	Experimental
		
		
		

## 7. Optimization of Ti-CFRP-Ti single lap joints

### 7.1. Different thicknesses

The analysis and discussion of the results accomplished experimentally and numerically led to some interesting conclusions about which configuration would be optimal for aerospace applications. The Ti-CFRP-Ti design, with a 0.8 mm thickness titanium laminates, reached the highest failure load numerically provided. So, it was considered the best design of those studied respecting the mechanical properties of the joint. The use of titanium laminates in an extremity of the adherend, for 12.5 mm overlap joints, and in the both edges, for 50 mm overlap joints, brought the best results in terms of the failure mode of the joints.

In an attempt to enhance the most interesting experimental and numerical joint, 50 mm overlap Ti-CFRP-Ti SLJ, two different approaches were made: changing the global thickness of the SLJs by reducing the thicknesses of the adherends and using different proportions of materials by reducing the thickness of titanium laminates. The software used was, once again, Abaqus®.

On the first approach, different thicknesses were considered for the Ti-CFRP-Ti adherends in order to conclude if there was any major optimization of the failure load or even a decrease in the peel stresses along the overlap. Figure 81 presents the numerical failure loads for different Ti-CFRP-Ti adherends, compared with the reference joint. The 2.3 mm case was the last thickness to be studied because for lower thicknesses, the failure mode was identical to that witnessed for the CFRP-only joints – delamination of the CFRP.

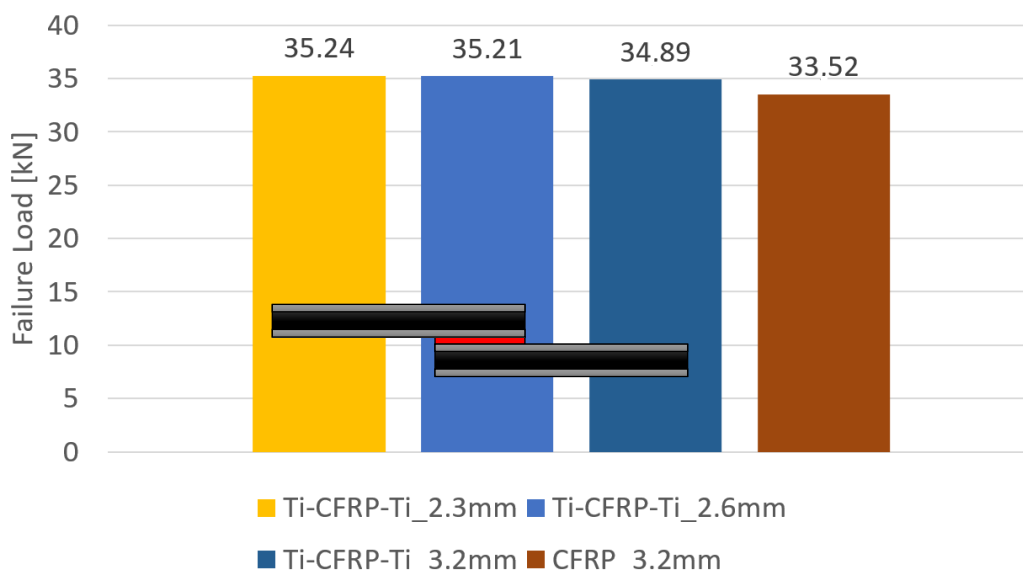


Figure 81 – Comparison between different Ti-CFRP-Ti adherend thicknesses in terms of failure load

It was possible to assume that, regarding the failure load, decreasing the thickness of the adherend did not have a positive influence. Instead, the failure load has remained similar to the one obtained numerically for the 0.8 mm thickness. Comparing the CFRP-only design with the others, not only was the failure load higher for the Ti-CFRP-Ti joints, but the failure mode was also different. The CFRP-only joint suffered delamination, while the others failed cohesively in the adhesive.

According to the peel stresses along the overlap (Figure 82), the same conclusions were taken while evaluating the same thicknesses. However, it is visible that when titanium laminates are used, the peak of peel stresses at both extremities of the overlap are higher for the CFRP-only joints. Consequently, the Ti-CFRP-Ti joints reduce the peel stresses along the overlap, especially at the edges where it reaches its maximum value.

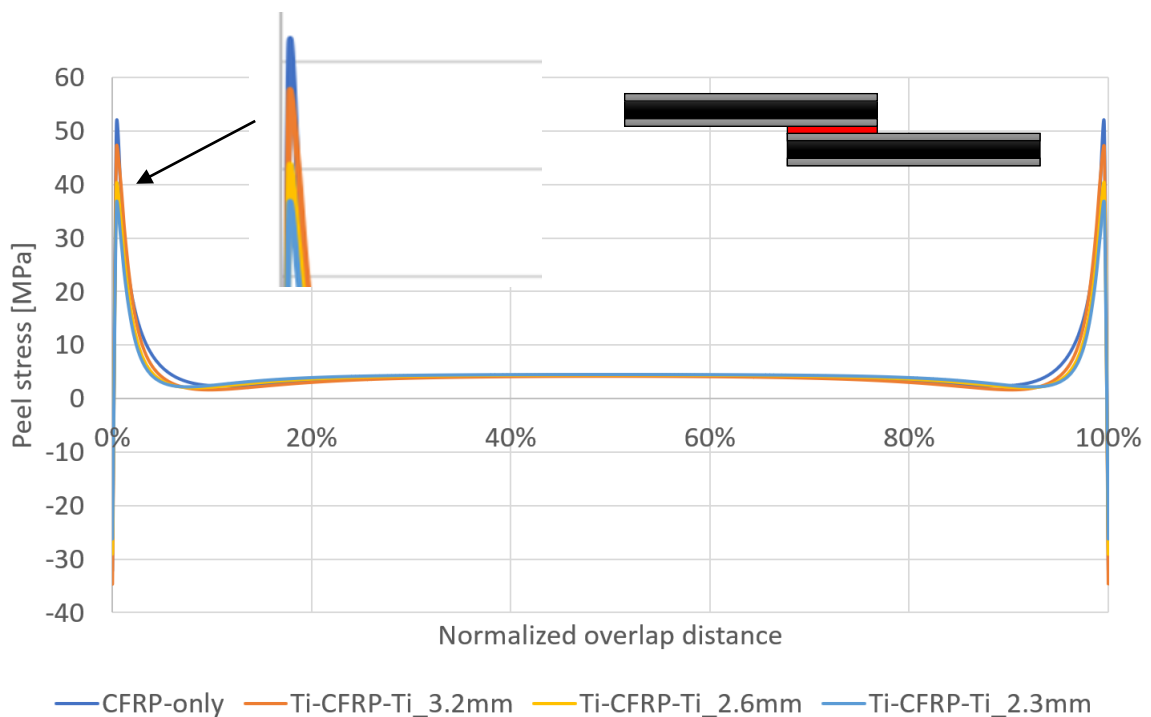


Figure 82 - Comparison between different Ti-CFRP-Ti adherends' thicknesses in terms of peel stresses



## 7.2. Distinct proportion of materials

On the second approach, distinct proportions of titanium and CFRP were considered for the Ti-CFRP-Ti adherends in order to conclude if there was any major optimization of the same parameters evaluated above. The different laminates of titanium that were evaluated were 0.4 and 0.3 mm of thickness. Any thickness under this value led to a failure in the composite, so it was not considered. The conclusions respecting the failure load were similar to those taken for different adherends thicknesses. The reduction of percentage of titanium in the adherend did not increase the failure load, although the value is similar for the various joints, as shown in Figure 83. Furthermore, the failure mode was cohesive in the adhesive for all Ti-CFRP-Ti SLJs. Regarding the peel stresses along the overlap, the same conclusions as commented in Figure 83 stand and are presented in Figure 84 for these cases.

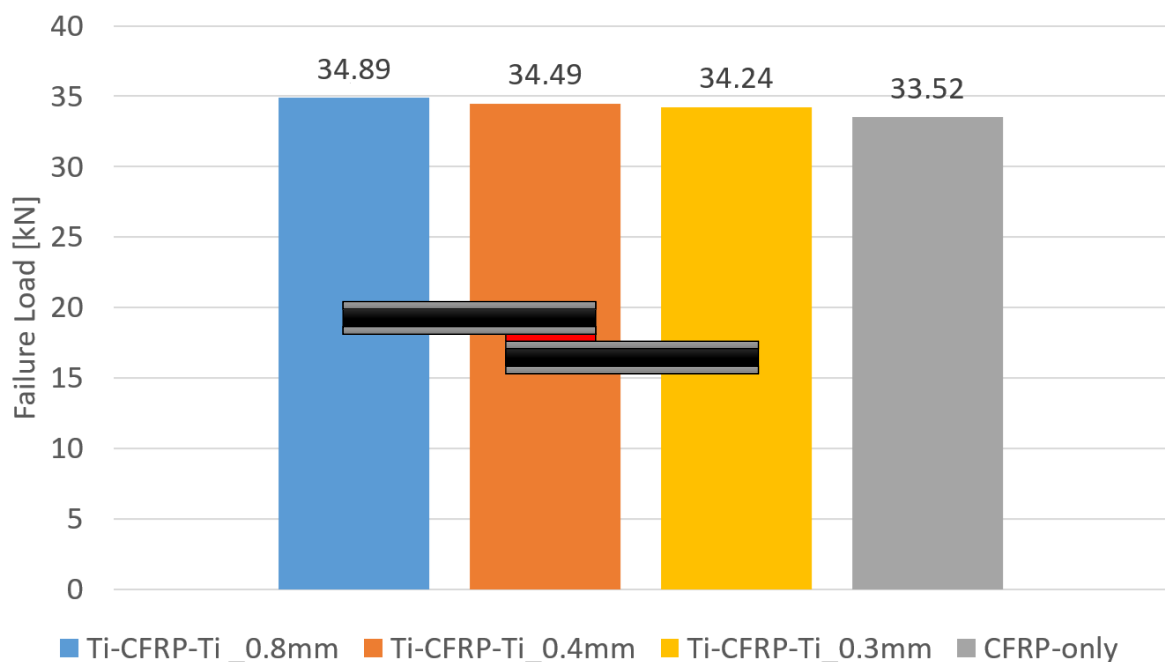


Figure 83 - Comparison of the failure load between different titanium laminates thickness in Ti-CFRP-Ti joints

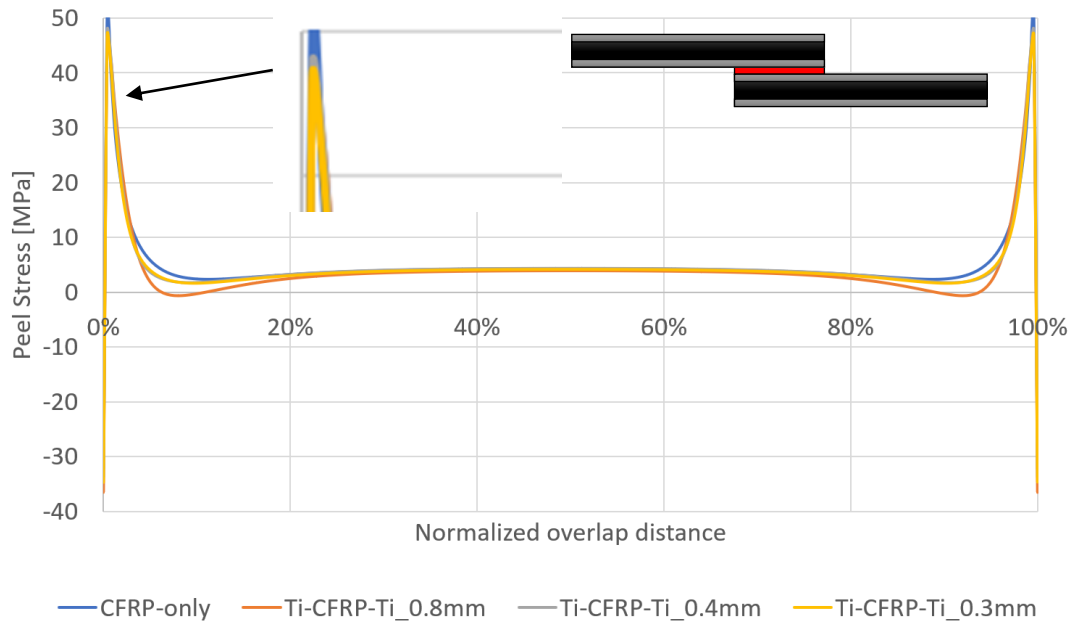


Figure 84 –Comparison of the peel stresses between different titanium laminates thickness in Ti-CFRP-Ti joints

### 7.3. Impact conditions

For the automotive industry, it is of major importance to evaluate the materials that compose several structural components of a vehicle under impact conditions. Nonetheless, in aerospace industry, there are some particular cases where it is also important to analyze the behavior of some structural components under impact solicitations. The performance of the aircraft's body while colliding with other materials, such as tools, animals or even another aircraft, should be studied to avoid the worst scenarios.

The 50 mm overlap joint designs experimentally and numerically studied for quasi-static situations were evaluated under impact conditions. This analysis was made using the same Abaqus® model described before for all configurations and only the boundary conditions were altered. A velocity was applied to a very rigid material associated to the joint part (Figure 85), so that an acceleration was created to simulate an impact solicitation to that same joint. The left extremity of the joint was fixed in all directions.



Figure 85 - Schematic view of the physical boundary conditions for SLJs under impact conditions in Abaqus®

Besides, the element type used in this model was different for all continuous elements (CFRP and metal). Instead of 8-node biquadratic plane stress quadrilateral elements, 4-node bilinear plane stress quadrilateral elements were used. The remaining steps were maintained for all SLJs under impact models.

The failure load was obtained for all configurations and then compared with the one associated to the quasi-static conditions. The “Load vs Time” curves obtained for all the joint designs are presented in Figure 86.

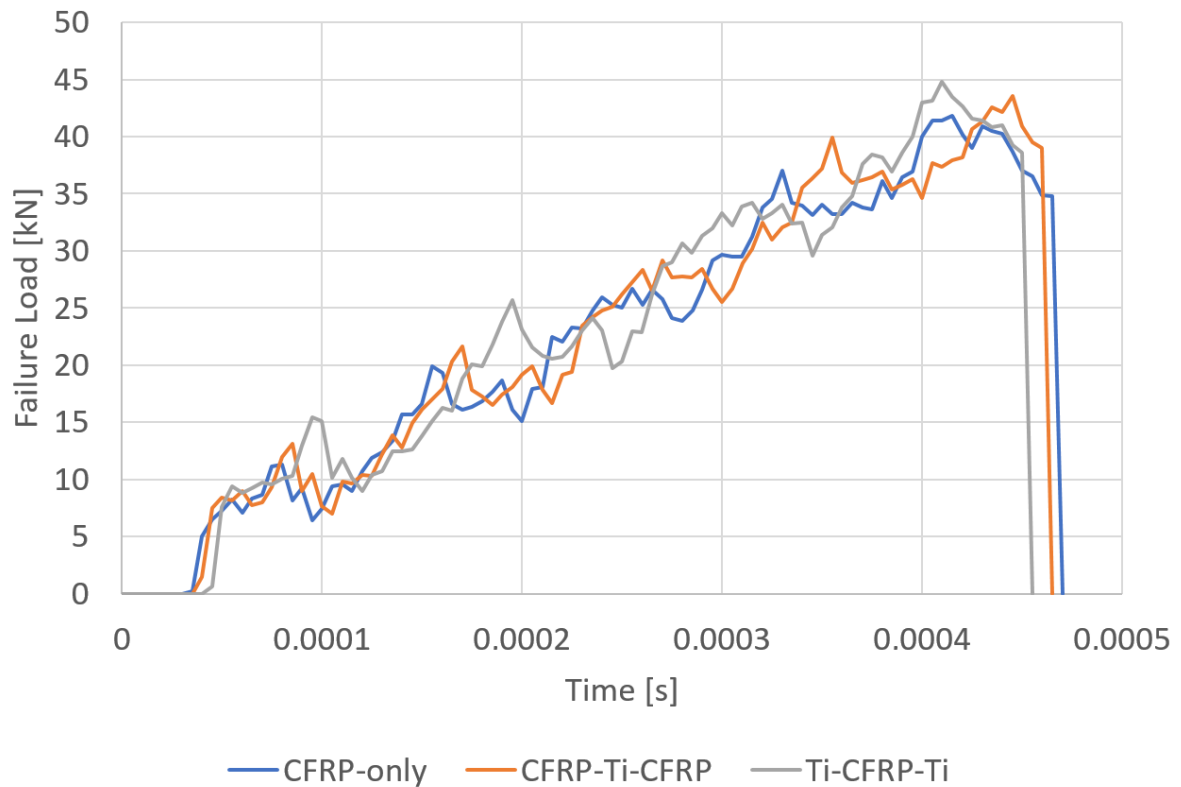


Figure 86 – Load vs Time curves for all SLJs under impact conditions

After the analysis of Figure 86, it is possible to affirm that there are some similarities between the curves. The failure load achieved for each SLJ's design and the failure mode were different when comparing the CFRP-only and the CFRP-Ti-CFRP configurations with the Ti-CFRP-Ti. In Figure 87, it is presented the failure load of all the SLJs numerically simulated. The best configuration under impact conditions was, once again, the Ti-CFRP-Ti one. It was clear that changing the titanium laminates thickness did not have a significant influence in the value of failure load. Additionally, an increase of the failure load was observed for SLJs under impact conditions when compared with the quasi-static situations.

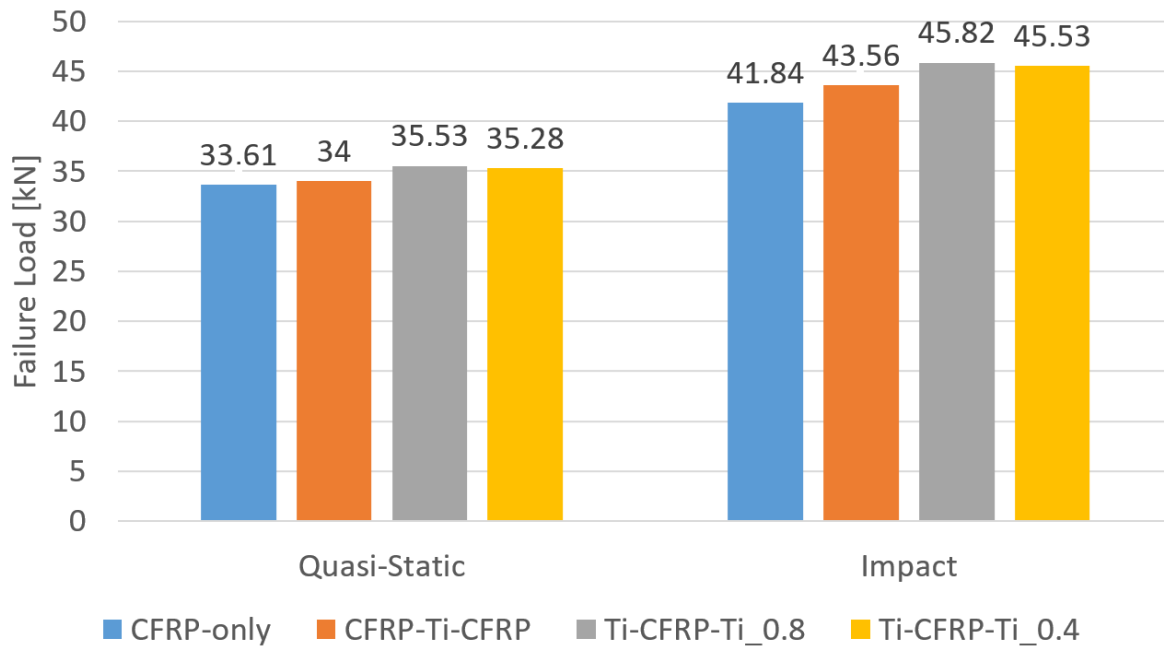


Figure 87 – Comparison of the failure load between quasi-static and impact conditions

The failure mode of the CFRP-only and the CFRP-Ti-CFRP SLJs was identical – cohesive in the CFRP. Figure 88 shows the delamination numerically suffered by the CFRP. The Ti-CFRP-Ti configuration failed cohesively in the adhesive (Figure 89).

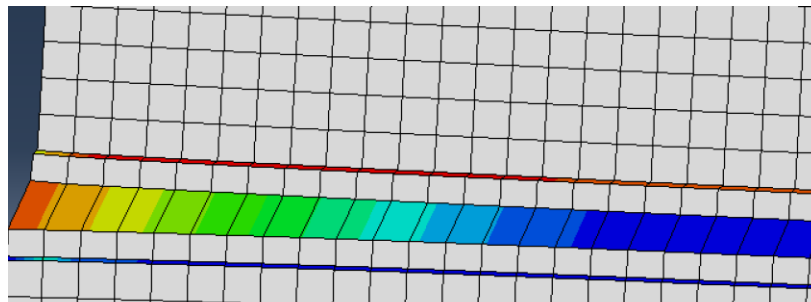


Figure 88 – Failure mode of CFRP-only and CFRP-Ti-CFRP SLJs under impact

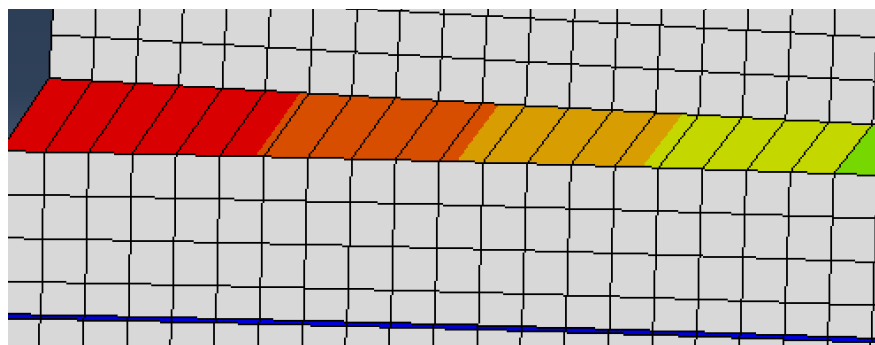


Figure 89 - Failure mode of Ti-CFRP-Ti SLJs under impact conditions

To conclude this analysis, the performance between a Ti-CFRP-Ti SLJ and an Al-CFRP-Al SLJ was compared, under the same impact and quasi-static conditions. The results of this comparison are presented in Figure 90.

The Ti-CFRP-Ti SLJ offered better results in terms of failure load than the aluminium joint. For both conditions, the titanium-CFRP hybrid joints reached higher values of failure load, exposing better mechanical properties than the aluminium-CFRP joints. Regarding the failure modes, both joints failed cohesively in the adhesive.

Finally, it is possible to conclude that the Ti-CFRP-Ti was the best SLJ's configuration under impact and quasi-static conditions.

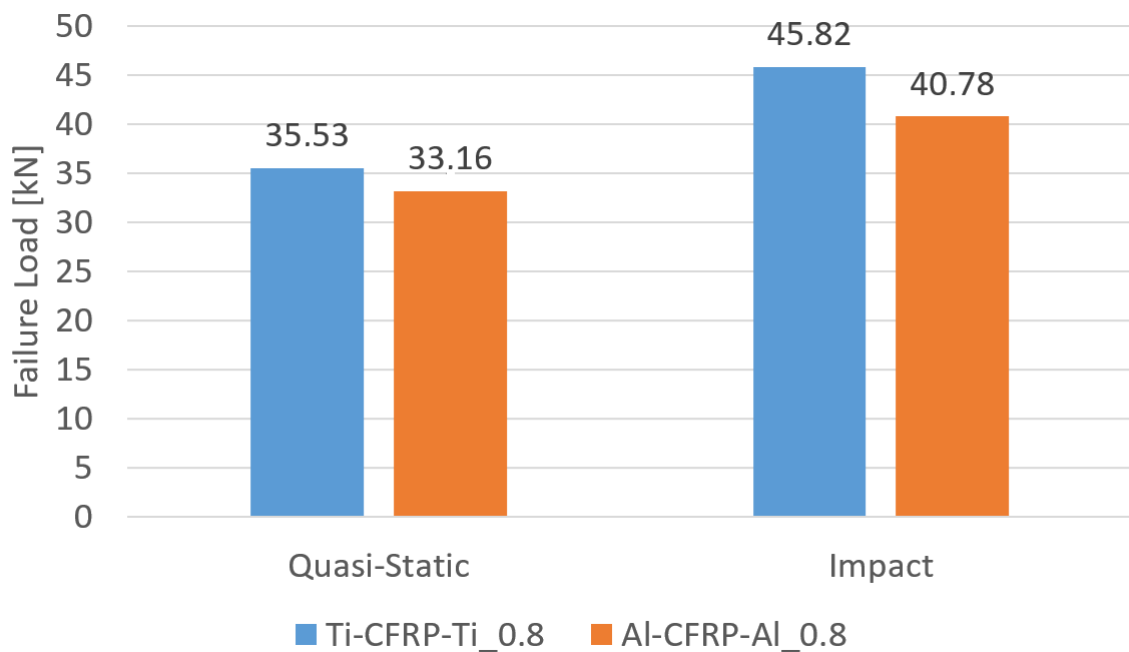


Figure 90 - Comparison between Ti-CFRP-Ti and Al-CFRP-Al failure loads under quasi-static and impact conditions

## 8. Conclusions

The key objective of this thesis was to use a concept similar to FML in order to improve the peel strength of a CFRP substrate, as well as the adhesively bonded joint strength itself when such hybrid materials are used as adherends. Consequently, several SLJs were manufactured and tested, with the main purpose of finding the best lay-up configuration of titanium-CFRP laminates that increased the peel strength of a reference CFRP-only joint. There were two overlap lengths evaluated:

- 12.5 mm, with the configurations CFRP-only, CFRP-Ti-CFRP and Ti-CFRP;
- 50 mm, with the configurations CFRP-only, CFRP-Ti-CFRP, Ti-CFRP and Ti-CFRP-Ti.

Regarding the 12.5 mm overlap joints, the failure load was similar between the different designs, slightly increasing with the introduction of a titanium laminate. The failure was cohesive in the adhesive for all the joints experimentally tested. Concerning the 50 mm overlap joints, there were dissimilar failures witnessed. On one hand, when comparing the CFRP-only and the CFRP-Ti-CFRP configurations, CFRP delamination occurred. However, the failure load was somewhat higher for the design with a titanium laminate in the middle of the adherend. On the other hand, for the Ti-CFRP and the Ti-CFRP-Ti configurations, a different type of failure was achieved, such that both designs revealed weak adhesion in the interface between the titanium and the CFRP, and failure was adhesive in that same interface. In the first case, the Ti-CFRP substrate suffered severe bending during the CFRP cure cycle, which caused the thermal stresses that damaged the adherend and the results were not interesting. In the second case, the neutralization of those thermal stresses by the existence of two titanium laminates in both adherend's extremities allowed the joint to have more resistance, leading to progressive failure caused by the titanium bonding. That progressive failure, instead of the abrupt one that was expected to occur (cohesive in the adhesive), was considered an exciting accomplishment regarding the safety of the aircrafts, as during service a structural component would not suddenly fail. Nonetheless, the failure would firstly occur in the metal-composite interface and, then, the remaining titanium joint would gradually deform until the adhesive failed.

The numerical models were coherent with all the configurations experimentally tested for the 12.5 mm overlap SLJs. Regarding the 50 mm overlap joints, the numerical analysis

results were similar to the experimental CFRP-only and CFRP-Ti-CFRP joints. However, the simulation of the Ti-CFRP-Ti joints did not match with the experimental results, because although the failure load was similar to the experimental tests, the failure mode was not the same. The software considered the adhesion between the titanium and the CFRP as perfect so the failure occurred in the adhesive. Nevertheless, the Ti-CFRP-Ti design was chosen, once again, as the best to increase the peel strength of a CFRP substrate as well as the global joint strength.

To sum up, the several analyses dictated that the introduction of a titanium laminate increased the failure load and the peel strength of a CFRP joint. However, changing the proportion of the materials or the global thickness of a SLJ, did not offer significant improvements, regarding the failure load and the peel stresses along the overlap. Under impact conditions, the Ti-CFRP-Ti SLJ shows a better behavior compared with the other designs, failing cohesively in the adhesive and achieving the highest failure load. The comparison between the Ti-CFRP-Ti and the Al-CFRP-Al joints revealed that using titanium as an alternative to aluminium is a better option, due to the higher failure load obtained in both quasi-static and impact conditions.



## **9. Future work**

1. Try different surface treatments for the titanium alloy in order to understand if the experimental results would be more coherent with those achieved numerically;
2. Optimize the best joint, Ti-CFRP-Ti, achieving higher failure loads and the type of failure previously expected;
3. Choose another metal to produce a new hybrid substrate, with better mechanical properties than the titanium alloy chosen. A compromise between low weight, high strength and low cost consists in an appealing challenge;
4. Try to improve the trapezoidal traction-separation law developed in order to better simulate the ductile behavior of the AF 160-2K adhesive;
5. Validate, experimentally, the numerical data obtained from the Abaqus<sup>®</sup> models that have simulated the behavior of SLJs under impact conditions.

## 10. References

- [1] Airbus, “A380 Technology – Advanced materials”, 2017. <http://www.airbus.com/aircraft/passenger-aircraft/a380-family/technology.html> (last accessed in October 2017)
- [2] T. Edwards, “Composite Materials Revolutionise Aerospace Engineering”, *Ingenia Issue*, vol. 36, pp. 25-28, 9 // 2008.
- [3] Airbus, “A350 XWB Family – Design Revolution”, 2017. <http://www.airbus.com/aircraft/passenger-aircraft/a350xwb-family.html> (last accessed in October 2017)
- [4] K. Fabricius, “Airbus A350: Composites on Trial Part I”, 2009. <http://scribol.com/technology/aviation/airbus-a350-composites-on-trial-part-i/> (last accessed in October 2017)
- [5] K. Lama, P. Patel, P. Varikoti, “Application of Composite materials in Aerospace Industry”, 2015. <https://pt.slideshare.net/KanchhaLama/application-of-composite-materials-in-aerospace-industry-1> (last accessed in October 2017)
- [6] The Atlas Group, “Latest Materials used for aircraft manufacturing”, 2016. <http://theatlasgroup.biz/latest-materials-used-aircraft-manufacturing/> (last accessed in October 2017)
- [7] C. A. J. R. Vermeeren, “An Historic Overview of the Development of Fibre Metal Laminates”, *Applied Composite Materials*, vol. 10, Issue 4-5, pp. 189-205, 7 // 2003.
- [8] Peter Dekker’s Mandarin Mansion, “Tiger’s tail patterned Mongolian composite bow”, 2006. <http://mandarinmansion.com/tigers-tail-patterned-composite-bow> (last accessed in October 2017)
- [9] Dytrade, “Fiberglass CSM”, 2004. [https://www.diytrade.com/china/pd/4617102/fiberglass\\_CSM.html](https://www.diytrade.com/china/pd/4617102/fiberglass_CSM.html) (last accessed in October 2017)
- [10] T. Johnson, “History of Composite: The Evolution of Lightweight Composite Materials”, *ThoughtCo.*, 4 // 2017.
- [11] Boats from USA, “Fiberglass Beetle Boat”, 2008. <https://boats-from-usa.com/not-specified/beetle-boat-93046> (last accessed in October 2017)
- [12] A. M. F. M. Ventura, “Os Compósitos e a sua Aplicação na Reabilitação de Estruturas Metálicas”, *Ciência & Tecnologia dos Materiais*, vol. 21, nº 3/4, 2009.
- [13] L. F. M. Da Silva, F. J. L. Alves, A. T. Marques, *Materiais de Construção*, Porto: Publindústria, Produção de Comunicação, Lda, pp. 375-396, 2013.
- [14] United States Department of Labor, “Polymer matrix materials: Advanced composites”, 2002. [https://www.osha.gov/dts/osta/otm/otm\\_iii/otm\\_iii\\_1.html](https://www.osha.gov/dts/osta/otm/otm_iii/otm_iii_1.html) (last accessed in October 2017)

- [15] 'Toray', "Torayca Prepreg", 2017.  
<http://cs2.toray.co.jp/news/toray/en/newsrrs02.nsf/0/28B83DB556D73DAE49257EF8000A3A15> (last accessed in November 2017)
- [16] H. Adam, "Carbon fibre in automotive applications", *Materials & Design*, vol. 18, n° 4/6, pp. 349-355, 7 // 1997.
- [17] C. Red, "Automotive CFRP: The shape of things to come", *Composites World*, 2013.
- [18] A. Quilter, "Composites in Aerospace Applications", *IHS ESDU*, 1 // 2001.
- [19] M. R. Al-Hadrayi Ziadoon, Z. Chwei, "Effect the stacking sequences of composite laminates under low velocity impact on failure modes by using carbon fiber reinforced polymer", *The International Journal of Engineering and Science*, vol. 5, pp. 53-62, 2016.
- [20] P. Cognard, *Adhesive and Sealants: Basic Concepts and High Tech Bonding - Handbook of Adhesives and Sealants Volume 1*, Oxford: Eksevier Ltd, pp. 21-99, 2005.
- [21] A. J. Kinloch, *Adhesion and Adhesives: Science and Technology*, London: Chapman & Hall, pp. 188-259, 1987.
- [22] P. Krishnan, "Fracture and failure analyses of plastics and reinforced plastics", 2015.  
<https://pt.slideshare.net/PadmanabhanKrishnan2/fracture-and-failure-analyses-of-plastics-and-reinforced-plastics> (last accessed in December 2017)
- [23] C. D. Radu, *Optimization of CFRP Joints with Fibre Metal Laminates*, 2015.
- [24] M. D. Banea, L. F. M. da Silva, "Adhesively bonded joints in composite materials: an overview", *Proceedings of the Institution of Mechanical Engineers, Part L: Journal of Materials: Design and Applications*, vol. 223, pp. 1-18, 2009.
- [25] M. J. Davis, D. A. Bond, "The Importance of Failure Mode Identification in Adhesive Bonded Aircraft Structures and Repairs", *Proceedings of the ICCM-12 Conference, Paris*, 1999.
- [26] L. F. M. da Silva, R. D. Adams, "Techniques to reduce the peel stresses in adhesive joints with composites", *International Journal of Adhesion & Adhesives*, vol. 27, pp. 227-235, 4 // 2007.
- [27] A. S. Paipetis, D. Katerelos, "Post-Impact-Fatigue behaviour of composite laminates: Current and novel technologies for enhanced damage tolerance", *Composite Laminates*, pp. 1-82, 2010.
- [28] R. B. Ladani, A. R. Ravindran, S. Wu, K. Pingkarawat, A. J. Kinloch, A. P. Mouritz, R. O. Ritchie, C. H. Wang, "Multi-scale toughening of fibre composites using carbon nanofibres and z-pins", *Composite Science and Technology*, vol. 131, pp. 98-109, 6 // 2016.
- [29] R. Matsuzaki, M. Shibata, A. Todoroki, "Reinforcing an aluminum/GFRP co-cured single lap joint using inter-adherend fiber", *Composites Part A: Applied Science and Manufacturing*, vol. 39, pp. 786-795, 2 // 2008.
- [30] A. Asundi, A. Y. N. Choi, "Fiber Metal Laminates: An Advanced Material for Future Aircraft", *Journal of Materials Processing Technology*, vol. 63, pp. 384-394, 1997.

- [31] T. Sinmazçelik, E. Avcu, M. O. Bora, O. Çoban, “A review: Fibre metal laminates, background, bonding types and applied test methods”, *Materials and Design*, vol. 32, pp. 3671-3685, 3 // 2011.
- [32] L. F. M. da Silva, M. Costa, G. Viana, R. D. S. G. Campilho, “Analytical Modelling for the Single-Lap Joint”, *Strength Prediction of Adhesively-Bonded Joints*, pp. 8-44, 2017.
- [33] O. Volkersen, “Die nietkraftverteilung in zugbeanspruchten Nietverbindungen mit konstanten laschenquerschnitten”, *Luftfahrtforschung*, vol. 15, p. 41, 1938.
- [34] M. Goland, E. Reissner, “The Stresses in Cemented Joints”, *J. Appl. Mech*, vol. 11, pp. 17-27, 1944.
- [35] L. J. Hart-Smith, “Adhesive-bonded single lap joints”, *NASA Langley contract report NASA CR-112236*, 1973.
- [36] D. Chen, S. Cheng, “Analysis of adhesive-bonded single-lap joints”, *Journal of Applied Mechanics, Transactions ASME*, vol. 50, pp. 109-115, 1983.
- [37] D. A. Bigwood, A. D. Crocombe, “Non-linear adhesive bonded joint design analyses”, *International Journal of Adhesion and Adhesives*, vol. 10, pp. 31-41, 1990.
- [38] R. D. Adams, V. Mallick, “A method for the stress analysis of lap joints”, *The Journal of Adhesion*, vol. 38, pp. 199-217, 1992.
- [39] L. F. M. da Silva, R. F. T. Lima, R. M. S. Teixeira, A. Puga, *Closed-form solutions for adhesively bonded joints*, 2008.
- [40] L. Goglio, “Continuum Mechanics Modelling by Finite Elements”, *Strength Prediction of Adhesively-Bonded Joints*, pp. 97-117, 2017.
- [41] L. F. M. da Silva, R. D. S. G. Campilho, *Advances in Numerical Modelling of adhesive joints*, Berlin: SpringerBriefs in Applied Sciences and Technology, 2011.
- [42] R. D. Adams, J. A. Harris, “Strength prediction of bonded single lap joints by nonlinear finite element methods”, *International Journal of Adhesion and Adhesives*, vol. 4, pp. 65–78. 1984.
- [43] R. D. Adams, J. A. Harris, “The influence of local geometry on the strength of adhesive joints”, *International Journal of Adhesion and Adhesives*, vol. 7, pp. 69–80. 1987.
- [44] R. D. Adams, J. Comyn, W. C. Wake, *Structure adhesive joints in engineering*, Berlin: Springer Science+Business Media, pp. 1-256, 1997.
- [45] J. W. Hutchinson, “Singular behavior at the end of a tensile crack in a hardening material”, *Journal of the Mechanics and Physics of Solids*, vol. 16, pp. 13–31, 1968.
- [46] J. R. Rice, G. F. Rosengren, “Plane strain deformation near a crack tip in a power law hardening material”, *Journal of the Mechanics and Physics of Solids*, vol. 16, pp. 1–12, 1968.
- [47] K. Duan, X. Hu, Y.W. Mai, “Substrate constraint and adhesive thickness effects on fracture toughness of adhesive joints”, *Journal of Adhesion Science and Technology*, vol. 18, pp. 39–53, 2004.

- [48] M. Ortiz, A. Pandolfi, “Finite-deformation irreversible cohesive elements for three-dimensional crack-propagation analysis”, *International Journal for Numerical Methods in Engineering*, vol. 44, pp. 1267-1282, 1999.
- [49] R. D. S. G. Campilho, M. F. S. F. de Moura, J. J. M. S. Domingues, “Modelling single and double-lap repairs on composite materials”, *Composite Science and Technology*, vol. 65, pp. 1948–1958, 2005.
- [50] C. D. M. Liljedahl, A. D. Crocombe, M. A. Wahab, I. A. Ashcroft, “Damage modelling of adhesively bonded joints”, *International Journal of Fracture*, vol. 141, pp. 147–161, 2006.
- [51] A. Turon, J. Costa, P. P. Camanho, C. G. Dávila, “Simulation of delamination in composites under high-cycle fatigue”, *Composites Part A: Applied Science and Manufacturing*, vol. 38, pp. 2270–2282, 2007.
- [52] R. D. S. G. Campilho, M. F. S. F. de Moura, J. J. M. S. Domingues, “Using a cohesive damage model to predict the tensile behavior of CFRP single-strap repairs”, *International Journal of Solids and Structures*, vol. 45, pp. 1497–1512, 2008.
- [53] R. D. S. G. Campilho, M. D. Banea, J. A. B. P. Neto, L. F. M. da Silva, “Modelling adhesive joints with cohesive zone models: effect of the cohesive law shape of the adhesive layer”, *International Journal of Adhesion & Adhesives*, vol. 44, pp. 48-56, 2013.
- [54] M. Scotch-Weld, "AF 163-2 Structural Adhesive Film, Technical Datasheet " 2009.
- [55] M. P. Palmares, *Strength of Hybrid Laminates Aluminium Carbon-Fibre Joints with Different Lay-up Configurations*, 2016.
- [56] R. D. S. G. Campilho, *Repair of composite and wood structures*, 2009.
- [57] Smiths Metal Centres, "Titanium Ti-6Al-4V (Grade5), Technical Datasheet " 2017.
- [58] ASM Aerospace Specification Metals Inc., “Titanium Ti-6Al-4V (Grade5), annealed, Technical Datasheet”, 1994.
- [59] I. Inagaki, T. Takechi, Y. Shirai, N. Ariyasu, “Application and Features of Titanium for the Aerospace Industry”, *Nippon Steel & Sumitomo Metal Technical Report N° 106*, 2014.
- [60] P. Molitor, V. Barron, T. Young, “Surface treatment of titanium for adhesive bonding to polymer composites: a review”, *International Journal of Adhesion & Adhesives*, vol. 21, pp. 129-136, 2001.
- [61] A. Mahoon, *Durability of structural adhesives*, London: Applied Science Publishers, p. 255, 1983.
- [62] H. M. Clearfield, D. K. McNamara, G. D. Davis, “Surface preparation of metals”, *Engineered materials handbook, volume 3: adhesives and sealants*, pp. 259-275, 1990.
- [63] L. F. M. da Silva, *Adhesive joints for low and high temperatures*, 2003.
- [64] G. W. Critchlow, D. M. Brewis, “Review of surface pretreatments for titanium alloys”, *International Journal of Adhesion and Adhesives*, vol. 15, pp. 161-172, 1995.